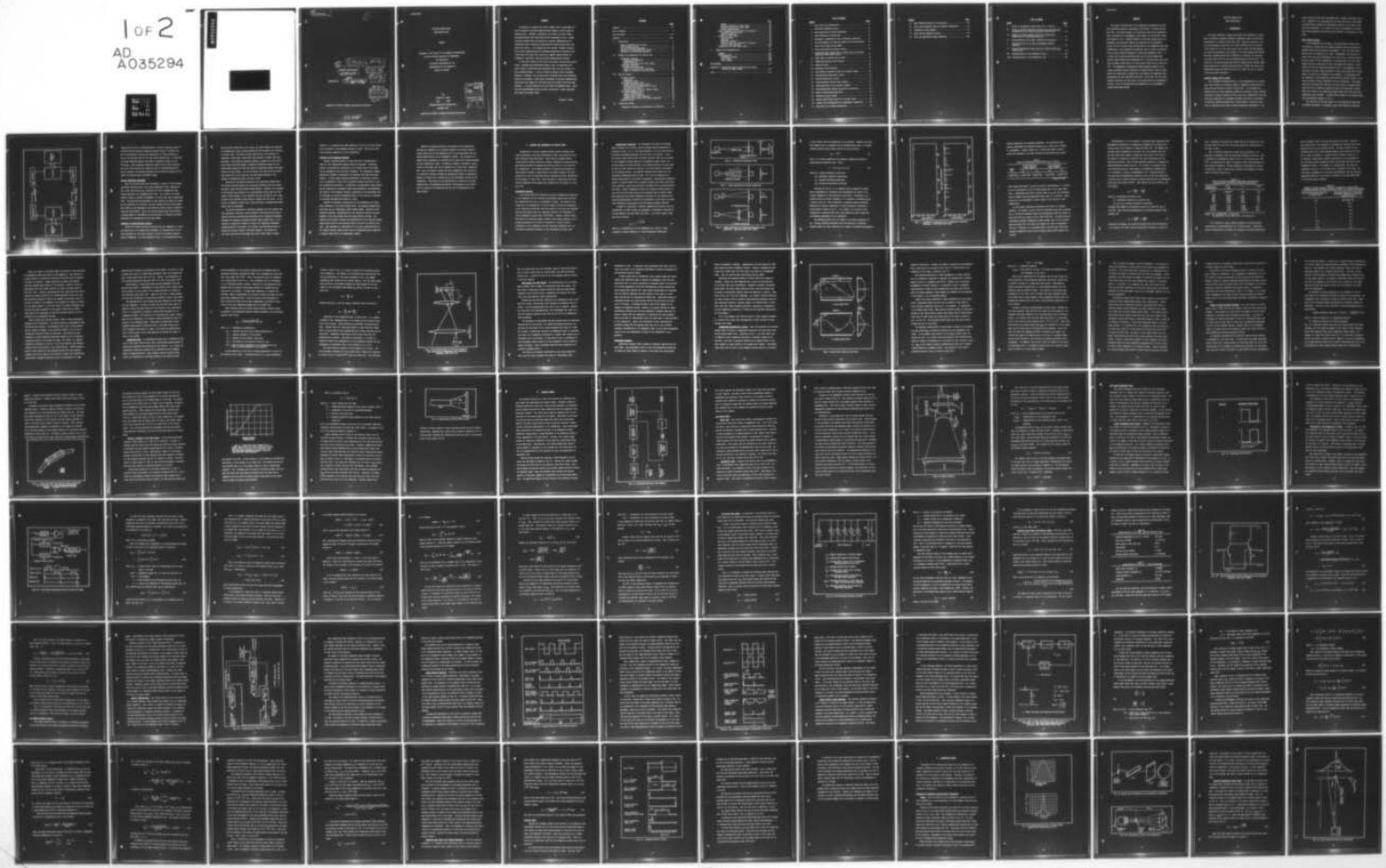AD-A035 294   AIR FORCE INST OF TECH WRIGHT-PATTERSON AFB OHIO   SCH--ETC   F/G 17/2
LOW-COST OPTICAL DATA LINK DESIGN STUDY.(U)
DEC 76   R G INNES
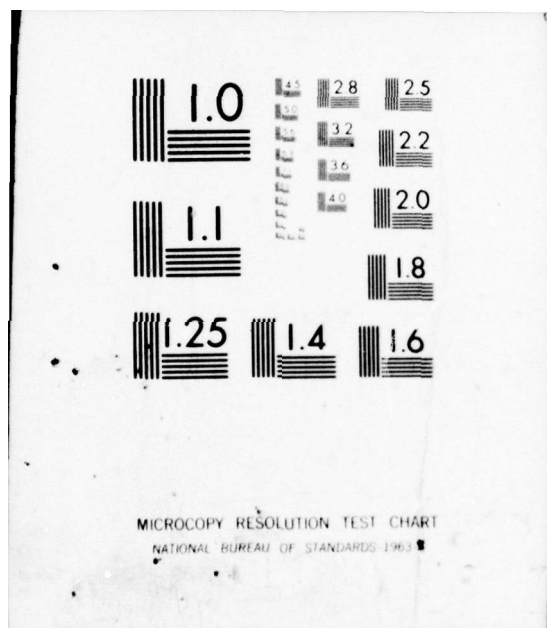
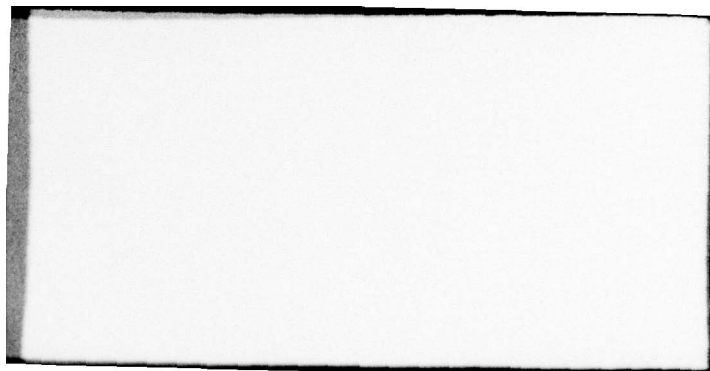UNCLASSIFIED   GE/EE/76D-25   NL

MICROCOPY RESOLUTION TEST CHART

NATIONAL BUREAU OF STANDARDS-1963

(6) (9) Master's thesis,

LOW-COST OPTICAL DATA
LINK DESIGN STUDY,

(11) Dec 76

THESIS

(12) 127 p.

GE/EE/76D-25

(10) Richard G. Innes
Capt   USAF

Approved for public release; distribution unlimited.

012225

LOW-COST OPTICAL DATA

LINK DESIGN STUDY

THESIS

Presented to the Faculty of the School of Engineering

of the Air Force Institute of Technology

Air University

In Partial Fulfillment of the

Requirements for the Degree of

Master of Science

by

Richard G. Innes

Capt   USAF

Graduate Electrical Engineering

December 1976

Preface

My decision to perform this study stemmed from a strong desire to see the promise of optical communications brought a little closer to practical use. Although I realized at the outset that this highly interdisciplinary area would pose serious challenges for me, I never-the-less believed that the potential of optical communications for conserving scarce natural and radio-spectrum resources more than warranted the effort. I am pleased that the results I present indicate that optical communications are becoming economically attractive, and I hope that this study will serve as an impetus toward further development of practical, low-cost optical communications systems.

As with most efforts of this type, this paper is truly not my work alone. Although many individuals played a part in completing this study, three in particular have sacrificed their time and talents in a most unselfish manner. I wish to thank my advisor, First Lieutenant Stanley R. Robinson, for his many hours of patient help and stimulation. Without his guidance, I know that my knowledge of optical communications could never have matured to the point where this paper could have been produced. I am also grateful to my wife Fran and daughter Diane. Their love and understanding during the many trying hours I spent preparing this paper were beyond value.

Richard G. Innes

ii

Contents

List of Figures

List of Tables

Abstract

This paper discusses some of the theoretical background and practical problems involved in designing a full duplex 1.5 Mb/sec optical data link. The actual design of a fiber-optic link and an atmospheric link is treated for an atmospheric path length of 1.372 Km and a fiber path length of 2 Km. Complete designs to the block diagram level are presented, and additional details are described for the modulator circuit for the CW laser diode and LED used in the atmospheric and fiber transmitters. Also presented is sufficient data to permit calculation of the various losses encountered in fiber and atmospheric links. It is shown that currently available LED's and low-loss graded-index optical fibers should permit production of a 2 Km long fiber optic data link to handle a data rate of 1.5 Mbit with an error rate of less than 10^{-5}. The atmospheric transmission theory presented permits use of readily available weather statistics to roughly predict that an atmospheric link operating in western Ohio can provide the comparable data performance for more than 99% of the time. Parts costs for the transmitters, receivers, and the cable in the fiber system are estimated at $21,800. Cost of the receivers and transmitters in the atmospheric system total about $4,030.

LOW-COST OPTICAL DATA

LINK DESIGN STUDY

I. Introduction

This paper describes a design study which was undertaken to deter-
mine if presently available commercial components permitted economical
construction of a duplex optical data link. Important features of the
link would include a data rate of 1.5 Mb/s (million bits per second),
a path length of 1 to 2 km, and a parts cost of about $15,000 maximum.
The study was performed at the request of the USAF Aeronautical Systems
Division's Communications Office (ASD/XOG) to determine the potential
of optical data links for use at Wright-Patterson Air Force Base. The
results of the study indicate that optical communications systems offer
great potential for solving Wright-Patterson's present and future data
transmission needs, and that the costs of at least one type of optical
system are highly attractive.

Specific Reasons for the Study

One of ASD/XOG's responsibilities is the implementation of digital
data links between the extensive number of computing systems and peri-
pheral devices located at Wright-Patterson AFB. As the number and
sophistication of these computing systems has continued to grow, ASD/XOG
has begun to receive requests for data links with transmission rates well
above the capabilities of equipment presently available to the agency.
In addition, ASD/XOG presently has a large number of relatively slow
links in operation which might be more economically implemented if the

1

various existing links were multiplexed onto a single, high-speed trunk line. Because of its increasing need for data links with a wide range of capabilities, ASD/XOG has considerable interest in all forms of new data link technology. As a result, the very high potential of optical data links appeared very attractive and resulted in the request for this study.

Basic Design Criteria

At the beginning of the study, a few broad design criteria were established to ensure that the designs developed would be suitable for ASD/XOG's known and anticipated requirements. First, the data transmission rate was selected as 1.5 Mb/s. Furthermore, the link was to handle this rate while maintaining a bit error rate of no more than one error for each 10^5 bits transmitted. The design was to be for a full duplex data link connecting two very intelligent data systems. Interfacing with the two computing systems was not to be addressed, but the link was to provide a NRZ (non-return to zero) data output and a timing signal for use by the interface at the receiver. It was assumed that the interface at the transmitter would provide a NRZ data signal to the link and require timing information from the transmitter. The assumptions were also made that control of the link start-up sequence would reside in the two computing systems and that error detection routines would also reside in the computing systems rather than within the link transmitters and receivers. A simple block diagram of the proposed data link configuration appears in Fig. 1.

The selection of the path length to be considered was based upon an ASD/XOG requirement to implement a data link between two existing

2
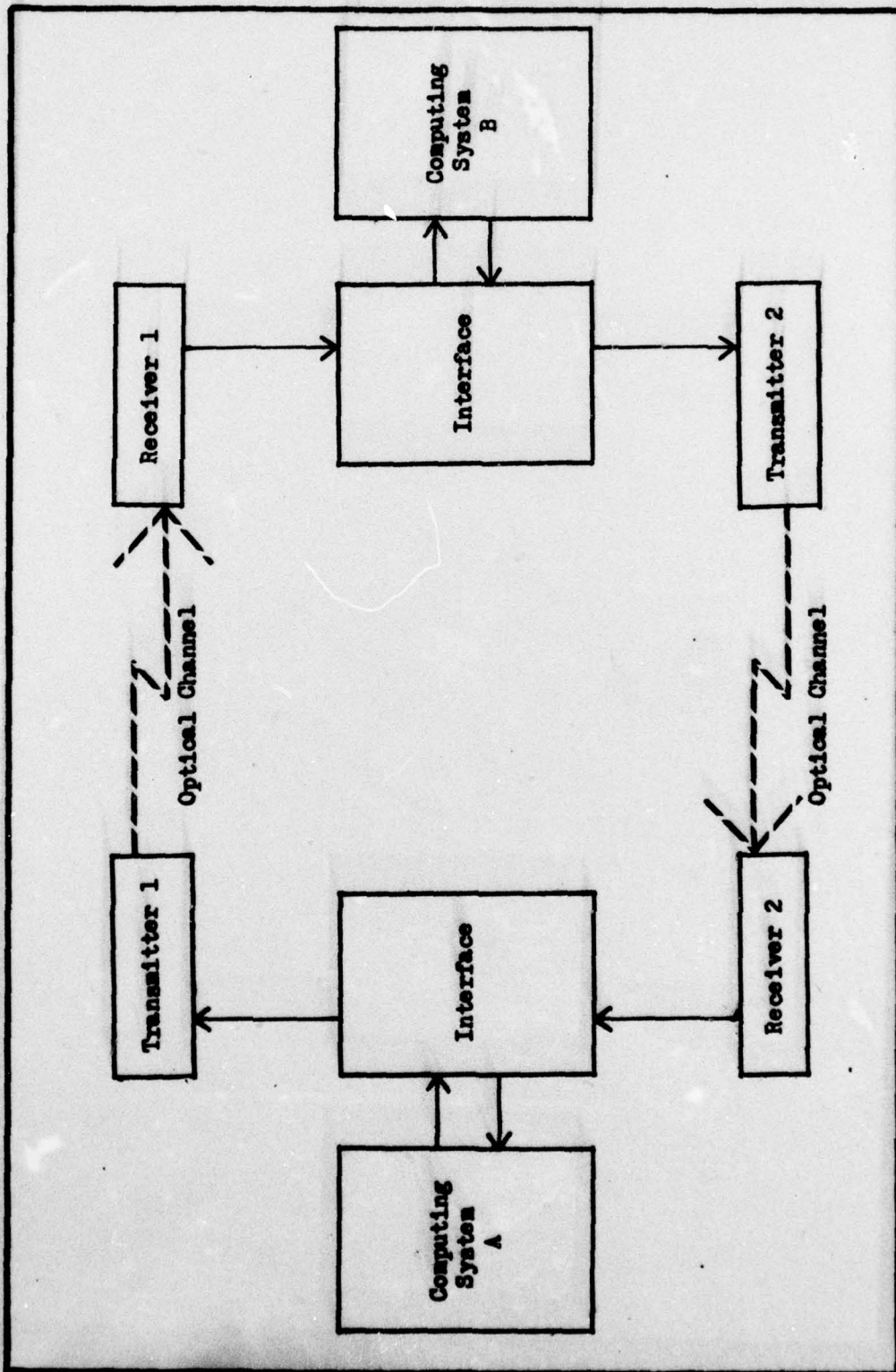
Fig. 1. Basic Data Link Configuration

3

computing facilities at Wright-Patterson, a DEC-10 computing system in Building 620 and extensive computing systems located in Building 676. Due to the physical location and construction of these buildings, a direct line-of-sight path 1372 m long exists between them. In addition, an unused telephone conduit 2 km long is available between the two buildings. These distances exceed the length of most other potential data link routes within the scientific area of Wright-Patterson AFB, and as a result, the designs developed for the link were expected to be useful for meeting many of ASD/XOG's needs.

Initial Technology Assessment

Once the criteria above were determined, a review of the available technology indicated that a link using atmospheric light transmission and a link using fiber optic waveguides for light transmission both offered potential for implementing the link. As a result, the author decided to make a parallel development of a fiber link and an atmospheric link. This decision was determined in part because the effects of atmospheric conditions on a low-cost link were unknown and the line-of-sight path needed by the atmospheric link would not exist in some of ASD/XOG's potential applications. Also, the designs derived would offer ASD/XOG a maximum amount of information on the potential of currently available components for implementing optical data links.

Selection of Electro-Optical Devices

Because the design criteria stipulated that the components to build the system were to be commercially available, an important part of the early research for this paper involved a survey of available electro-optical components. For the atmospheric link, it was accepted that the

4

optical source would have to be a laser, but some research was required to determine what type of laser offered the most potential for building a low-cost link. The device finally selected was a CW (carrier, or continuous, wave) laser diode which could operate at normal room temperatures. This diode was selected because it appeared to offer sufficient output power and because a potential modulation scheme for the diode showed promise of being two orders of magnitude cheaper than modulators for other lasers. As will be shown, this early intuitive selection turned out to be a good one, and the design proposed in the chapter on transmitters uses a CW laser diode.

Selection of the optical source for the fiber-optic system was a little more involved because the literature indicated that both lasers and LED's (light emitting diode) showed promise. However, the lifetimes of LED sources were reported to be significantly better than the lifetimes of laser diodes, so the tentative decision was made to use a LED, provided that sufficient power could be coupled into the fiber. As the results in Chapter IV show, such a LED was found, so designs based upon lasers were not developed.

The initial selection of front-end components for the receiver was also important, involving a choice between a PIN (positive-intrinsic-negative junction construction) photodiode and an avalanche photodiode. Although the avalanche photodiode offered higher sensitivity, it also required a complex bias scheme to counter the temperature dependent characteristics of the diode. As a result, the decision was made to design the receiver around a PIN diode detector. The results of the study show that the PIN diode will work in both types of links,

5

however, it is possible that some reduction in cost of the fiber system can be realized if the avalanche detector is used. Time has not permitted further examination of this possibility.

Overview of the Following Chapters

Before a detailed design of a data link can be accomplished, a model for the transmission channel should be developed. Therefore, Chapter II describes the derivation of the models used in this paper for the atmospheric and fiber-optic channels. The atmospheric channel description includes a discussion of attenuation and beam scattering effects. A simple model relating attenuation to prevailing visibilities is presented to allow use of available weather statistics to predict attenuation statistics. In addition, the phenomena of beam bending and spot dancing are discussed, along with appropriate countermeasures. The results of the analysis include a prediction of the percentage time of occurrence of various attenuation levels in the link and a selection of the beam divergence half angle of 1 mrad.

Chapter III presents a description of the atmospheric and fiber-optic receivers at the block diagram level. The designs presented are based upon use of a Manchester signal coding scheme. Analysis of the receivers includes a determination of the effects of noise on the performance of the data decoder and the timing decoder circuits. The results of the chapter include the determination of the required optical signal power levels at the detector diode to provide the desired error rate. Also included is a description of the jitter characteristics of the timing recovery circuit, which uses an integrating phase comparator to decode timing data in the Manchester signals.

Chapter IV presents details on the design of the transmitters. Included are comments on the possible design of the laser's optical system (which has not been completed due to time constraints) and the desired beam pattern for the atmospheric system. Also included is a sample safety calculation to determine the closest safe viewing distance for the transmitter's beam. In addition, Chapter IV presents a calculation of the power that can be coupled into a fiber from a commercial LED. Also, the amount of power that each transmitter will provide to its respective receiver through the appropriate channel is determined. Chapter IV closes with a description of the electronics section of the transmitter. While most of this description is limited to the block diagram level, the modulator description is developed to the circuit level to indicate the simplicity and low cost of modulators for CW laser diodes.

II. Channels and Components for Optical Links

Transmission of optical signals presents special problems which differ appreciably from those encountered in more traditional wire and radio frequency based data links. These special problems concern electro-optical energy conversion, channel transmission characteristics, and coupling between the channel and optical devices in the receivers and transmitters. This chapter presents a discussion and analysis of these special problems. Specifically, the chapter examines the characteristics of the two candidate optical channels and their implications on the design of a data link. Also included is a description of those optical components which appear most promising for the design of a low-cost link.

Atmospheric Channels

This section describes background noise and transmission properties of the atmosphere and the resulting requirements placed upon receivers and transmitters for use in an atmospheric system. The reader is cautioned that the transmission of optical signals through the atmosphere is not completely understood, and that workers in the area have reported that existing theory does not completely describe the performance of actual atmospheric systems (Ref 1:2193-2195). However, present theory does seem to be accurate enough to permit first order estimates of the average percentage of the time of occurrence of various levels of attenuation in the atmosphere, and the resulting information will be invaluable for making estimates of link performance and down time.

Transmission Properties. The atmosphere can alter the received signal strength at an optical receiver through several mechanisms as depicted in Figs. 2 to 4. From these sketches, it can be seen that the attenuation phenomena generally fall into one of two groups. First, the overall power level across the entire receiver plane can be reduced if the atmospheric medium absorbs the transmitted beam; second, the received power will also diminish if the medium scatters the light beam so that the power density is reduced in the area actually intercepted by the receiver optics. The physical elements which account for the attenuation mechanisms shown in Figs. 2 to 4 are the molecular and aerosol constituents of the earth's atmosphere. The molecular components consist of various gases such as oxygen, nitrogen, and water vapor which occur naturally, along with man-added pollutants such as carbon monoxide and ozone. Aerosol components include such things as water droplets in the form of fog and rains along with pollutants such as factory smoke. Both molecular and aerosol components contribute to the absorption and scattering mechanisms, although the contribution to each type of attenuation mechanism varies greatly with the physical element involved.

A number of researchers in optical communications believe that the transmission of light through the atmosphere is adequately described by the Beer-Lambert law (Ref 2:128; Ref 3:10). In its most general form, this law is written

$$T_a = e^{-\int_0^L \gamma ds} \tag{1}$$

where T_a = transmissivity of the atmosphere as a ratio of output intensity to input intensity; γ = total extinction coefficient;

9
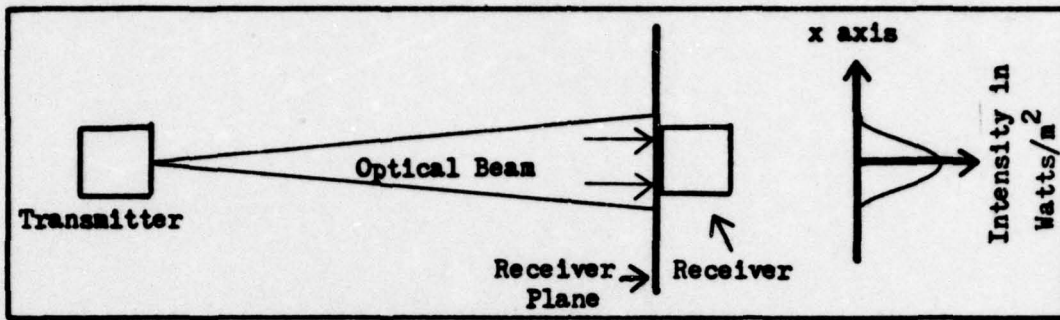
Fig. 2. Unaffected Atmospheric Beam
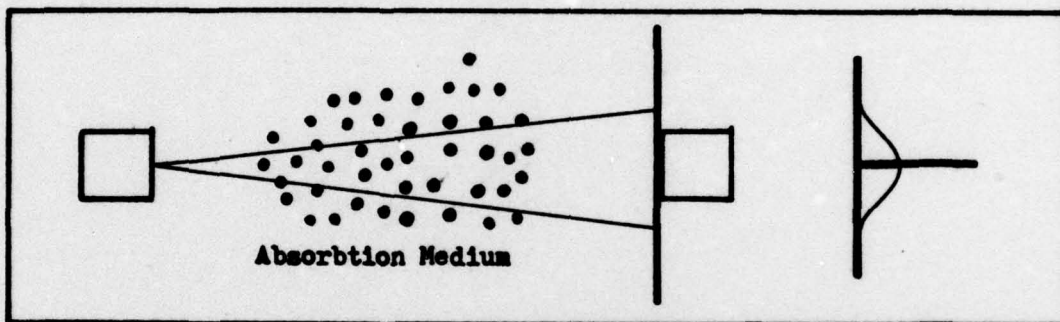
Fig. 3. Beam Attenuated by Uniform Absorbtion
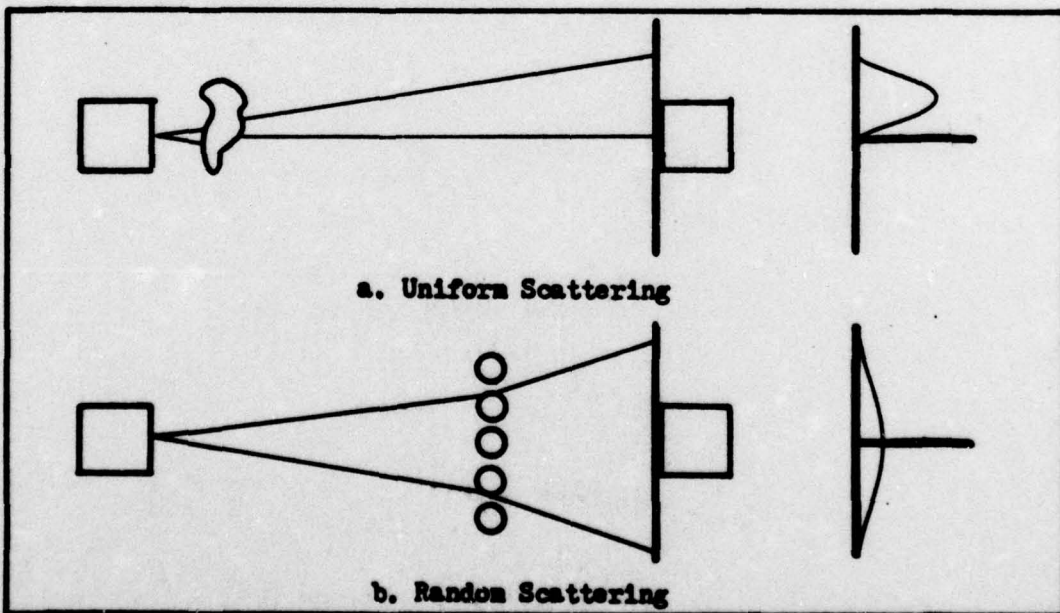
Fig. 4. Beam Attenuated by Scattering (Reproduced with
permission, Copyright 1969) (Ref 2:134)

ℓ = path length from the transmitter to the receiver. Usually, for short path lengths such as considered for the proposed data link, γ is fairly constant along the path length, and Eq (1) may be written

$$\tau_a = e^{-\gamma\ell} \qquad (2)$$

Also, γ is usually broken down into separate components related to scattering and absorption (Ref 3:10):

$$\gamma = K_a + K_m + \sigma_a + \sigma_m \qquad (3)$$

where K_a = aerosol absorption coefficient

K_m = molecular absorption coefficient

σ_a = aerosol scattering coefficient

σ_m = molecular scattering coefficient

From Eqs (2) and (3), it is apparent that an analysis of atmospheric transmission is concerned with determining the values of the various components of the extinction coefficient. Fortunately, by a careful choice of optical frequency, it is possible to eliminate K_m as a factor in Eq (3). This elimination is possible because molecular absorption of optical frequencies is highly selective, occurring in narrow bands as shown in Fig. 5. As a result, if the laser in the transmitter is operated away from a high absorption band, losses due to molecular absorption will be negligible.

The remaining terms in Eq (3) cannot be as easily eliminated as K_m. Instead, modeling techniques have been employed to determine average values for these constants for a number of different wavelengths,
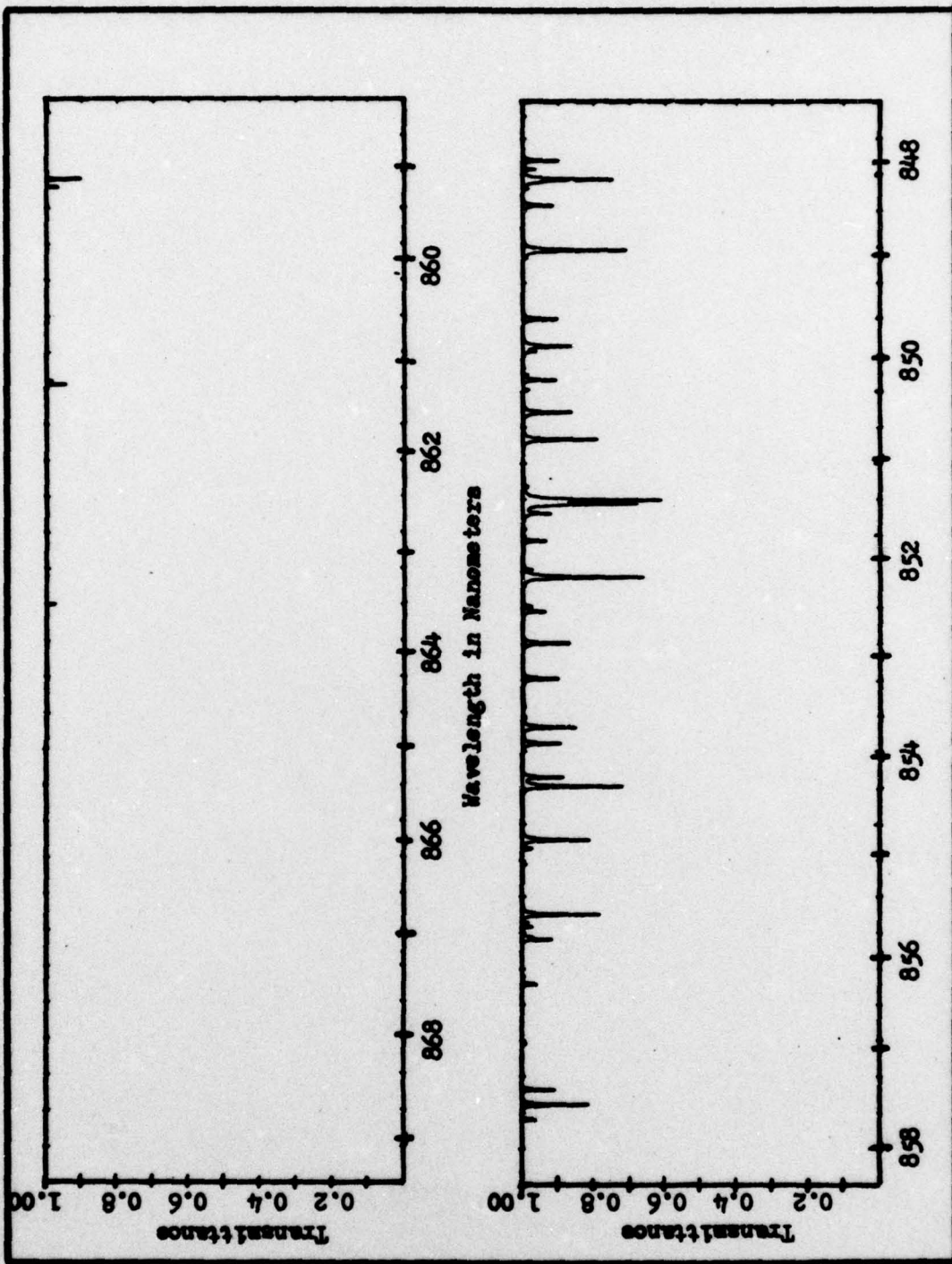
Fig. 5. Atmospheric Transmittance Due to Molecular Absorbtion
(Through a 10 km Path) (Ref 5:98)

weather conditions, and seasonal variations. For relatively clear weather, McClatchey has tabulated values σ_m, K_a and σ_a for a variety of wavelengths. Typical values for $\lambda = 860$ nm are shown in Table I since this frequency is the most suitable for available laser diodes.

Table I
Values of Attenuation Coefficients for $\lambda = 860$ nm

Summer σ_m	23 km Visibility "clear" weather		5 km Visibility "hazy" weather	
	K_a	σ_a	K_a	σ_a
1.93×10^{-3}/km	1.52×10^{-2}/km	9.03×10^{-2}/km	7.43×10^{-2}/km	4.40×10^{-1}/km

(From Ref 3:20)

Using values from Table I in Eqs (2) and (3), and assuming $\ell = 1.372$ km, τ_a can be calculated as 0.86 in clear weather and 0.49 in hazy conditions. (McClatchey also lists a winter value of σ_m, but the difference from the summer value has negligible effect when $\ell = 1.372$ km). These values of τ_a are equivalent to power losses of 0.66 dB and 3.1 dB, respectively.

As the weather conditions deteriorate, the value of γ changes markedly. For example, using a 632.8 nm wavelength laser and a receiver with a 10 minute acceptance angle, Chu and Hogg have measured losses of more than 40 dB on a path of 2.6 km (Ref 5:742-751). The same series of experiments recorded transmission losses greater than 65 dB in heavier fogs and nearly 30 dB in heavy rain showers for light of wavelength 632.8 nm. Therefore, it is probable that a low-cost data link using moderate transmitter power will not operate under severe weather conditions.

13

Unfortunately, it is not possible to correlate many theoretical and experimental descriptions of atmospheric propagation to available statistical data on the weather at Wright-Patterson AFB. For example, Chu and Hogg relate attenuation to the rain rate in millimeters per hour and fog liquid water density in grams per cubic meter, while much of the theory of scattering is based on drop size distributions of the scattering particles. None of these physical quantities is measured by Wright-Patterson's weather service. As a result, to correlate available statistical data on local weather to atmospheric transmissivity, it is necessary to resort to Koschmieder's law. Coolidge discusses this law and the modifications required to use the law with prevailing visibility data (a value recorded by weather services) and at wavelengths other than 550 nm (Ref 6:91-96). When modified for use at 860 nm, the law becomes

$$\gamma_a = \frac{2.07}{V_k} = \frac{1.28}{V_s} \tag{4}$$

where V_k = prevailing visibility in km

V_s = prevailing visibility in statute miles

$\gamma_a = \sigma_a + K_a$ = aerosol attenuation coefficient

Coolidge also comments on attenuation during fog conditions (Ref 6: 126-128). When fog exists Koschmieder's law becomes wavelength independent, and

$$\gamma_a = \frac{2.934}{V_k} = \frac{1.823}{V_s} \tag{5}$$

According to Coolidge, the transition between haze and fog conditions is not abrupt, but occurs when the prevailing visibility is about 3/4

14

mile. Therefore, this paper will assume that Eq (4) applies for visibilities above 3/4 mile, and that Eq (5) applies for visibilities of 3/4 mile or less.

Now, if the path length and a value for σ_m are known, it is possible to assemble a table of prevailing visibility versus τ_a. Such a tabulation is presented in Table II for $\ell = 1.372$ km and $\sigma_m = 1.93 \times 10^{-3}$. The derivation of Table II assumes no water vapor absorption at the selected wavelength. Given a frequency of occurrence of various visibilities, Table II can be used to predict the frequency of occurrence of various values of τ_a.

Table II
Values of Aerosol Attenuation Coefficient and Resulting
Transmissivity for Various Prevailing Visibilities

Visibility in Statute Miles	γ_a in /km	τ_a	τ_a dB
14.3[1]	1.055×10^{-1}	0.86	0.66
5[2]	0.256	0.70	1.5
4[2]	0.320	0.64	1.9
3[2]	0.427	0.56	2.6
2[2]	0.640	0.52	2.8
1[2]	1.280	0.172	7.6
0.75[3]	2.431	0.036	14.5
0.5[3]	3.646	0.006	21.7
0.25[3]	7.292	4.5×10^{-5}	43.4

Notes: $\sigma_m = 1.93 \times 10^{-3}$/km, $\ell = 1.372$ km
(1) From Table I, (2) From Eq (4), (3) From Eq (5)

It is possible to obtain computer summaries of hourly weather observations at Wright-Patterson for a 36-year period. Tabulations permit determining the frequency of occurrence of various visibilities

during different times of the day and months of the year. There are also tabulations of the frequency of occurrence of various visibilities averaged over the entire 36-year period. The data in Table III was developed from the all years average summary, while other sets of data may be found in Appendix A. Using the data in Tables II and III, it is possible to make fairly accurate predictions of the percentage of the time that various attenuation levels (at 860 nm) will exist in the atmospheric channel. For example, on a yearly basis, the link will experience a loss of 7.6 dB no more than 1.9 percent of the time. By using data in Appendix A, it can also be ascertained that the link will experience losses of 7.6 dB about 6.3 percent of the time during 0900 to 1100 local time in January.

Table III
Summary of Annual Average Visibility Occurrences at Ground Level
at Wright-Patterson AFB (Data Processing Branch, Air Weather Service/MAC)

Tabulated Prevailing Visibility in Statute Miles	Percentage Frequency of Occurrence of Actual Visibilities lower than Tabulated Value
14.3	more than 62%
5	20.7
4	14.0
3	8.5
2	4.8
1	1.9
0.75	1.3
0.5	0.7
0.25	0.4

Again, the reader is cautioned about the accuracy of the statistics of transmission based upon Table III and Appendix A. The accuracy of a human observer in determining prevailing visibility even in daylight is subject to question. Muench reports that primary duty weather observers commonly make errors of ± 36 percent in daytime visibility measurements when the actual visibility is about 3 statute miles or less (Ref 7:34). However, considering the very large data base used to develop the weather statistics for Wright-Patterson and the fact that many different observers' results are compiled, the overall errors in the data of Table III and Appendix A are probably not nearly as extensive as Muench reports. At the very least, the results obtained from the data and model presented in this report should give at least a rough idea of the percentage of time that various losses will be encountered in the atmospheric channel.

Before closing this section, another class of laser propagation phenomena will be mentioned. The class includes the phenomena of beam bending and spot dancing. The phenomena occur even in clear weather and are caused by changes in the refractive index of the air due to temperature variations along the beam path. Spot dancing is most pronounced in windy conditions when small masses of air at different temperatures exist in the larger air mass. The result is a bending mechanism as depicted in Fig. 4a. As its name implies, spot dancing produces fairly rapid shifts in the beam direction. Chiba's measurements of power spectra of spot dancing indicate that spot dancing changes occur on the order of 1/10 second or longer (Ref 8:2460-2461). Using Chiba's standard derivation of the x displacement of a beam

17

undergoing spot dancing, and combining a path length ℓ of 1372 m, it can be shown that there is a significant probability that spot dancing will bend a laser beam by more than 30 μ rad. However, the probability of spot dancing bending the beam more than 0.5 m rad is only about 10^{-46}.

Beam bending is a much more slowly varying phenomenon than spot dancing (Ref 8:2456). Measurements by Ochs indicate that diurnal bending variation is on the order of 40 μ rad/km and about 3 μ rad/km in the horizontal plane (Ref 9:12). Based on this data, it seems reasonable that the likelihood of beam bending exceeding 1 mrad is very small.

The implications of spot dancing and beam bending for link design are very important. In order to ensure that the beam cannot bend far enough to reduce the power density at the receiver to an insufficient level, it is necessary to include a planned beam divergence in the transmitter design. This results in an increased power output requirement for the transmitter, the increase varying approximately with the square of the divergence angle. Based upon the magnitudes of beam movements experienced by Chiba and Ochs, it has been decided that a safe divergence half angle is 1 mrad. This selection should ensure only a remote chance of the beam wandering far enough off target to cause a link outage.

Background Noise. An inescapable problem with an atmospheric data link is that light from the sun, stars, and man-made sources cannot be completely eliminated from detection by the receiver. As a result, an atmospheric system must contend with an additional noise component known as background noise. Pratt presents several relations which permit the calculation of the power falling on the detector given

18

several parameters of the receiver systems and the measured value of background irradiance expressed as power into a hemisphere or power per unit solid angle (Ref 2:119). Pratt also provides plots of irradiance for a zenith angle of 45° (i.e., a sky irradiance) and for irradiance of the illuminated earth's surface. Selection of the appropriate plot depends upon the physical relationship between the transmitters and receivers in the system. In cases where receivers in a system view different types of backgrounds, the receiver viewing the earth will have more input background noise. Since the actual noise calculation is quite similar for either sky or earth backgrounds, only Pratt's relations for an earth background example will be treated here.

Pratt indicates that the optical power reaching a detector diode is related to the background spectral radiant emittance by the following relation (Ref 2:119):

$$P_B = \frac{\pi \, \tau_a \, \tau_{ro} \, \lambda_B \, \theta_R^2 \, d_R^2}{4} \, W(\lambda) \tag{6}$$

where τ_a = atmospheric transmissivity

τ_{ro} = receiver lens and filter system transmissivity

λ_B = optical bandwidth of the receiver

d_R = diameter of the receiver input lens

θ_R = full angle of the receiver's field of view

$W(\lambda)$ = spectral radiant emittance of the background for the center optical frequency of the receiver.

In this equation λ_B is set by the optical bandwidth of a filter in the receiver optics train. A practical value for λ_B using inexpensive

19

filters is about 10 nm. θ_R is also a function of the selected optics train components. For reasons to be discussed later when optical filters are considered, it was found necessary to use a two element collimating lens system for the receiver optics. For this lens system, Pratt provides a relationship between the focal lengths of the two lenses in the collimating lens system, θ_R, and θ_R' as shown in Fig. 6 (Ref 2:8):

$$\theta_R = \frac{F_2}{F_1} \theta_R' \tag{7}$$

However, since $\theta_R' = \arctan(r_d/s_d)$, relation 7 may be written as

$$\theta_R = \frac{F_2}{F_1} \left(\tan^{-1} \frac{r_d}{s_d}\right) \tag{8}$$

Evaluation of the transmissivities is fairly easy. τ_r is simply a product of the transmissivities of the lenses and the optical filter used in the systems. These relations are available in manufacturers' data. Typical value for crown glass lenses is about 90% while lenses made of acrylic plastic have transmissivities of about 83% when used as collectors. Economical interference filters offer only about 50% transmissivity, however. From earlier discussions, it is best to assume the worst case transmissivity of the atmosphere applies for the propagation of background light to the receiver, i.e., $\tau_a \cong 1$.

The final relation required to solve equation (6) is $W(\lambda)$. For the wavelength considered for this system Pratt's figure 6-11 indicates an average value of around 8×10^{-3} watts per cm^2-micron. Pratt mentions

20
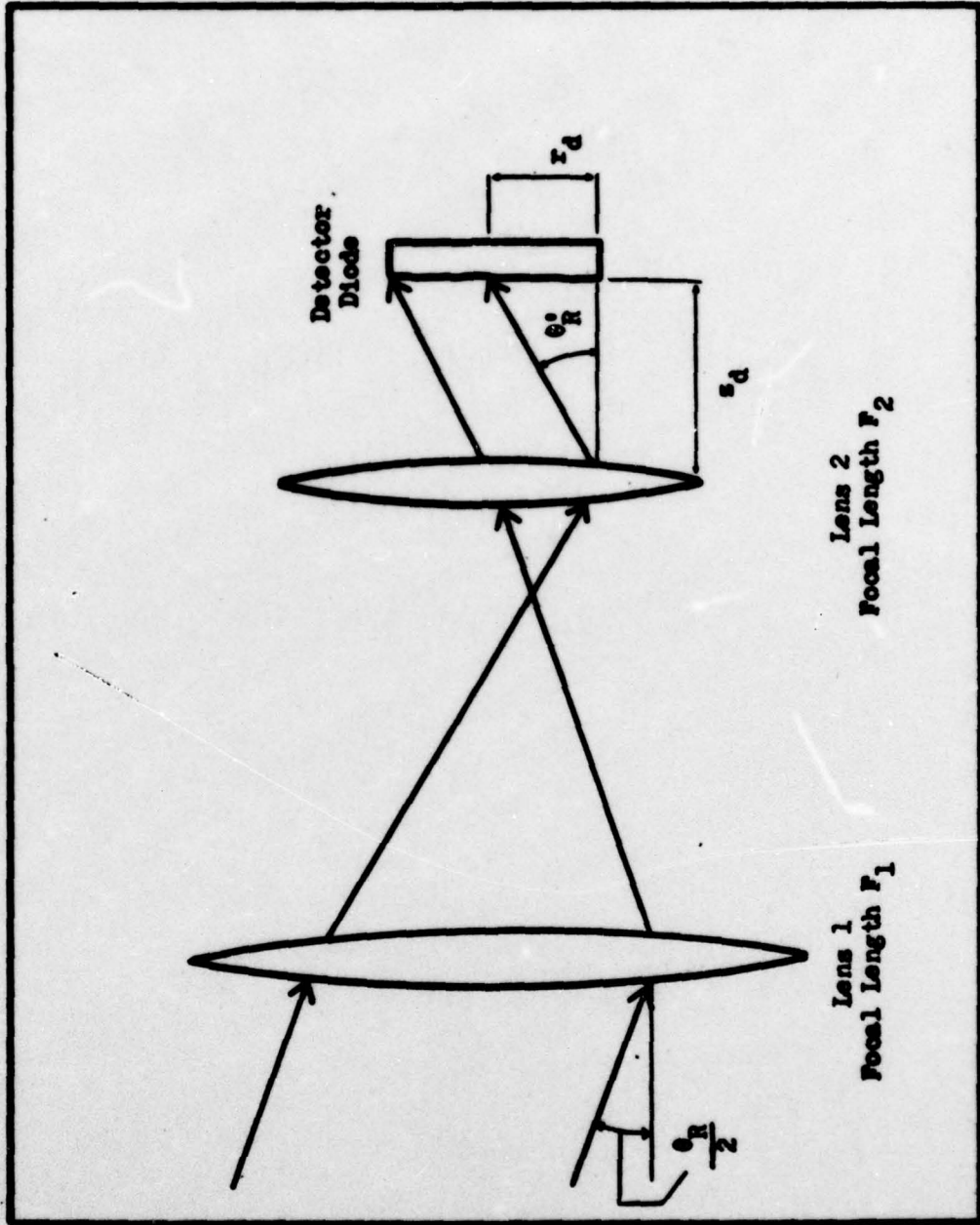
Fig. 6. Ray Relationships for Receiver Angle of
View Calculations (Reproduced with permission.
Copyright 1969) (Ref 2:8)

that this figure may vary with different types of reflecting material such as rocks, trees, water or plowed fields, but does not provide further data. A solution of Eq (6) for the proposed receiver follows in the next chapter.

Implications for Link Design. The characteristics of the atmospheric channel place a number of constraints upon link design. The main areas of importance concern transmitter power and beam spread, transmitter and receiver optics, transmitter and receiver site locations, and some important safety implications.

Perhaps the most obvious limitation on an atmospheric link is the need for a clear, line-of-sight path between the transmitter and receiver. For the proposed data link, this is not a problem. However, for other data link implementations, this requirement may result in a need for repeater stations or may rule out the use of an atmospheric link altogether.

The phenomena of beam bending and spot dancing also have important implications on link design. For reasons discussed previously, the decision has been made to use a beam divergence half angle of 1 mrad. As a result, a significant increase in transmitter output is required, but there is no inexpensive alternative if erratic link outages due to turbulence are to be avoided. On the positive side, an advantage of this divergence angle selection is that transmitter optics should be easier to design. Also, a divergent beam will make transmitter and receiver alignment easier.

The effects of molecular absorption on light beam propagation make clear the need to operate the laser at a wavelength where

attenuation is low. In addition, laser wavelength drift must be low so there is no shift to an absorption wavelength or beyond the passband for the receiver's optical filter.

A final restriction on atmospheric links concerns human eye safety. Lasers with sufficient power to operate an atmospheric link also emit sufficient power to require safeguards to personnel under the provisions of Air Force Regulation 161-32 and corresponding civilian regulations. These regulations indicate that laser hazard calculations are concerned with the optical frequency and power density of the beam at a point where the beam can be intercepted by human eyes. Additional factors in determining safety for pulsed lasers involve the duty cycle and pulse rate of the beam. A calculation based on AFR 161-32 appears in the chapter on transmitter design. However, the general results of safety calculations indicate that for most atmospheric systems, steps must be taken to ensure that the transmitter is controlled and that personnel must not be able to inadvertently enter the laser beam in close proximity to the transmitter. Again, this restriction is not a particularly difficult problem for the proposed data link, but it can virtually eliminate consideration of an atmospheric link in cases where controlling access to the area immediately in front of the transmitter is not possible.

Fiber-Optic Channels

Fiber-optic channels offer a number of excellent possibilities for data links. One outstanding virtue is that the transmission properties of fibers are quite stable as opposed to the larger time fluctuations

found in atmospheric channels. Consequently, the only reason for fiber
link outages should be component vailures. Further, transmission path
losses can be made lower for fiber links, and there is no background
noise. Too, the line-of-sight restriction does not apply.

Offsetting the numerous benefits of fiber links are a number of
problems. Perhaps the most important one is that the cost-per-foot
of the fiber link can be substantial. Presently, suitable two-channel
fiber cables cost about three dollars per foot, and these cables must
be placed in underground conduits which are expensive to install. Also,
fiber optics are a very new technology. As a result, optimum solutions
for some problems, such as low-loss field-installed couplings, have not
been completely resolved. However, despite its problem areas, a fiber
optic data link offers excellent potential, warranting an examination
of the transmission properties of fibers and the resulting implications
for link design.

All of the comments that follow pertain to fiber channels composed
of a single fiber, since this configuration is most suitable for long
distance data links.

Transmission Properties of Fibers. There are presently two different
general types of fibers in large-scale production, the step index fiber
and the graded index fiber. Referring to Fig. 7, the step index fiber
is composed of two transparent materials of different indexes of re-
fraction. The fiber is generally coated with an opaque buffer to pre-
vent transfer of light outside of the single-fiber channel. The graded
index fiber does not have a sharp boundary between regions of different

24

Buffer

Ray 2

θ

n_1

Ray 1

n_2

n_2

n

a. Step Index Fiber

Index Profiles

Buffer

Ray 2

θ

Ray 1

n

b. Graded Index Fiber
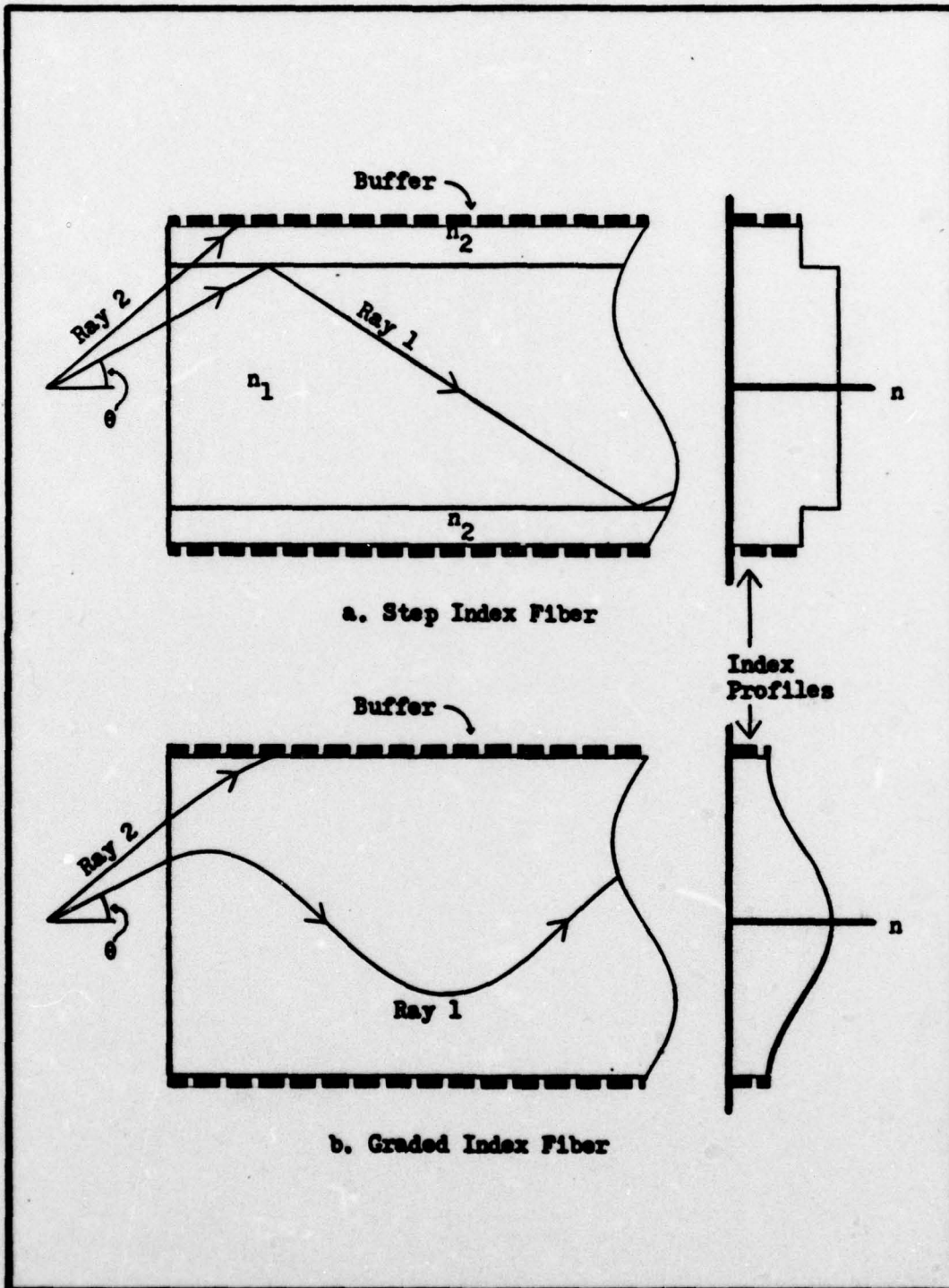
Fig. 7. Basic Fiber Types and Ray Paths

25

indexes of refraction. Instead, the index of refraction varies smoothly from a high level in the center of the fiber to a lower value at the boundaries of the fiber, as shown in Fig. 7b.

The detailed description of light propagating in fibers involves the use of Maxwell's equations to describe the transmission of electro-magnetic waves in a waveguide (Ref 10:8). However, due to the short wavelengths of optical signals, it is possible to gain a reasonable understanding of fibers by using geometrical ray optics (Ref 10:1-8). Since the second approach is much simpler and adequate for the purposes of this paper, it is the approach adapted.

Using a ray optics description, light propagating in a step index fiber is contained within the core (the n_1 region) of the fiber by total internal reflections from the $n_2 - n_1$ boundary. By comparison, in the graded index fiber, light rays are guided by means of refraction. Because of the index profile, graded index fibers tend to continuously focus rays of light toward the center axis of the fiber as shown by ray 1 in Fig. 7b. This focusing process keeps the rays from exiting through the wall of the fiber.

An important characteristic of both types of fibers is the maximum ray entry angle θ_{max} for which an entering ray will propagate in the fiber. If the general entry angle θ is too large, neither fiber can contain the ray. As a result, the ray proceeds to the cladding region where its energy is dissipated as in the case for ray 2 in Figs. 7a and 7b. θ_{max} is not usually listed in manufacturer's data, but a closely related quantity is commonly listed. This quantity is the fiber's numerical aperture, and it is given by (Ref 10:2)

26

$$N.A. = \sin(\theta_{max}) \qquad (9)$$

where N.A. = Numerical aperture

θ_{max} = max value of θ in Fig. 7 for which the associated ray will propagate in the fiber.

Upon initial examination Eq (9) implies that the best fibers are those which have a large numerical aperture, since these fibers would be easiest to couple to a large area light source. Unfortunately, another important characteristic of fiber channels implies that the numerical aperture should be small. This quality is the group delay propagation of the fiber, and it concerns the pulse spreading effect that fibers have on input signals. Pulse broadening effects limit the maximum data handling rate of a fiber, and broadening complicates receiver design.

To gain a qualitative understanding of group delay, consider the fact that practical light emitters for fibers are area sources of considerable size when compared to the cross-sectional area of practical fibers. As a result, rays from the source may arrive at the entrance wall of the fiber at various angles from $\theta = 0^{\circ}$ to $\theta \approx 90^{\circ}$. Those rays which arrive at an angle larger than θ_{max} are absorbed and do not propagate, but all other rays are contained and do propagate. Due to the fact that each ray propagates through a different path length, the various rays depart the opposite end of the fiber at different times, and the pulse detected by the receiver can undergo significant pulse broadening. For example, rise and fall times of roughly 35 nsec would be experienced with a 2 Km length of cable which had a specified bandwidth of 20MHz for a one kilometer length.

27

Now, to reduce the degree of pulse broadening, it is necessary to reduce the difference in travel time of the various rays propagating in the fiber. For a step index fiber, the only way to accomplish this is to reduce the number of different rays the fiber can propagate. Unfortunately, this also reduces the number of different ray angles that the fiber will accept, and the fiber becomes more difficult to optically excite. As a result, it is apparent that step index fibers do not offer an efficient system for low cost data links because the improved bandwidth of the fiber comes at the cost of increased complexity in the optical transmitter.

Fortunately, graded index fibers offer a method to control pulse spreading without complicating optical driver requirements. Graded index fibers can be constructed so that rays entering the fiber at different angles travel essentially the same "effective" path length even though the true path lengths differ widely. This effective path equalization occurs because rays which have high entry angles θ have propagation routes which spend a significant amount of time in areas of low indexes of refraction. Since light propagates faster in the low index regions, it is possible for a ray propagating down the center of the fiber and a skew ray to both arrive at the exit end of the fiber at nearly the same time. The result is that graded fibers with the proper index profile have much better pulse responses than step index fibers. To give a quantitative measure of pulse response, most manufacturers denote the pulse broadening characteristics of their fibers in terms of fiber bandwidths per kilometer length. Typical bandwidths for step and graded index fibers of equal numerical aperture are about

20 MHz/Km and 200 to 400 MHz/Km respectively, indicating the superiority of graded fibers over step fibers.

In addition to the pulse broadening effects of fibers, the other major concern is attenuation. As in atmospheric transmission, the output signal of fibers is attenuated by both scattering and absorption. However, thanks to carefully controlled manufacturing processes, attenuation in fiber links can be much lower than the atmosphere can provide. Presently, fibers are available from several sources in commercial quantities with total attenuations of only 6 to 10 dB/Km. As in atmospheric propagation, the fibers do have important molecular absorption bands, and the low loss figures apply only when an appropriate frequency is used.

Losses in Fiber-to-Fiber Couplings. As is the case for an atmospheric link, a fiber link must be coupled to both the light emitter and detector. Additionally, the fiber should be capable of fiber-to-fiber coupling to facilitate cable installation and repair. The area of couplings for single fiber cables is still in a developing stage, and the author has not been able to obtain data on commercially available low loss (<1 dB) coupling devices. However, much of the technology seems to be worked out at the laboratory level, and a brief review of some demonstrated splicing techniques follows.

An important consideration for efficient fiber-to-fiber coupling is preparation of the fiber ends. The ends should be broken absolutely square across with a smooth surface if scattering losses are to be low. Suitable ends can be prepared by grinding and polishing, but the equipment required is bulky, and there is a good chance for dust contamination

29

of the fiber end surface. A better way to prepare fibers is through use of a fairly simple fiber breaking machine developed at Bell Laboratories (Ref 11). This machine uses a spring tensioner to hold the fiber in controlled tension over a slightly curved anvil. The fiber is then scored on the side opposite the anvil and automatically fractures with a clean, smooth surface. The machine's developers report that setup of the fiber for breaking is not critical, and the author of this paper believes the Bell Labs machine offers the most potential for simple fiber end preparation.

As important as fiber preparation is the alignment of the two fiber ends in the coupling and reflective losses at the interfaces. An inescapable loss in coupling is caused by Fresnel reflections. These occur at any interface between two materials of different indexes of refraction. The loss at each interface is described mathematically by (Ref 12:5-55)

$$\text{Fresnel Reflection Loss (dB)} = 10 \, \text{Log} \left[1 - \left(\frac{n' - n}{n' + n} \right)^2 \right] \quad (10)$$

where n = index of refraction of transmitting material

n' = index of refraction of receiving material.

Now, in a realizable coupler which does not involve fusing the fibers together, air will always be present at the fiber to fiber interface, and Eq (10) indicates that fairly significant losses result. For example, if fibers with center cores of n = 1.5 are used, the Fresnel loss at the splice is about 0.35 dB. However, if the air is displaced by an index matching fluid with an index of refraction near that of the core material, Eq (10) reveals Fresnel losses can be substantially

30

reduced. Suitable index matching "fluids" include a series of epoxy cements and glycerin. Couplers using these fluids may cause as little as 0.1 dB loss.

In addition to Fresnel losses, mechanical problems can also affect coupling losses. Bisbee has measured losses in fibers of 10.8 micron core diameters due to end separations and offsets (Ref 13). He found that losses increased by about 0.5 dB if the fibers in index matching fluids were separated by 10.8 microns, and that losses increased by about 3.3 dB for an axis offset of only 5.4 microns. Thus, accurate three-dimensional alignment is important if low losses are desired. One of the best answers to this problem seems to be a splicing technique developed by Miller (Ref 14). In Miller's system, shown in Fig. 8, the fiber ends are placed into a small tube with a square shaped cross-section.
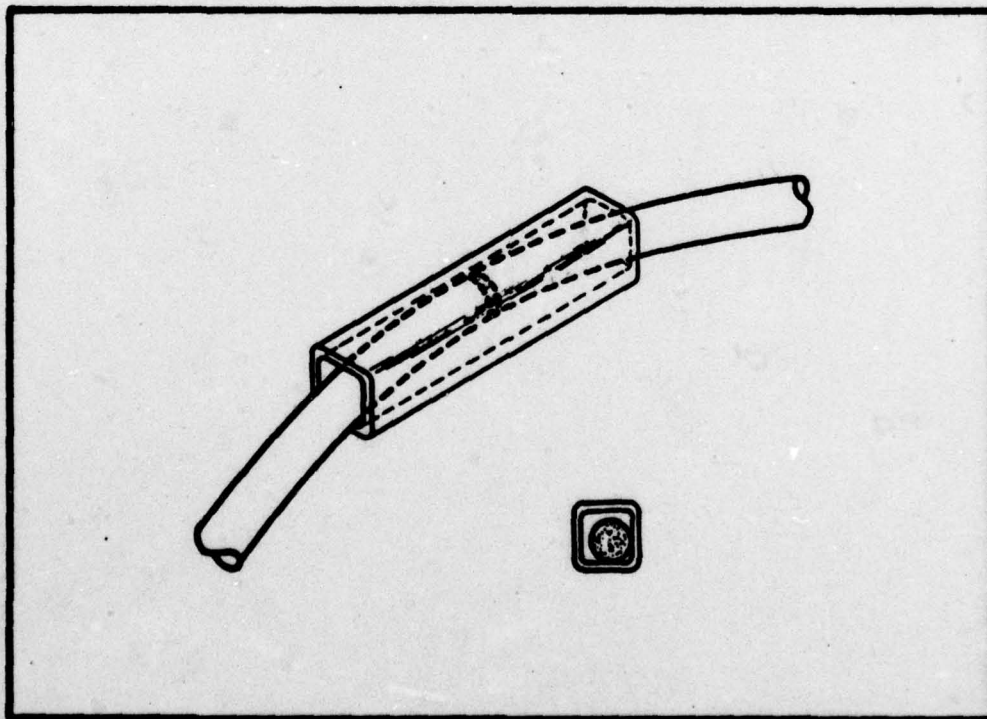
Fig. 8. Loose Tube Splice for Optical Fibers (Reprinted with permission from The Bell System Technical Journal, Copyright 1975) (Ref 14:1216)

The fibers are butted together and then flexed slightly so that the tube rotates until one of the diagonals of the square cross-section lies in the same plane as the flexing plane of the fibers. The resulting splice can be either held in a simple jig for temporary fittings or can be permanently glued with epoxy cement (which also serves index matching duties). Miller reports that splices made using the Bell fiber breaking tool and epoxy cementing have a mean loss of only 0.077 dB. Miller does point out that a series connection of 10 splices has a bit higher loss per splice rate, but even so the series connection's total loss was only 1.37 dB, on a mean loss of 0.137 dB per splice. So, the Bell Laboratories experiments indicate that simple field splicing is possible, and that the resulting losses can be quite small.

Losses in Coupling to and from Fibers. As previously mentioned, coupling a light emitter to a fiber can be difficult. A number of studies using both LED's and solid stage G_aA_s lasers have been conducted to determine the best coupling system such as butt joints or focusing lenses (Ref 12:5-34 to 5-53). Additionally, studies in the optimal physical construction of light emitters have been conducted to produce the best possible emission pattern for coupling to fibers. The indication of these studies is that the best driver efficiency is obtained when the light emitter is carefully matched to the fiber.

Fairly easy calculation of the power coupled into a fiber is possible using some results of an analysis by Marcuse (Ref 15). Fig. 9 shows the relationship between the normalized power coupled into a fiber from a LED and the relative sizes of the LED emitting surface and
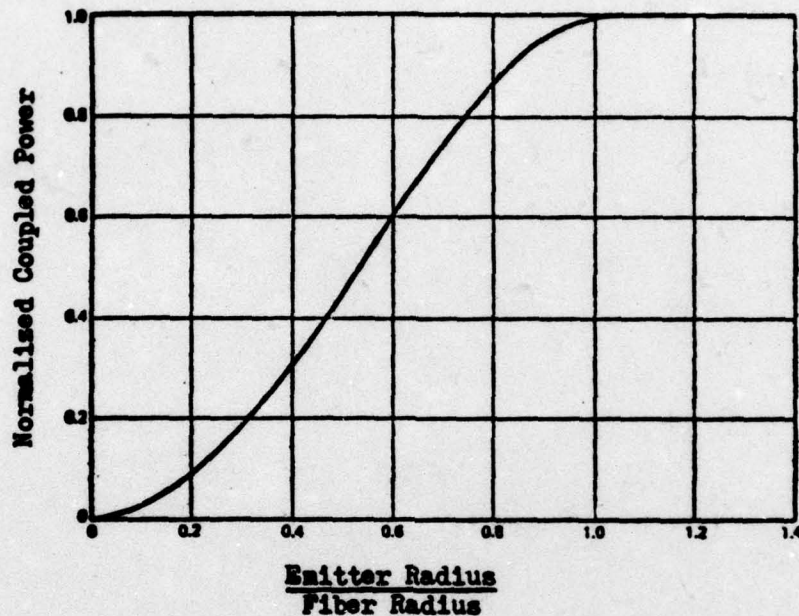
Fig. 9. Normalized Power Coupled Into a
Graded Index Fiber for Various Emitter-to-Fiber
Radius Ratios (Reprinted with permission from
The Bell System Technical Journal, Copyright
1975, AT & T) (Ref 15:1521)

the fiber's core size. In this figure, b is the radius of the LED sur-
face while a is the radius of the fiber core. The quantity plotted on
the vertical axis, P_n is the coupled power, P_f times a normalizing
constant. Fig. 9 assumes that the fiber is in direct contact with the
LED, but other data from Marcuse indicates that the fiber can be
separated from the LED by an amount equal to the radius of the fiber
with no change in results (Ref 15:1516).

Now, P_f is related to P_n by

$$P_f = P_n (\pi^2 B_a^2 \Delta) \tag{11}$$

where P_f = Power coupled into the fiber

P_n = Normalized power coupled into the fiber as given by Fig. 9

B = Brightness of the diode in watts/cm^2-steradian

a = Radius of the fiber core

Δ = Maximum refractive index difference in the fiber (See Ref 15:Eq 18).

All of the information needed to solve Eq (11) is available from manufacturers' specifications for LED's and fiber cables. An example of the use of the equation appears in Chapter IV.

Output coupling from the fiber to the detector diode is not an critical as input coupling. Provided that the diode's sensitive area is larger than the fiber's core, essentially all the light emitted from the fiber can be collected by the diode. Actually, commercially available detector diodes generally have active surfaces much larger than optical fibers cross-sections, and efficient output coupling may require expanding the output beam cross-section to match the detector's active area, as shown in Fig. 10. Here θ_{max} is the maximum angle of emission from the fiber. The literature indicates that the value of θ_{max} varies with a number of factors such as source wavelength, input coupling characteristics, and fiber length, and that an analytic expression for θ_{max} has not yet been developed (Ref 12:5-57). Therefore, an experimental placement of the detector from the fiber will have to be conducted when the link is put into operation. However, despite this
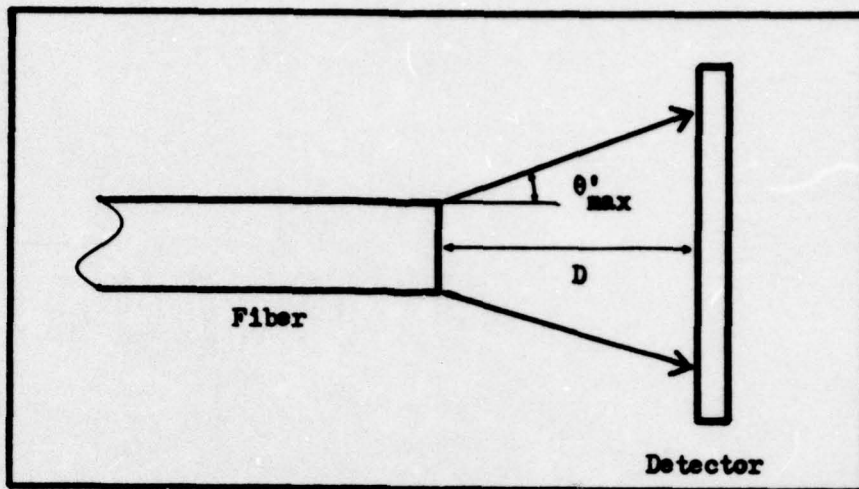
Fig. 10. Light Beam at Detector End of Fiber

problem, the major losses in output couplings should be due to Fresnel
reflections. Assuming that a fiber core of index of refraction 1.5 is
used, Eq (10) indicates the coupling loss from the fiber to the detector
diode is only about 0.17 dB.

III. Receiver Design

The primary functions of a data link receiver are recovering the
data signal and regenerating the signal timing. Although a number of
different methods for doing this job have been developed, an economical
optical channel can only use those techniques which are compatible with
mono-polar signals. This restriction played an important part in the
selection of the coding scheme for the system. Additional restrictions
involved the need for post-diode amplifiers which could efficiently
amplify very small signals and the need to keep the receiver's timing
circuits accurately synchronized to the transmitter. After considering
these constraints, the decision was made to use Manchester coding.
Manchester coding allows a timing reference to be transmitted continu-
ously, regardless of the data pattern. Further, this coding scheme
permits AC coupling of amplifiers in the receiver, simplifying design
of the amplifiers. Unfortunately, this coding scheme does require a
certain amount of complexity in the receiver, but the indications are
that the implementation of the receiver can still be accomplished at
reasonable cost.

Once the coding scheme was selected, a block diagram of the re-
ceiver was developed, as shown in Fig. 11. Tracing the signal through
the system, the first step in the process is the optics train. This
train couples the detector diode to the optical channel and also filters
out unwanted light. Next, the detector diode converts the optical
signals to electrical signals to be amplified in the post-diode ampli-
fier. The amplified signals are then routed to two different circuits.
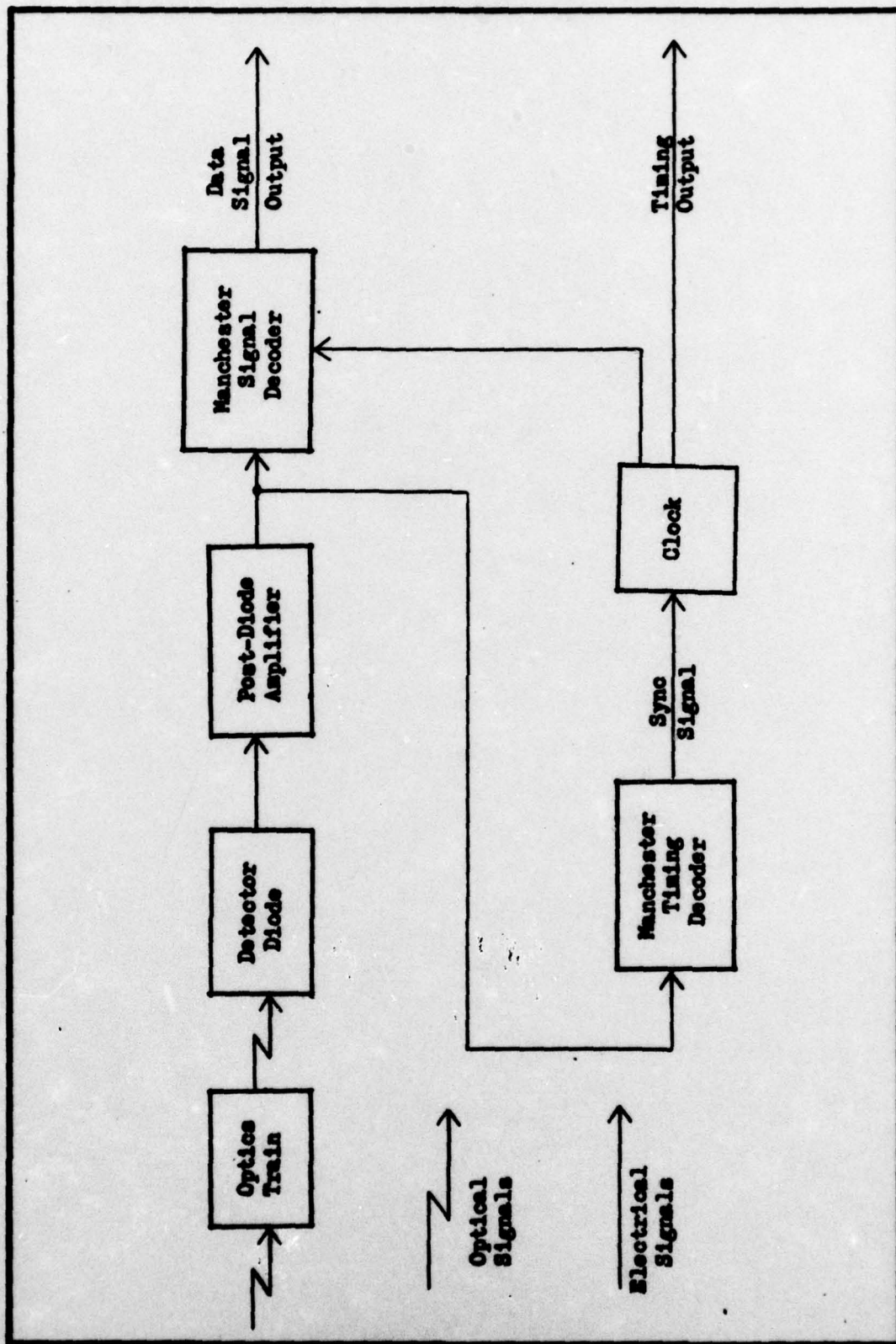
Fig. 11. Simplified Receiver Block Diagram

37

One circuit decodes the Manchester signals into simple NRZ (non-return to zero) signals. The other circuit uses the Manchester signal to synchronize the receiver's clock circuits to the signal so that an accurate clock waveform is available to operate the receiver circuits and to be passed on along with the decoded signal for further handling. The remaining part of this chapter will analyze the various blocks shown on this diagram.

The Optics Train

Fiber Link. The optics train design is determined by whether the receiver will work with a fiber or atmospheric link. For a fiber link, the optics train consists of nothing more than butting the fiber end against the detector, possibly with an index matching fluid. The unit is then surrounded by an opaque material so that ambient light cannot leak onto the detector diode surface. As mentioned in Chapter II, losses incurred with this approach are almost entirely due to Fresnel reflections. Now, losses from the reflection at the input surface of the diode are included in the manufacturers' data for the diode. So, assuming no index matching fluid, the fiber link's input loss is due to the one reflection at the fiber-air interface. For fibers with cores of $n = 1.5$, this loss is given by Eq (10) as 0.177 dB.

Atmospheric Link. Design of the optics train for an atmospheric link is considerably more complicated than for the fiber link. For high efficiency, it is desirable to have the input aperture of the receiver as large as economics permit (Ref 2:55). Additionally, the optics train must reduce the amplitude of stray light reaching the detector diode. This task is accomplished by using an optics design

38

which limits the maximum angle of off-axis illumination which can reach the detector diode, and by using an optical bandpass filter.

A sketch of the atmospheric receiver optics selected for the low cost link is shown in Fig. 12. This design was evolved around the 317.5 mm focal length Fresnel lens, the largest aperture lens available at reasonable cost. This lens is made of acrylic plastic, which has good transmission properties at near-infrared frequencies and permits low-cost manufacturing.

Originally, it was hoped that just the single Fresnel lens and optical filter would be sufficient for the optics train. Unfortunately, it was discovered that familiar dyed glass type optical filters could not provide the 10 nm wide passband needed to match the stability of a CW laser diode transmitter. As a result, the optical filter selected for the design was a multi-cavity optical interference filter. Since optical interference filters work as designed only with light incident at approximately normal angles, an extra lens was required to collimate the beam from the Fresnel lens (Ref 16:129-130). The exact spacing of the lenses was determined using matrix methods, although other methods would serve as well (Ref 17:84-94). The spacing shown produces a circular spot size on the detector diode of 1.274 nm radius, matching the diode's sensitive area. Light passing through the optical filter is in near perfect collimation, with the largest incident angle at the detector diode being less than 2.4°. At this small angle, the interference filter provides the desired bandpass, and essentially all the optical signal passes the interference filter without undergoing extra loss (Ref 16:130).

1.27mm

Detector Diode EG&G SHS-100

Optical Filter

Limiting Aperture Radius = 1.61 mm

37 mm

Lens 2 Focal Length = -5 mm

Lens 1 Focal Length = 317.5 mm, Aperture = 0.0506 m^2

313 mm

254 mm
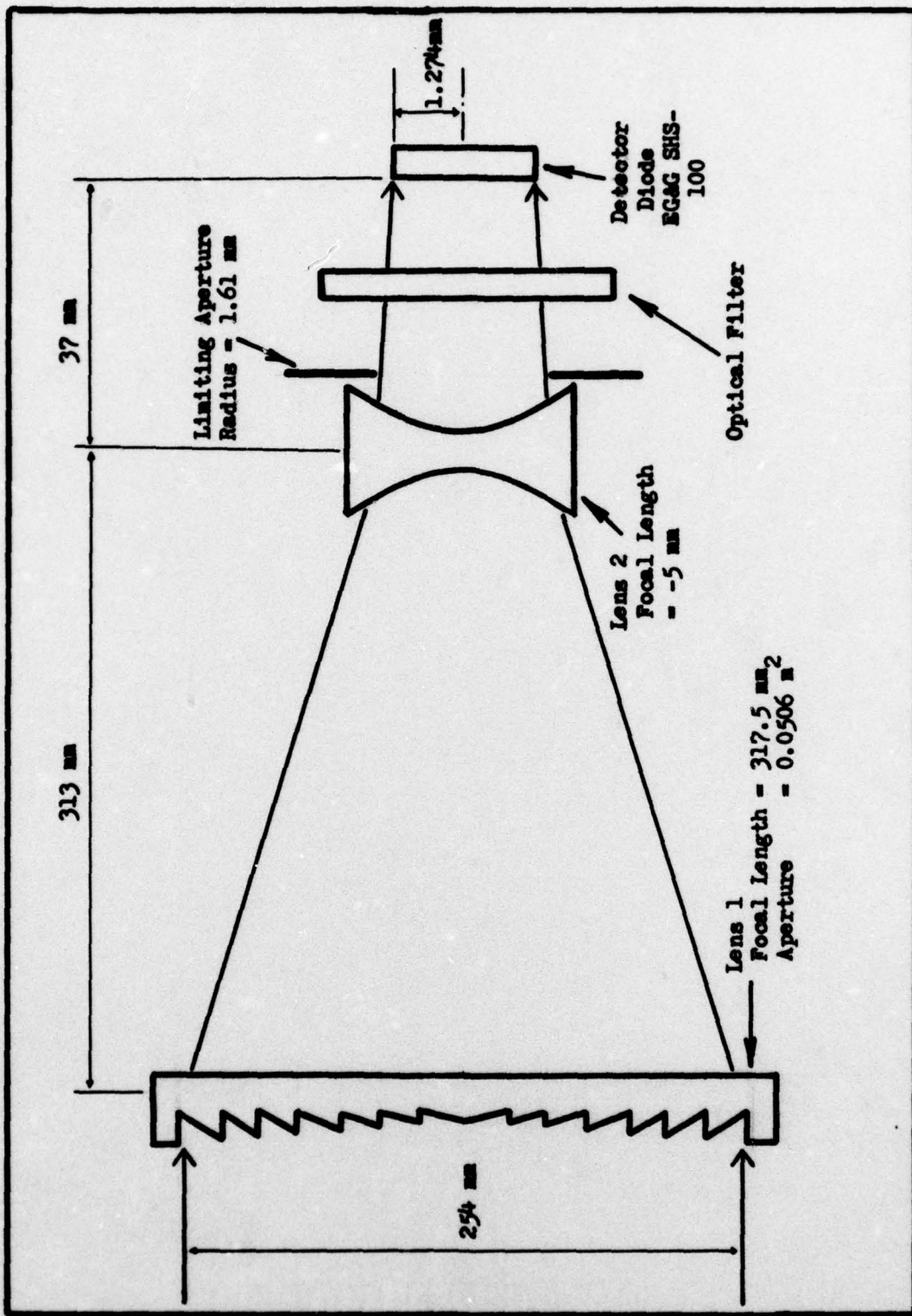
Fig. 12. Receiver Optics

Now, there are two crucial characteristics of the optics train which must be known in order to complete other design steps for the atmospheric receiver. These characteristics are the transmissivity of the optics train and the angular field of view of the optics system. Calculation of the transmissivity of the lens system is calculated from Eq (12):

$$\tau_{ro} = (\tau_{lens\ 1}) \cdot (\tau_{lens\ 2}) \cdot (\tau_{filter}) \tag{12}$$

where τ_{ro} = Total transmissivity of the receiver optics train

τ_{lens} = Transmissivity of the appropriate lens

τ_{filter} = Transmissivity of the selected optical filter in the passband.

An appropriate value of τ_{lens} for an acrylic plastic Fresnel lens used in collimation is about 0.83 (Ref 16:50). Likewise, an appropriate value for a crown glass lens suitable for use as lens two is $\tau_{lens\ 2}$ = 0.91 (Ref 16:23). Optical filters which are available at low cost for wavelengths near 860 nm are quite a bit less efficient, however, and $\tau_{filter} \approx 0.50$ (Ref 16:154). As a result, Eq (12) yields a value for the proposed optics system of

$$\tau_{ro} = 0.378 \approx 4.2\ dB\ loss \tag{13}$$

The angular field of view of the lens concerns the maximum angle of off axis rays that will cause significant illumination of the detector diode surface as was discussed in Chapter II. For the detector diode and diode to lens two spacing in the selected optics design, the value of θ_R' in Fig. 6 becomes $2.49°$. Therefore,

$$\theta_R = 0.039° = 0.68\ mrad \tag{14}$$

41

The Signal Processing Train

The signal processing train must decode the noise-corrupted
Manchester data in a manner which ensures the maximum probability that
the receiver's output signal is the same as the transmitted signal. The
error rate (the number of errors made per bits transmitted) of the re-
ceiver is determined by the receiver configuration selected for the
decoder, the received optical power level, and the level of noise
present in the optical signal and the receiver systems. In this section,
the receiver's signal processing train is described and analyzed in de-
tail. Also presented is a determination of the required optical power
to yield a BER (bit error rate) of one error in 10^5 bits.

Signal Processing Train Circuit. Samples of the Manchester coding
of a binary "1" and "0" are shown in Fig. 13. The change in signal at
the mid-period point is essential to the timing recovery scheme (to be
described later) but complicates signal recovery. Now, an important
point to note about the code is that despite the mid-period change, the
value of the signal in each half of the bit period is uniquely determined
by the transmitted data bit. As a result, decoding the signal can be
made more efficient if the received signal is processed for the entire
bit period T rather than for only the first half of the period.

In addition to problems posed by the nature of Manchester signals
decoding of the signal may be complicated by the presence of noise. As
a result, use of a signal processor which provides the lowest possible
error rate is required. Assuming, as is usual, that the noise in the
system is white and Gaussian, and also assuming perfect square wave
signals, then one form of optimum detection is the integrate and dump

42

Data Bit   **Manchester Coded Signal**

1

0

One Bit Period T
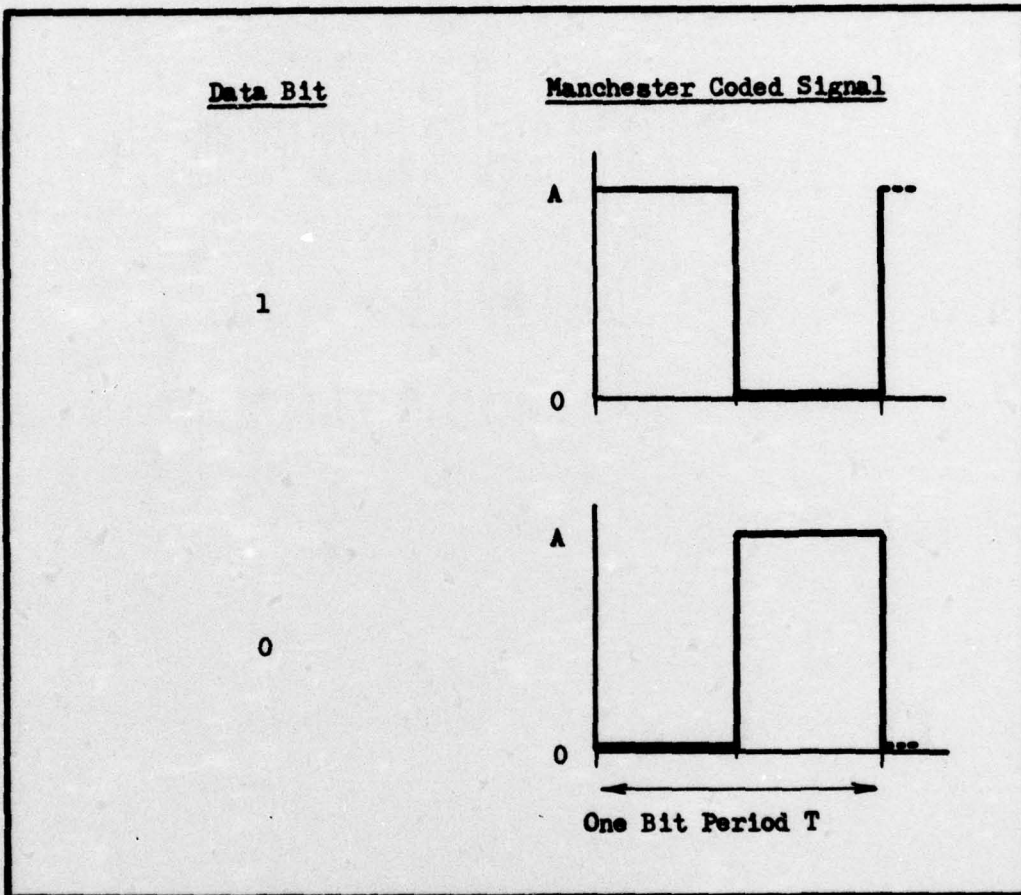
Fig. 13. Manchester Code Waveforms

detector scheme (Ref 18:378). Because of the discontinuity in the
Manchester data, two separate integrators are required to make full use
of all the information coded in the Manchester signal. The resulting
configuration of the data signal processing train is shown in Fig. 14.

The operation of the circuit in Fig. 14 may not be immediately
apparent, so a brief description is presented. To begin, each IHD
(Integrate-Hold-Dump) circuit is served by two independent control lines,
an integrate control line and a dump line. While an IHD integrate con-
trol line is high, the circuit continuously integrates the input signal.
While the integrate control line is low, the IHD initially stores the
value of the integrated signal. Then, the IHD circuit is reset by the
dump line at some time prior to beginning a new integration.

Derivation of the Probability of Error. As shown in Fig. 14, each
IHD integrates over different halves of the bit period. As a result,
in a noiseless case, one IHD output will be high and the other will be
low when the end of the bit period is reached. Thus, at the end of each
bit period, the output of the comparitor will be high if a "1" was sent
and low when a "0" was sent. This result is then gated into a storage
register and the two IHD circuits are reset by the dump line so the
next bit can be processed.

Now, when noise is added to the signal, the output of the comparitor
will still tend to select the proper output due to the noise filtering
action of the IHD circuit. However, there is a possibility that noise
can corrupt the input signal strongly enough to cause the outputs of the
IHD circuits to have incorrect relative magnitudes. When this happens,
the comparitor output becomes incorrect, and an incorrect data output
occurs.
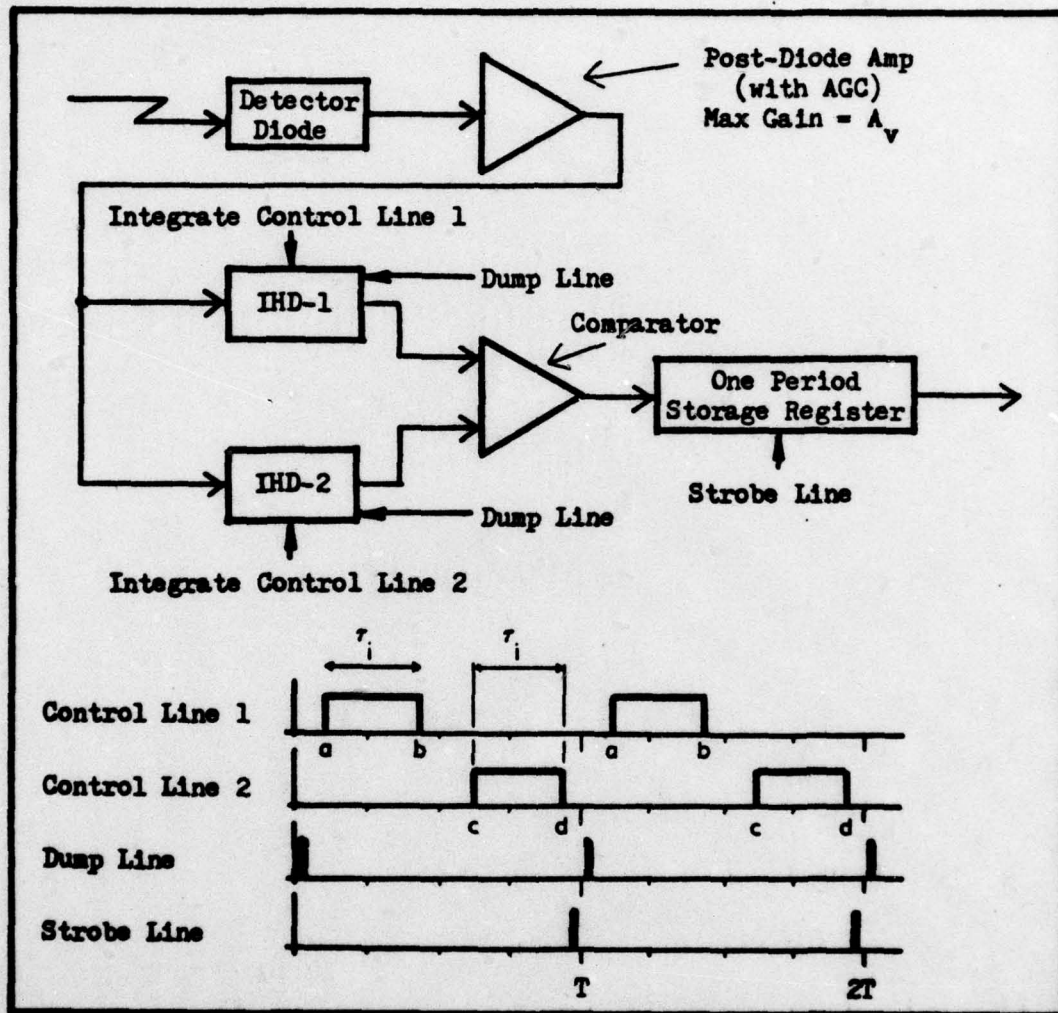
Fig. 14. Data Signal Processing Circuit and Control Timing

To treat this more rigorously, consider that the input to each integrator is composed of the signal $s(t)$ plus additive noise. Further, assume that the noise is zero mean, stationary and white with a two-sided power spectral density G_s' watts/Hz. As a result the autocorrelation function of the noise is:

$$E\left[n(t)\, n(t + \tau)\right] = G_{sv}' \,\delta(\tau) \tag{15}$$

where $\delta(\ )$ = Dirac delta operator.

Now, if we assume that a Manchester 1 is being decoded, the output of IHD 1 at the end of the integrating period is given by:

$$I_{1/1} = \int_a^b \left[s_1(t) + n(t)\right] dt$$

$$= \int_a^b s_1(t)\, dt + \int_a^b n(t)\, dt \tag{16}$$

where $I_{1/1}$ = output of IHD 1 after the integration period, given that a 1 was sent

$s_1(t)$ = Manchester signal for a "1" data bit (see Fig. 13)

$n(t)$ = Noise signal

a = time at start of the IHD sampling period (Fig. 14)

b = time at the completion of IHD sampling period (Fig. 14)

In a similar way, the output of IHD 2 can be described as:

$$I_{2/1} = \int_c^d s_1(t)\, dt + \int_c^d n(t)\, dt \tag{17}$$

where the time interval c to d corresponds to the sampling time for IHD 2 (see Fig. 14).

Now, it is assumed throughout this paper that the signal input to the integrators has a constant amplitude in each half of the bit period. From Fig. 14, it is apparent that if the input signal has constant magnitude A during the first half of the bit period, then the integral of the signal over time interval a to b is equal to $\tau_1 A$, where $\tau_1 = b - a$. Similarly, the integral of the signal over time period c to d is zero since the signal is zero in this time interval. As a result Eqs (16) and (17) become

$$I_{1/1} = \tau_1 A + \int_a^b n(t) \, dt = \tau_1 A + N_1 \tag{18}$$

$$I_{2/1} = 0 + \int_a^b n(t) \, dt = N_2 \tag{19}$$

Next, the probability that the comparitor output will be incorrect, given that a 1 is sent, is given by the probability that $I_{1/1}$ is less than $I_{2/1}$. Symbolically,

$$P_{e/1} = P\left[I_{1/1} < I_{2/1}\right] = P\left[\tau_1 A + N_1 < N_2\right]$$

$$= P\left[N_1 - N_2 < \tau_1 A\right] \tag{20}$$

where substitution of Eqs (18) and (19) along with some rearrangement has been accomplished.

If the assumption is made that n(t) is a Gaussian random process, then N_1 and N_2 are Gaussian random variables. Since n(t) has been assumed to have zero mean, N_1 and N_2 also have zero mean. Further, if we define a new random variable N' equal to $(N_1 - N_2)$, then N' is also

47

a zero mean Gaussian random variable, with variance

$$VAR(N') = E\left[(N' - 0)^2\right] = E\left[(N_1 - N_2)^2\right]$$

$$= E\left[N_1^2\right] + E\left[N_2^2\right] - 2E\left[N_1 N_2\right] \qquad (21)$$

Since N_1 and N_2 are zero mean, this further reduces to

$$VAR(N') = VAR(N_1) + VAR(N_2) - 2E\left[N_1 N_2\right] \qquad (22)$$

Next, recalling the comments about the correlation function of noise samples as shown in Eq (15), $E\left[N_1 N_2\right]$ is zero and Eq (22) reduces further to

$$VAR(N') = VAR(N_1) + VAR(N_2) \qquad (23)$$

Recall that time intervals a - b and c - d are both equal to length τ_1. Since the noise process is assumed wide sense stationary, the variance of N_1 is equal to the variance of N_2 and Eq (23) becomes

$$VAR(N') = 2 \, VAR(N_1) \qquad (24)$$

For an integrator with white Gaussian noise plus signal at the input, Taub and Schilling show that the variance of the output signal is (Ref 18:368)

$$VAR(N_1) = G'_{S_V} \tau_1 \qquad (25)$$

where G'_{S_V} = the two sided normalized power spectral density of the noise in (volts)^2 (Note that Taub and Schilling's integration constant is assumed 1 in Eq (25) as was done for Eq (18)). So, the variance

48

of N' becomes

$$VAR(N') = 2G'_{s_v} T_1 = \sigma^2 \qquad (26)$$

With Eq (26) and Eq (20), it is now possible to write

$$P_{e/1} = \int_{-\infty}^{-AT_1} f_{N'} (N') \, dN' \qquad (27)$$

where $f_{N'} (N')$ is the Gaussian probability density function of the random variable N'. Using the symmetry property of the Gaussian probability density function, Eq (27) becomes

$$P_{e/1} = \int_{AT_1}^{\infty} f_{N'} (N') \, dN' = \int_{N'=AT_1}^{\infty} \frac{1}{\sqrt{2\pi\sigma^2}} e^{-\frac{(N')^2}{2\sigma^2}} \, dN' \qquad (28)$$

This can be transformed into a standard form of the complementary error function by using a change of variable with $x = N'/\sigma$. The result is (Ref 12:A-1)

$$P_{e/1} = \frac{1}{\sqrt{2\pi}} \int_{x=\sqrt{\frac{A^2 T_1}{2G_{s_v}'}}}^{\infty} e^{-\frac{x^2}{2}} \, dx = Erfc\left(\sqrt{\frac{A^2 T_1}{2G'_{s_v}}}\right) \qquad (29)$$

Now Eq (29) relates the conditional error probability in terms of signal level and noise power spectral density at the input to the IHD circuits. In general, the controlling signal to noise ratio for receivers with low noise amplifiers is usually determined at the output of the signal detector. As a result, it is worthwhile to be able to relate Eq (29) back to the signal levels present at the detector diode output.

49

To begin, assume the post-diode amplifier's voltage gain is A_v (see Fig. 14). Then, if V_d is the output voltage of the detector diode, $A = V_d A_v$. Next, consider the output noise power spectral density of a perfect amplifier. The amplifier then has a transfer function of A_v. If the input power spectral density of the amplifier is G_{s_v}, then (Ref 18:250)

$$G'_{s_v} = \left| A_v \right|^2 G_{s_v} \tag{30}$$

Placing the equivalent relations for A and G'_{s_v} into Eq (29) yields

$$P_{e/1} = \text{Erfc} \sqrt{\frac{V_d^2 A_v^2 \tau_1}{2 \left| A_v \right|^2 G_{s_v}}} = \text{Erfc} \sqrt{\frac{V_d^2 \tau_1}{2 G_{s_v}}}$$

$$= \text{Erfc} \left(\sqrt{\frac{E_{b_v}}{2 G_{s_v}}} \right) \tag{31}$$

where E_{b_v} = input energy of that portion of the signal processed by IHD 1 in volts^2 units. From Eq (31), it can be seen that the probability of error is set by the ratio of signal power to noise power spectral density at the detector diode's output, and that the amplifier has no effect.

While Eq (31) has been derived for the case of a 1 being transmitted, the symmetry of the Manchester code and the detector circuit result in $P_{e/0}$ being equal to $P_{e/1}$. The derivation is not shown since it is similar to the one given for $P_{e/1}$. Now, the total probability of the detector making an error is given by

$$P_e = P_{e/1} \left[P(1) \right] + P_{e/0} \left[P(0) \right] \tag{32}$$

where P(1) = Probability of a one occurring in the data stream

P(o) = Probability of a zero occurring in the data stream.

If the assumption is made that one and zero data bits are equally likely, then $P(1) = P(0) = 1/2$. Next, recalling that $P_{e/1} = P_{e/0}$, Eq (32) becomes

$$P_e = P_{e/1} \tag{33}$$

Finally, recall that the desired error rate for the system is 10^{-5}. This is equal to the desired probability of error. Thus, from Eqs (31) and (33)

$$10^{-5} = \text{Erfc} \left(\sqrt{\frac{E_{b_v}}{2G_{s_v}}} \right) \tag{34}$$

Using tabulated values of the complementary error function, this becomes

$$\sqrt{\frac{E_b}{2G_s}} = 4.25 \tag{35}$$

where E_{b_v} and G_{s_v} in Eq (31) have both been divided by the load resistance of the detector diode so that E_b and G_s are expressed in joules and watts per Hertz respectively.

Eq (35) is very important because it determines the minimum ratio of signal energy to noise power spectral density that the receiver needs to provide the desired error rate. Once a value for G_s can be determined for a given detector circuit, Eq (35) can then be used to determine the required input signal to provide at least a 10^{-5} BER. The determination of G_s follows in the next section.

The Diode Noise Model. As mentioned in the previous section, a noise model for the diode detector must be developed before the required signal power can be determined. This section develops that model.

To begin, the various sources of detector noise should be identi-fied. For a PIN photodiode, Pratt indicates that two important noise sources are thermal noise and shot noise. Shot noise is caused in part by the leakage current, called dark current, present in the diode when no optical signals are present (Ref 2:145-150). Pratt also indicates that due to the random generation of hole-electron pairs in a solid-state detector, both the optical signal and the background light (in atmospheric systems) also will cause shot noise (Ref 2:151). Finally, due to the very low level signals involved, input noise to the post-diode amplifier must also be included. Pratt indicates that a noise model of the diode and its various noise generators can be represented by a circuit similar to the one shown in Fig. 15 (Ref 2:157). Here current sources are used because the PIN diode acts like a current source.

Now, it is necessary to present the two-sided power spectral den-sity relations for each of the noise terms. To begin, Pratt shows that the signal noise due to I_{sn} (also called signal shot noise) and the noise due to background radiation have very similar power spectral densities. This is evident from the relations for their power spectral densities (Ref 2:151).

$$G_{sn} = qI_sR_L \text{ watts/Hz} \tag{36}$$

$$G_B = qI_BR_L \text{ watts/Hz} \tag{37}$$

52

I_s — Signal Current Due to Optical Signal

I_d — Average Dark Current Noise Source

I_b — Average Noise Current Due to Background
      Light(Atmospheric Link Only)

I_t — Average Thermal Noise Current

I_{sn} — Average Noise Current Due to Signal
      Detection Noise

I_A — Average Noise Current Contributed by
      the Post-Diode Amplifier

C_{D+A} — Combined Capacitance of the Diode and
      Input to the Post-Diode Amplifier

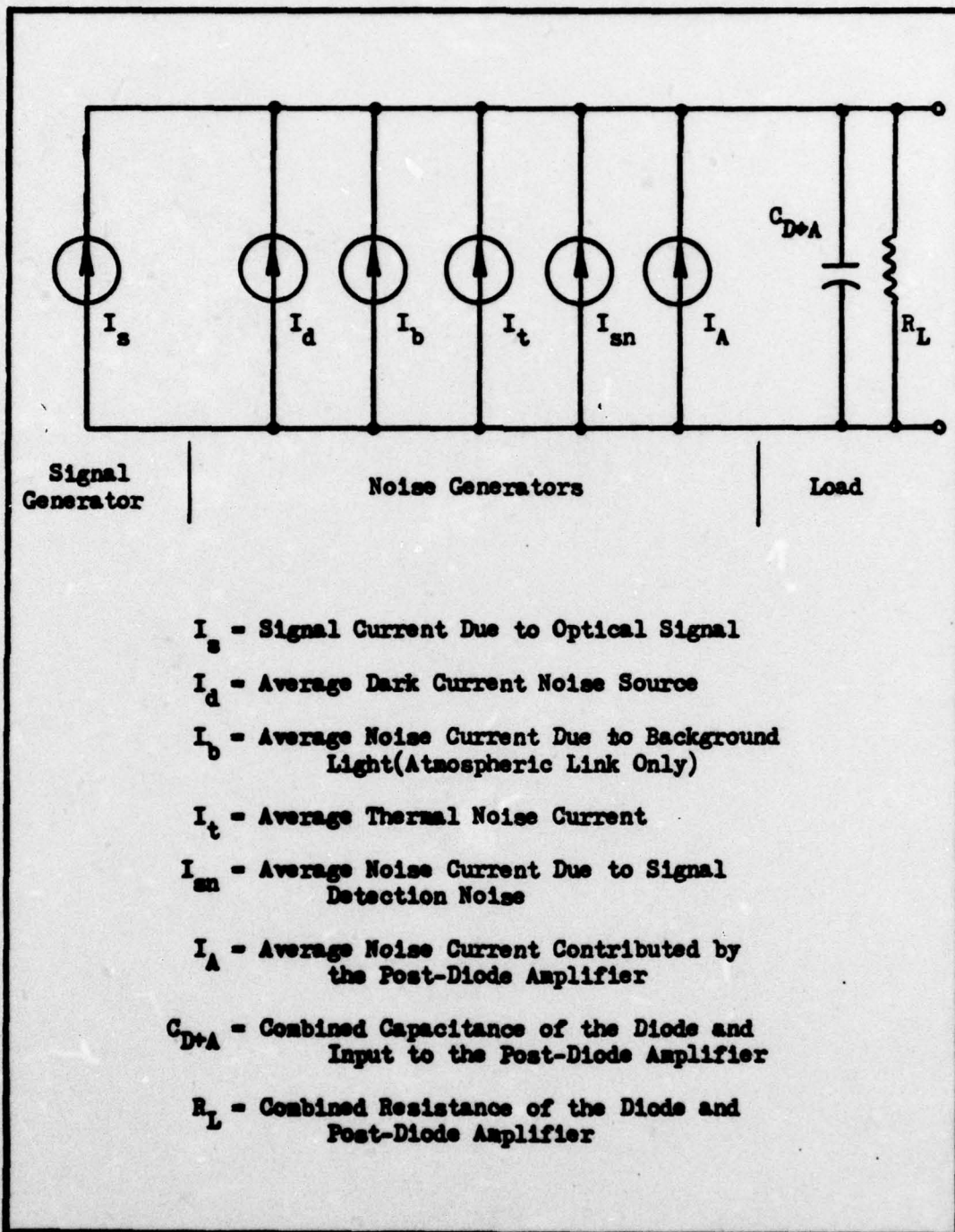R_L — Combined Resistance of the Diode and
      Post-Diode Amplifier

Fig. 15. PIN Photodiode Equivalent Circuit

53

where q = charge of an electron in Coulombs

I_s = average current due to on portions of the signal

I_B = average current due to background illumination

R_L = combined diode-amplifier net load resistance.

Notice here that Pratt's power spectral densities in current squared
units have been converted to watts units by multiplying by R_L. Pratt's
equations are also adjusted to agree with accepted PIN diode shot noise
relationships as presented by Riess and others (Ref 19:995). These
conversion conventions are followed in the rest of the relations as
well. Also, an AC-coupled circuit is assumed, so a DC term normally
present in Eqs (36) and (37) is deleted. Recall Eq (37) only applies
to atmospheric links.

The power spectral density of the thermal noise (in amps^2 units)
generated in the diode is given by $G_{TI} = 2KT/R_d$ where R_d is the channel
resistance of the diode, T is the temperature in degrees Kelvin, and
K is Boltzman's constant (Ref 2:156). Converting this to a power
spectral density in watts units yields

$$G_T = \frac{2KT}{R_d} R_L \tag{38}$$

Eq (38) takes advantage of the fact that $R_L \approx$ input impedance of the
post-diode amplifier for practical high-speed circuits. For purposes
of this calculation, it will be assumed that the diode and the post-
detector amplifier are both at room temperature, 300°K. Finally, the
noise due to the average dark current I_d has a power spectral density
of

$$G_D = q I_d R_L \text{ watts/Hz} \tag{39}$$

Again, a DC term is not shown.

If the assumption is made that all of the noise generating processes described above are pairwise uncorrelated with one another, then the power spectral density of the total noise process is given by

$$G_s = G_D + G_T + G_B + G_A + G_{sn} \tag{40}$$

where $G_B = 0$ for fiber links.

<u>Required Input Power with Perfect Timing</u>. Now that G_s has been related to quantities available in manufacturing specifications, it is possible to solve Eq (35) for the required electrical signal power out of the diode to get a 10^{-5} BER. First, squaring Eq (35) and substituting for G_s yields

$$E_b = 36.13 \, (G_D + G_T + G_B + G_{sn} + G_A) \tag{41}$$

Recalling that E_b is the integrated energy of the high portion of the Manchester bit, E_b is equal to τ_1 times the load resistor R_L and the square of the signal current GI_s. Thus, substituting for E_b and the various power spectral densities yields

$$\tau_1 R_L I_s^2 = 36.13 \, \left[G_D + G_T + G_B + q \, R_L I_s + G_A \right] \tag{42}$$

This is then solved for I_s, resulting in the relation

$$I_s = \frac{36.13 \, q + \sqrt{1.305 \times 10^3 \, q^2 + 1.45 \times 10^2 \, \frac{\tau_1}{R_L} \, (G_D + G_T + G_B + G_A)}}{2\tau_1} \tag{43}$$

The reader will gain a better appreciation for some of the work to follow if a numerical value of I_s is determined. For this design

study, an EG and G SHS-100 PIN diode has been selected for the detector. Some of this diode's characteristics are tabulated in Table IV. Also, the post-diode amplifier selected is the Texas Instruments TIXL 152 integrated circuit, whose characteristics and equivalent circuit are shown in Table V and Fig. 16 respectively.

Table IV
Characteristics of the EG&G SHS-100 PIN Photo Diode

Spectral Responsivity, R_λ at $\lambda = 860$ nm	0.62 A/W
Rise time (10-90%)	4×10^{-9} Sec
Dark current at 125 volt Bias	10^{-8} A
Capacitance	4 pf
Area of active surface	5.1 mm^2
Minimum channel resistance	1×10^6 ohms

Table V
Characteristics of the T.I. TIXL 152 Amplifier

Input Noise "Current", i_n	3 PA/$\sqrt{Hz}$
Forward Transfer Impedance, R_f	12×10^3 volts/amp
Input Impedance, z_i	300 ohms
Bandwidth	20 MHz

For the diode and amplifier, the load resistance is almost totally determined by the low input impedance of the amplifier. As a result, $R_L = 300$ ohms. Using this with the diode dark current of 10^{-8} amperes

36
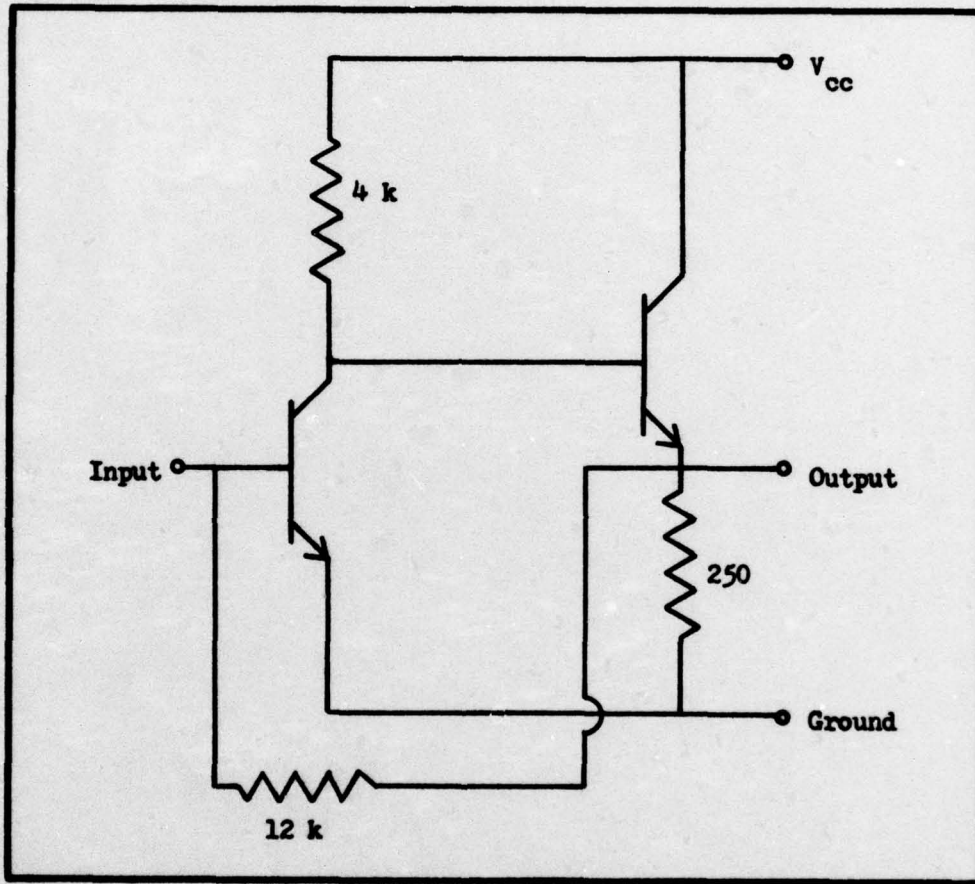
Fig. 16. TIXL-152 Equivalent Circuit (Reproduced with permission, Copyright 1976) (Ref 20:330)

provides a value G_D of

$$G_D = 2q \; I_d R_L = (1.6 \times 10^{-19})(10^{-8})(300) = 4.8 \times 10^{-25} \; \text{W/Hz}$$

(44)

Next, assuming a room temperature of 300°K

$$G_T = 2KT = \frac{2(1.38 \times 10^{-23})(300)}{1 \times 10^6} = 8.28 \times 10^{-27} \; \text{W/Hz} \qquad (45)$$

Finding a value for G_B is not quite so easy. First, the optical power falling on the detector diode must be found. This is given by Eq (6). The result using values for the optics system given in Eqs (13) and (14) is

$$P_B = \frac{\pi(\tau_{ro}) \; \lambda_B \theta_R^{\;2} d_R^{\;2}}{4} \; W(\lambda)$$

$$= \frac{\pi(0.378)(0.01)(6.8 \times 10^{-4})^2 (25.4)^2}{4} \; (8 \times 10^{-3})$$

$$= 7.09 \times 10^{-9} \; \text{W} \qquad\qquad (46)$$

The responsivity of a photodiode relates the average diode output current to the amount of incident optical power. Since the diode selected has a responsivity of 0.62 amp/watt, the resulting value of I_B is

$$I_B = (0.62)(7.09 \times 10^{-9}) = 4.4 \times 10^{-9} \; \text{amp} \qquad (47)$$

So

$$G_B = (1.6 \times 10^{-19})(4.4 \times 10^{-9})(300) = 2.1 \times 10^{-25} \; \text{W/Hz} \qquad (48)$$

58

Next, the noise current of the TIXL 152 must be converted to a power spectral density. First, the noise current i_n listed is a single-sided term. So

$$G_A = \frac{(i_n^2 R_L)}{2} = \frac{(3 \times 10^{-2})^2 \, 300}{2} = 1.35 \times 10^{-21} \text{ W/Hz} \qquad (49)$$

Finally, limitations posed by the timing performance of realizable circuits mean that the integration period must be slightly shorter than one-half a bit period (this will be further discussed in the section on timing recovery). Therefore, a reasonable value for τ_1 is 2.8×10^{-7} sec. Using this and the values in Eqs (44), (45), (48), and (49), Eq (43) yields a value for I_s of

$$I_s = 2.42 \times 10^{-8} \text{ amp} \qquad (50)$$

Note that this value is for the atmospheric link because G_B was added to the value for G_s. However, since G_B is small compared with the sum of the other noise terms, Eq (50) is valid for either link for the number of significant digits shown.

Next, recalling that the PIN diode's responsivity is 0.62 amp/W, the required signal optical power P_0 at the photodiode is 3.9×10^{-8} W.

Now, it is necessary to show that the value for I_s in Eq (50) does not require alteration when the performance of the timing recovery circuit is considered. This analysis follows in the next section.

The Timing Recovery Circuit

The timing recovery circuit is required to synchronize operation of the IHD circuits in the signal processing chain with the incoming

signal. Additionally, the timing recovery circuit provides an output clock which is necessary for simple computer interfacing.

Accurate operation of the timing recovery circuit is essential if the error calculations for the signal processing train are to be valid. Referring to Fig. 14, it is evident that if the time periods a-b and c-d are displaced sufficiently with respect to the signal's timing, then the IHD circuits will integrate an incorrect sample of the received signal. The timing circuit can shift its timing interval with respect to the input signals in two ways. First, the timing circuit may be nominally locked to the transmitted signal but may drift, or jitter, back and forth around the proper synchronization point. Second, the timing recovery circuit can become totally unsynchronized. In either case, if timing intervals a-b and c-d are displaced excessively from the desired position, the output of the signal processing section will become totally invalid. Therefore, design of the timing recovery circuit must insure that total loss of lock is extremely unlikely and that the amount of the jitter present in a nominally locked timing circuit is low enough so that very few errors result.

Circuit Configuration. The timing recovery circuit selected for this receiver employs a phase-locked-loop detector with an integrating phase comparator. This circuit is capable of decoding the timing information in Manchester signals and takes advantage of the superior noise performance of integrating detection schemes. In addition to the phase-locked-loop circuit, the timing recovery section of the receiver also includes necessary control circuits to drive the signal processing train. A block diagram of the circuit appears in Fig. 17 and a description of the components shown in Fig. 17 follows.
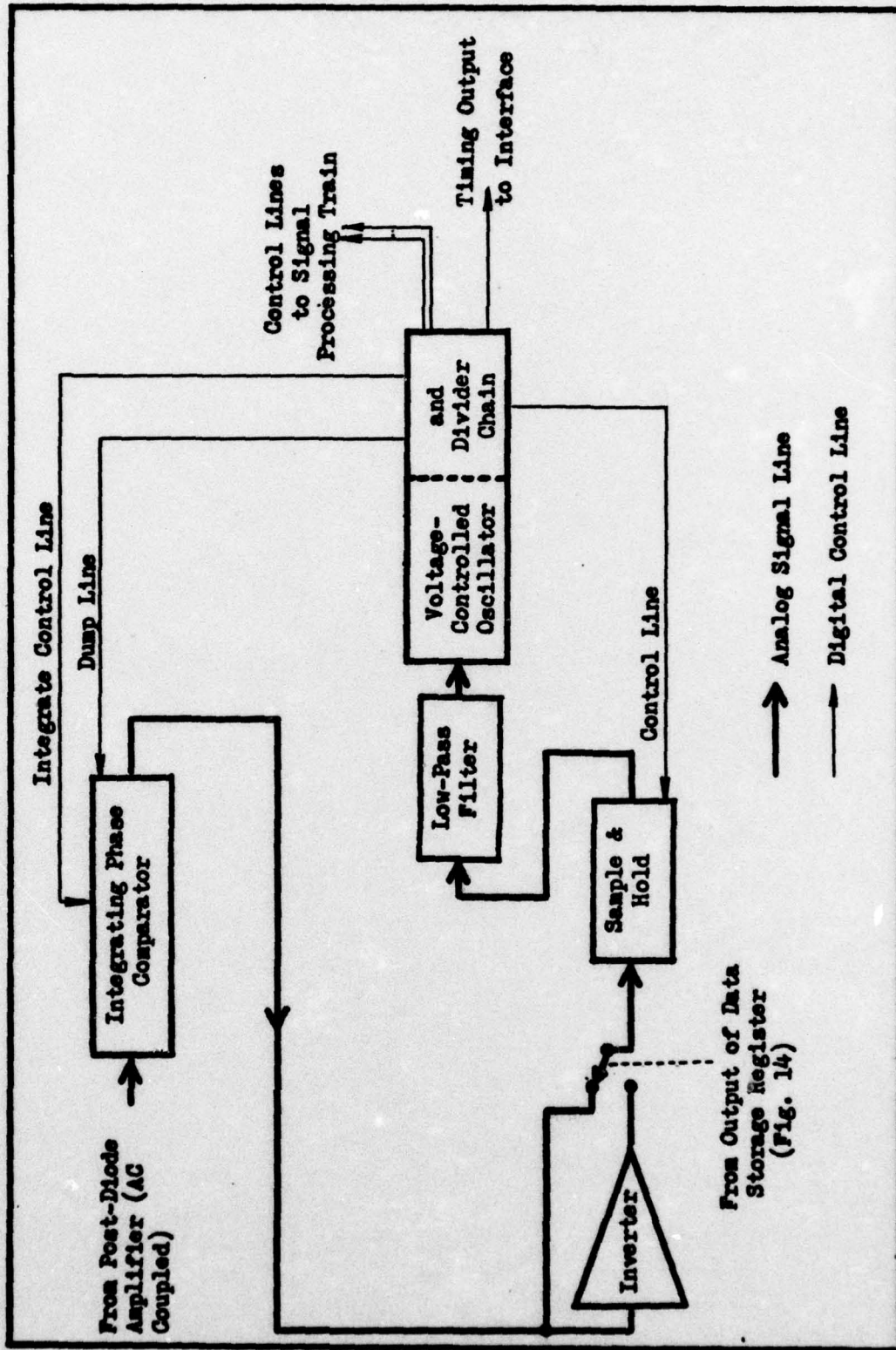
60

Fig. 17. Timing Recovery Section Block Diagram

61

The integrating phase comparator circuit for the phase-locked-loop is composed of another IHD circuit, identical in construction to the ones already described for the signal processing train. However, both the control and dump lines for this phase comparator are independent of other lines in the receiver.

The output of the phase comparator passes through a polarity selection circuit composed of an inverter and selector switch. The selector's operation is controlled by the output signal from the signal processing train. This decision-directed feedback circuit is required because the polarity of the error signal from integrating phase detector changes with the type of data bit transmitted as well as with the direction of drift in timing error. The exact operation of the polarity selector will be detailed later.

Following the polarity selector is a sample-and-hold circuit. It stores error information calculated in the previous bit interval while the error information in the current bit interval is being processed by the phase detector and polarity selector.

The output of the sample-and-hold circuit is filtered prior to reaching the control input to the VCO (voltage-controlled oscillator). The low-pass filter has a relatively low cutoff frequency, so the control voltage to the VCO varies slowly in time compared to the change in the values from the sample-and-hold circuit.

The VCO actually operates at some integer multiple frequency of 1.5 MHz. The output of the VCO is passed through a divider chain so that the eventual output is 1.5 MHz. In addition, a series of precisely timed pulses are generated by the divider chain during each timing

interval to control time-critical events such as the integration periods of the three IHD circuits.

The feedback loop for the phase-locked-loop is closed by using timing signals derived from the VCO to control the integration period of the integrating phase comparator. As timing changes occur, the timing of the integration period changes with respect to the midpoint of the Manchester signal, resulting in the error signals needed to change the VCO frequency to resynchronize the receiver. As will be shown, the closed-loop response of the phase-locked-loop can provide excellent stability and accuracy for the system.

Timing Circuit Operation. Basically, the circuit outlined in Fig. 17 is a form of digital phase-locked-loop. Additionally, the phase comparator circuit used has a sawtooth shaped phase error versus output signal curve. The operation of this general class of loops has been described by several authors, including Byrne (Ref 21). As a result, only special characteristics of this particular circuit will be covered. In the description to follow, the reader may find it helpful to refer to the signal timing diagrams in Fig. 18. It should be noted that Fig. 18 assumes perfect timing between the input signal and the VCO. Also, even when a loss of synchronization does occur, all signals, except for the input signal, retain the same relative time relationships with one another.

To begin the description of the circuit's operation, assume that a string of Manchester coded ones is being received and that the VCO is synchronized. Due to AC coupling in the post diode amplifier and the symmetry of a Manchester coded signal, the output of the integrating
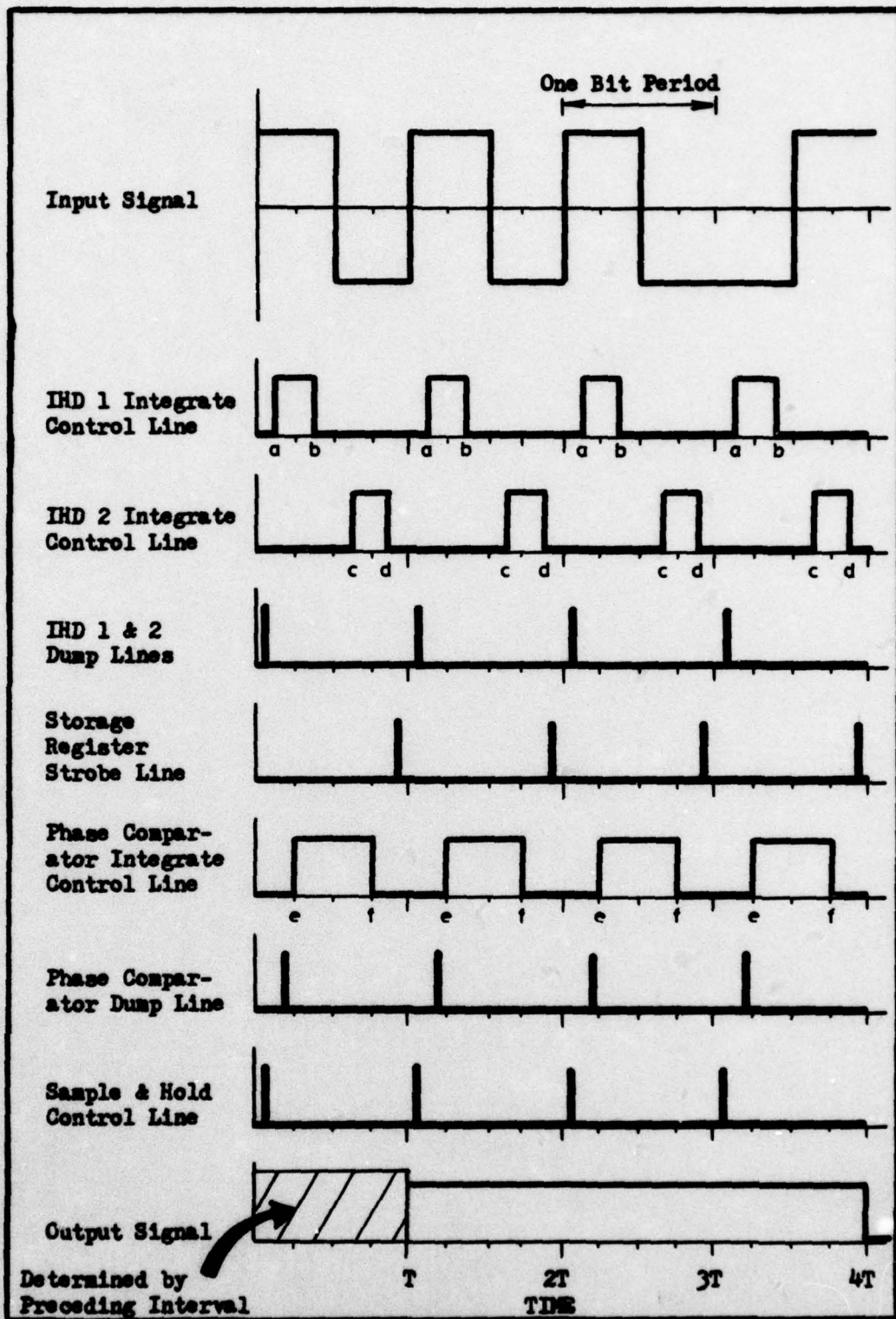
63

Fig. 18. Timing Relations of the Receiver Signals

64

phase detector is zero because the detector integrates symmetrically around the point where the polarity change occurs. This means that the output of the polarity selector and sample-and-hold circuits are also zero (in the absence of noise). Assuming perfect synchronization has existed for some time, the low-pass filter output has been at zero. The new output of the sample-and-hold circuit causes no change in the low-pass filter output, and the VCO frequency stays constant.

Next, assume that a drift in synchronization occurs, perhaps due to noise. Now, the integration period is not symmetrical around the mid-point of the transmitted signal. As a result, the phase comparator's output varies from zero with a magnitude related to the amount of drift. This error signal is coupled through the polarity selector and sample-and-hold circuits to the low-pass filter. The output of the low-pass filter slowly follows the error signal, and the VCO begins to alter frequency to resynchronize with the transmitted signal. Error signals continue to be generated in each bit period until the timing error has been eliminated.

At this time, the reason for the polarity selector circuit should be discussed. Assume that a timing error exists as shown in Fig. 19. Notice that the output of the phase comparator has a different sign at the completion of the integration period depending upon whether a Manchester coded one or zero is received. This occurs even though the actual direction of the phase error is the same in both cases. Also, note that the magnitude of the error is always correct. As a result, if the type of bit sent in the interval is determined (1 or 0), then the sign of the error signal can be adjusted so that the error signal will give a true representation of both the amount and direction of the
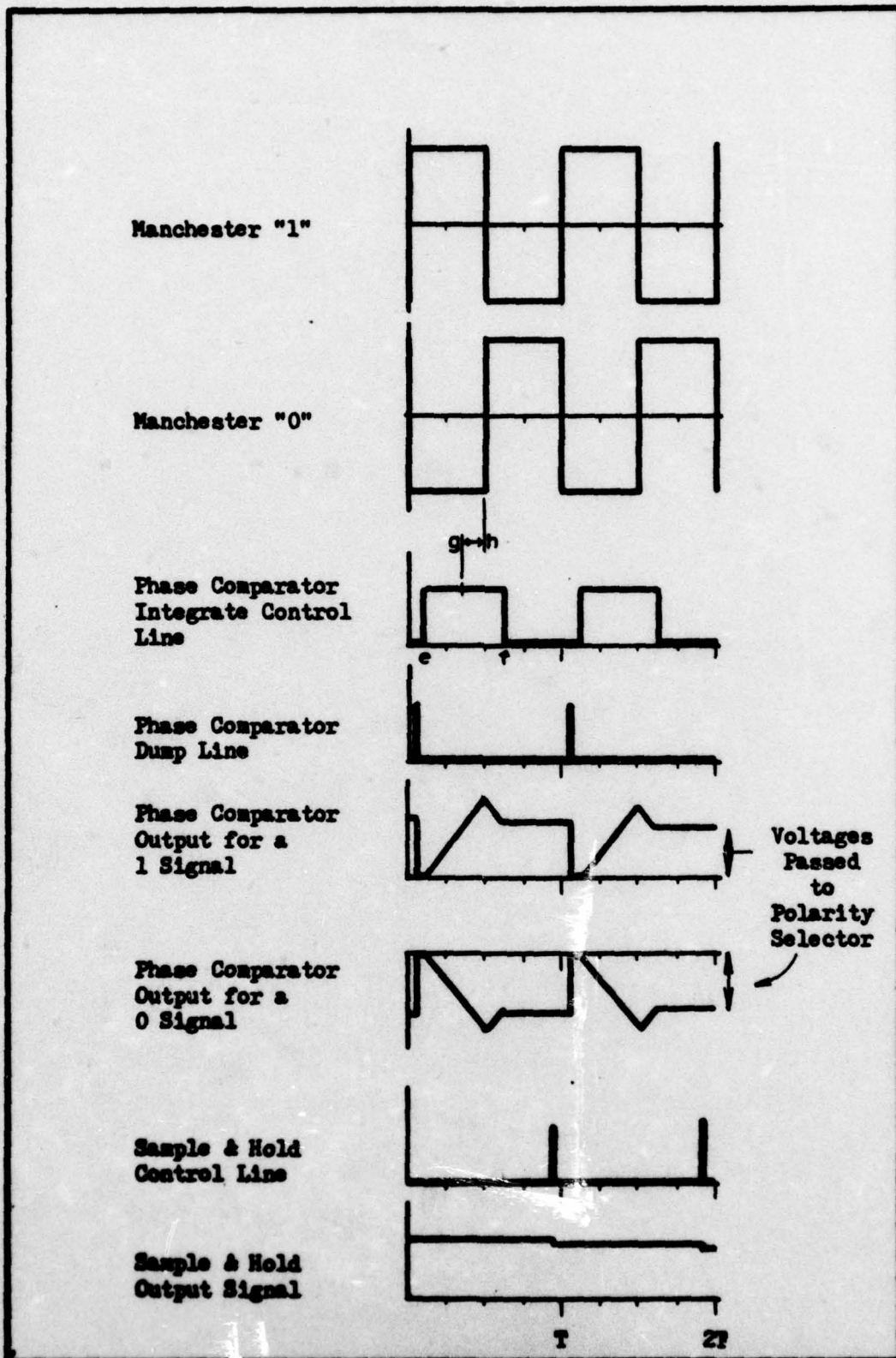
Fig. 19. Phase-Locked-Loop Signals During Error Correction

66

phase error. This need to correct the sign of error signals is the reason for the polarity selector circuit. The preceding arguments also explain why the sample-and-hold circuit and the integrating phase detector's dump control lines are strobed early in each bit period. Actually, this early strobing controls processing for an error signal that was developed in the preceding bit period but which could not have a sign assignment made until the data bit was decoded. Thus, the polarity selector and sample-and-hold circuits are important elements in the phase-locked-loop circuit.

For this receiver, the most important requirements for the timing circuit are that jitter variance must be low and that the receiver phase-locked-loop must not loose lock when the clock in the transmitter drifts. Both characteristics are related to the low-pass filter bandwidth. If the time constant of the low-pass filter is too long, then fast drifting of the transmitter clock can exceed the tracking capability of the loop, and a loss of lock results. On the other hand, if the time constant is too short, the jitter bandwidth is large and phase jitter of significant amounts will be present.

Timing Circuit Jitter Analysis. This section provides an estimate of the effects of noise on the timing circuit. It will be argued that the noise filtering action of an IHD circuit being used as a phase comparator provides additional filtering relative to the closed-loop response of the phase-locked-loop. As a result, it will be argued that for noise analysis a phase-locked-loop using an integrating phase comparator can be modeled by a phase-locked-loop with a linear phase comparator preceded by an independent integrating filter. The reader

67

is cautioned that there is some doubt about the validity of considering the integrating filter to be external to the phase-locked-loop. Thus, total reliance cannot be placed in the analysis. On the positive side, the assumptions made in 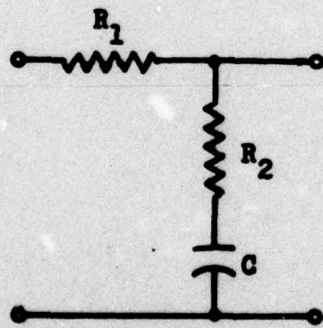the following derivation do seem reasonable, and the numerical results agree closely with the demonstrated performance of other phase-locked-loop circuits. As a result, the author feels that this section provides a set of reasonable starting parameters for the design of an experimental circuit to confirm the actual loop's performance.

In the following analysis, the jitter bandwidth of a linear phase-locked-loop model developed by Byrne is used to relate the phase jitter in the clock circuit output to the resulting effect on the error performance of the data processing train. The results show that the amount of jitter present in the timing circuit will have a negligible effect upon the error performance of the data processing train. As a result, the value of I_8 given by Eq (50) for a 10^{-5} error rate is essentially correct even when timing errors are considered.

Before beginning the jitter analysis, a brief overview of Byrnes' phase-locked-loop model is given. A block diagram of the model appears in Fig. 21 (Ref 21:561,564). Here, the phase comparator output is a linear function of the relative phase difference of the incoming signal and the VCO signal (divided down to match the frequency of the incoming signal). The phase comparator output is passed through a low pass filter of the form shown in Fig. 20b, and the filter output is used to control the VCO frequency. The performance of Byrnes' loop is determined by the selection of constants α_1 and α_3, and the low-pass filter

68

a. Loop Circuit

$$V_1 = \alpha_1 \varphi_e$$
$$\varphi_e = \varphi_1 - \varphi_0$$

$$V_2 = H(s)V_1$$

$$\phi_0 = \frac{\alpha_3}{s} V_2$$

$$\alpha = \alpha_1 \alpha_3$$
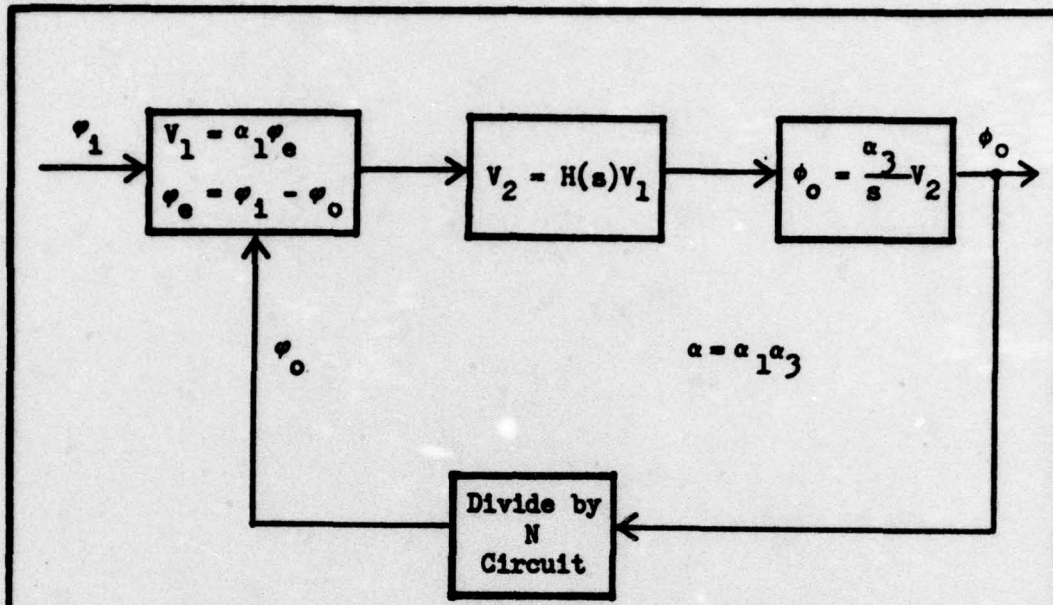
Divide by N Circuit

$$T_1 = (R_1 + R_2) C$$

$$\tau_1 = (R_1 + R_2) C$$

$$T_2 = R_2 C$$

$$\tau_2 = R_2 C$$

$$H(s) = \frac{1 + sT_2}{1 + sT_1}$$

b. Phase Lag Filter and Associated Relationships

Fig. 20. Byrne's Phase-Locked-Loop Model (Reprinted with permission from The Bell System Technical Journal, Copyright 1962, AT&T) (Ref 21:561, 564)

components. Of particular importance is the phase comparator constant α_1. It has units of volts per radian, and describes the conversion efficiency, or gain, of the phase comparator. The value of α_1 is determined by the physical construction of the chosen phase comparator circuit, and a numerical value for the IHD type of phase comparator will be given later.

To begin the jitter analysis, several assumptions will be made. Byrne assumed that noise in his loop was Gaussian, and that assumption is also made here. In addition, it will be initially assumed that a data string of ones is being sent, and that the polarity selector is fixed in the proper position for one type data bits. As a result, errors in the data output will not affect the operation of the phase-locked-loop, and the polarity selector and sample and hold circuits may be considered to be removed from the feedback loop.

In the development of the characteristics of his phase-locked-loop model, Byrne states that when the filter constant ratio T_2^2/T_1 is much greater than unity, the following relations hold (Ref 21:595)

$$\frac{2 B_1}{\pi \alpha} = \frac{T_2}{T_1} \tag{51}$$

and

$$\frac{2\pi \Delta f_1}{\alpha \hat{\rho}_e} = \frac{T_2}{T_1} \tag{52}$$

where T_1 and T_2 = filter constants (Fig. 20)

$\hat{\rho}_e$ = peak value of phase error due to a step change in input signal frequency

α = loop gain of the PLL (Fig. 20)

70

Δf_1 = step change in input frequency in Hz

B_j = equivalent closed loop jitter bandwidth of the PLL.

Using Eqs (51) and (52), it is possible to show that

$$B_j \hat{\rho}_e = \pi^2 \Delta f_1 \tag{53}$$

For a given set of timing signals such as shown in Fig. 18, it is possible to specify the largest value of phase error $\hat{\rho}_{e \ max}$ between the VCO and incoming signal which will not cause integrations over improper regions of the data signal. Also, for a given clock circuit in the transmitter, it is possible to determine a largest expected value of Δf_1. Therefore, Eq (53) enables the calculation of the smallest value B_j which will not result in loss of lock due to normal transmitter clock drift.

Next, reference to Fig. 14 indicates that the "voltage" power spectral density G_{s_v}' given by Eq (30) is present at the input to the phase comparator as well as the two signal-processing IHD circuits. However, the value of G_{s_v}' in voltage units must be converted to the equivalent radian "power" spectral density perceived by Byrne's simple phase comparator before the relationship for B_j will permit calculation of the variance of the VCO output.

To begin the development, consider the output of the integrating phase detector when a timing error exists. The input to the phase detector is the signal $s(t)$ plus additive Gaussian noise $n(t)$. For the timing periods e-f and g-h related as depicted in Fig. 19, the output voltage from the IHD circuit is

$$V_o = \frac{1}{K} \int_e^f \left[s(t) + n(t) \right] dt = \frac{1}{K} \int_e^f s(t) \, dt + \frac{1}{K} \int_e^f n(t) \, dt$$

$$= \frac{1}{K} \int_g^h s(t) \, dt + \frac{1}{K} \int_e^f n(t) \, dt \tag{54}$$

where $K =$ an integrator constant

$V_o =$ the integrator's output voltage.

Now, time g-h is directly related to the phase error between the signals ρ_1 and ρ_o. Since $s(t)$ is constant in each half of a bit period, the first part of Eq (54) can be written

$$\frac{1}{K} \int_g^h s(t) \, dt = \alpha_1 (\rho_1 - \rho_o) \tag{55}$$

where α_1 is simply the same constant as in Byrne's model. As a result, Eq (54) can be written as

$$V_o = \alpha_1 (\rho_1 - \rho_o) + \alpha_1 \left(\frac{1}{\alpha_1 K} \int_e^f n(t) \, dt \right)$$

$$= \alpha_1 \left(\rho_1 - \rho_o + \frac{1}{\alpha_1 K} \int_e^f n(t) \, dt \right) \tag{56}$$

Next, assume that time e-f is essentially constant, so that the integral of the noise does not depend upon the phase error $\rho_1 - \rho_o$. This assumption seems reasonable because time e-f varies very little for the normal range of frequency change encountered in practical phase-locked-loop VCO's. If this assumption is made, then the portion of V_o caused by the input noise is

$$V_{on} = \alpha_1 \left(\frac{1}{\alpha_1 K} \int_o^{T_{1\emptyset}} n(t) \, dt \right) \tag{57}$$

where $\tau_{1\phi} = f-e$ is a constant equal to the average integration time of the IHD circuit.

Now Eq (57) is very interesting. It indicates that V_{on} could be considered to be the result of passing the noise voltage from the post-diode amplifier through a series combination of an integrating filter and a linear phase comparator element with a transfer function α_1. Thus, in comparing Eq (57) to Eq (56), it is evident that the noise power spectral density at the input to Byrne's linear phase comparator element in Fig. 20 will be the result of passing G'_{s_V} through an integrator with an integrator constant

$$K' = \alpha_1 K \tag{58}$$

As a result, the phase jitter at the output of the VCO can be considered to result from passing G'_{s_V} through the integrating filter in series with a phase-locked-loop filter of equivalent bandwidth B_j.

Taub and Schilling have shown that the magnitude squared transfer function of an integrating filter is (Ref 18:252)

$$\left| H_1(f) \right|^2 = \left(\frac{\tau_{1\phi}}{K'} \right)^2 \left(\frac{\sin (\pi \tau_{1\phi} f)}{\pi \tau_{1\phi} f} \right)^2 \tag{59}$$

Also, the magnitude-squared transfer function of a perfect rectangular filter of bandwidth B_j is given by

$$\left| H_\phi(f) \right|^2 = \begin{cases} 1, & |f| < B_j \\ 0, & \text{else} \end{cases} \tag{60}$$

73

As a result, the variance of the output phase jitter due to a cascade
of these filters is

$$\sigma_{\rho_0}^2 = \int_{-B_j}^{B_j} G_{s_v}' \left| H_1(f) \right|^2 df$$

$$= \frac{G_{s_v}' \tau_{1\phi}^2}{(K')^2} \int_{-B_j}^{B_j} \left(\frac{\sin(\pi \tau_{1\phi} f)}{\pi \tau_{1\phi} f} \right)^2 df \qquad (61)$$

A change of variable gives

$$\sigma_{\rho_0}^2 = \frac{G_{s_v}' \tau_{1\phi}}{\pi(K')^2} \int_{-\pi \tau_{1\phi} B_1}^{\pi \tau_{1\phi} B_j} \left(\frac{\sin(X)}{X} \right)^2 dx \qquad (62)$$

Now, because $\tau_{1\phi}$ is on the order of 10^{-7} and B_j for a phase-locked-
loop is usually much less than 10^7, the integral in Eq (62) is approxi-
mately equal to $2\pi \tau_{1\phi} B_j$. Also, recall that $G_{s_v}' = \left| A_v \right|^2 G_s R_L$ from
Eq (30) and the comments following Eq (35). As a result, Eq (62) may
be solved to yield

$$\sigma_{\rho_0}^2 \approx \frac{2 G_s \tau_{1\phi}^2 \left| A_v \right|^2 R_L}{\alpha_1^2 K^2} B_j \quad \text{radians}^2 \qquad (63)$$

provided that $B_j \ll 10^7$ and the phase lag filter constants are such
that $\tau_2^2/\tau_1 \gg 1$.

It should be recalled that Eq (63) has been derived under the
assumption that errors in the data output do not affect the jitter
performance of the timing recovery circuit. To justify this assumption,

74

a numerical answer for Eq (63) will be presented. Then, using the results of this numerical analysis, it will be argued that the actual phase-locked-loop circuit with decision-directed feedback will have essentially the same value of output phase variance given by Eq (63).

The numerical evaluation which follows is based upon use of an IHD circuit which has an integrator constant $K = 6.8 \times 10^{-8}$ and which is designed for use with Manchester coded signals which vary ± 4 volts around a zero volt mean. These values match those of an existing low-cost circuit being developed by the author.

To evaluate Eq (63) several assumptions must be made. To begin, the value of $T_{1\phi}$ will be arbitrarily selected as equal to 1/2 bit period, or 3.33×10^{-7} sec. Using this, the value of A_v can be determined from a knowledge of the required signal amplitude at the IHD input and the signal level present at the output of the detector diode. To determine the signal level out of the diode, the assumption is made that the signal-to-noise ratio of the receiver is ultimately determined by the noise performance of the data processing train rather than the timing recovery circuit. Allowing this assumption means that the required value of I_s is given by Eq (50) as 2.42×10^{-8} amp. Since this current drives the 300 ohm load in the post-diode amplifier, the peak-to-peak output voltage of the diode is 7.26×10^{-6} volts. This level must be boosted to the eight volt peak-to-peak value needed by the IHD circuit. Thus, $|A_v|$ is 1.10×10^6.

Next, a value for α_1 can be determined by noting the resulting output voltage of the IHD circuit when the input phase is shifted a known amount. For example, consider a timing shift of $\pi/2$ radians occurs. This corresponds to shifting timing period e-f in Fig. 19 to

75

the left by 1/4 bit period. As a result of the timing shift, the input voltage to the phase comparator V_{in} is constant at +4 volts for the entire timing period. The output of an integrator with a constant input is given by $V_{out} = V_{in} \tau_1/K$ (Ref 18:367). Therefore, $V_{out} = 19.6$ volts. Since this corresponds to the output due to a $\pi/2$ radian phase shift, $\alpha_1 = 19.6/(\pi/2) = 12.5$ volts/rad.

Finally, a value for G_s is needed. From the assumption that $I_s = 2.42 \times 10^{-8}$ amp, Eq (36) permits calculating that $G_{sn} = 1.16 \times 10^{-24}$. Then using values of the other components of G_s given by Eqs (44), (45), (48) and (49), $G_s = 1.35 \times 10^{-21}$ W/Hz.

Using the values determined above, Eq (63) gives a value for the variance of the output phase signal as

$$\sigma_{\rho_0}^2 \approx \frac{2(1.35 \times 10^{-21})(3.33 \times 10^{-7})^2(1.10 \times 10^6)^2(300)}{(12.5)^2(6.8 \times 10^{-8})^2} B_j$$

$$= 1.51 \times 10^{-7} B_j \tag{64}$$

The author's experience with crystal-controlled clocks indicates that short-term frequency shifts are very small, and that Δf_1 in Eq (53) can probably be made on the order of 1 Hz. If the timing in Fig. 19 is assumed, then $\hat{\rho}_e = 0.047$ radians when integration errors begin in the data processing train. Thus Eq (53) indicates that $B_j = 209$ Hz. As a result

$$\sigma_{\rho_0}^2 = 3.16 \times 10^{-5} \tag{65}$$

This means the standard deviation of the output jitter is only 5.61×10^{-3} radians. Therefore, for the timing values selected here, and assuming that data errors do not affect the polarity selector, the probability that ρ_0 will differ from the proper value by more than $\hat{\rho}_e = 0.047$ radians (a value of about 8 standard deviations) is very small, being on the order of 10^{-15}.

Now, the previously made assumption that the data errors would have no effect on the performance of the phase-locked-loop will be discussed. To begin, reference to Fig. 17 indicates that the polarity assignment circuit output passes through the low-pass filter before reaching the VCO. Because of the very low cutoff frequency of the low-pass filter, one isolated sign assignment error due to an incorrect data output will have negligible effect on the control voltage to the VCO. Since a properly synchronized receiver will only make one data error in every 10^5 output bits, and since these errors are presumed to be randomly spaced, the effect of the signal-train-dependent errors on the phase-locked-loop will be very small. From the numerical analysis just completed, it can also be concluded that additional data errors which result from timing errors due to noise input to the phase-locked-loop comparator are negligible. Thus, the frequency of incorrect data selections for a synchronized receiver is so low that the low-pass filter should virtually eliminate the added effects of polarity-selector-induced jitter.

Required Input Power with Timing Considered. From the preceding arguments, it is apparent that additional errors in the data output of the receiver caused by noise effects on the timing circuit should be

77

small enough to be ignored when compared to the error rate of 10^{-5} which results when perfect timing is assumed. Hence, the important timing consideration is not jitter, but is rather the amount of time realizable circuits for the functions in Fig. 14 and 17 need to dump and transfer signals. From experimental results with the prototype IHD circuit, it appears that the timing relations shown in Fig. 21 are approximately correct. So τ_i for IHD 1 and 2 is about 2.8×10^{-7} sec. Using this value in Eq (43) indicates the required level of I_s to get a 10^{-5} BER yields

$$I_s = 2.42 \times 10^{-8} \text{ amps} \tag{66}$$

which is the same result as Eq (51). As was also shown previously, the required optical power at the diode with a diode responsivity of 0.62 Amp/watt remains

$$P_0 \approx \frac{2.42 \times 10^{-8}}{0.62} = 3.9 \times 10^{-8} \text{ watts} \tag{67}$$

even when the anticipated effects of the timing circuit are considered.

Receiver Costs

Although the hardware design of the receiver is not complete, some experimental results with an IHD circuit and the calculations made in this chapter do permit some rough estimates of the parts cost for the fiber and atmospheric receivers. Since both receivers use a common electronics package, this item will be discussed first. Then, the costs of the additional items for the atmospheric system optics will be addressed.

The author believes that the detector diode and post diode amplifier can be built with about $100 worth of parts. The main items
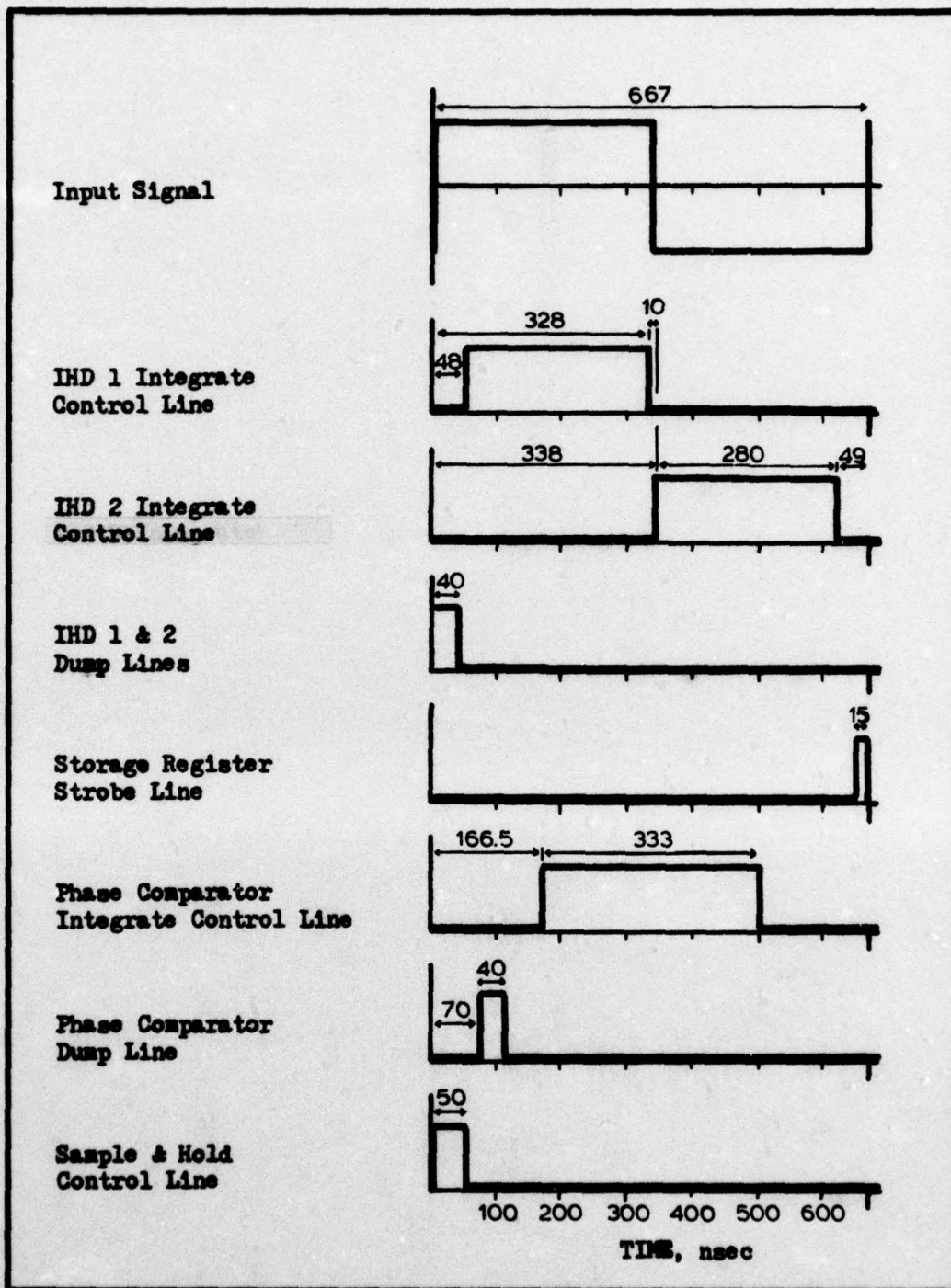
78

Fig. 21. Proposed Receiver Timing

included are the SHS-100 photo-diode, a TIXL-152 diode amplifier, and two LM 733 wide-band amplifiers. An AGC amplifier using an LM 308 operational amplifier is also included.

The IHD circuits should cost about $40 each. This is based upon use of LM 318 high-speed operational amplifiers. Since three IHD circuits are required for the receiver, the total cost of the IHD's runs about $120.

The polarity selector and the sample-and-hold circuits are also constructed from LM 318's. Cost for the combined circuit is expected to be $40.

The VCO and its divider train will be constructed from an LM 375 oscillator IC and appropriate Schottky-clamped TTL logic chips. Schottky logic will be necessary because the oscillator must run at about 90 MHz to provide the closely-spaced timing signals necessary to control the IHD circuits. Cost for this unit is expected to be $30.

The signal output section will use an LM 361 high speed comparator and a 74$74 D type latch. Cost is expected to be $10.

In addition to the functional blocks mentioned above, the receiver costs also must include amounts for power supplies and packaging. It is estimated that these units will add about $300 to the total.

For the fiber receiver, the only added cost is that for connecting the fiber to the detector diode. Since this will probably be done simply by clamping the diode in position in front of the fiber, the cost for the fiber receiver will be roughly equal to the cost of the electronics and packaging, about $600 total.

80

In addition to the costs cited above, a receiver for the atmospheric system must also include an allowance for the optics train. For the optics train presented in this chapter, the cost of the lenses is $350 according to the 1976 Melles Griot Optical Catalog Price List. An additional allowance for focusing mounts must also be included, and this is expected to bring the total optics train cost to $500. Thus, the atmospheric receiver total cost for electronics, optics, and packaging is expected to be $1100.

In closing this section, it should be noted that some of the components used in making the parts cost analysis have not been completely designed into the receiver. However, the components all appear to be suitable for their intended applications, and the author believes that few if any major changes will be necessary to complete a formal design.

IV. Transmitter Design

The design of the electro-optic section of the transmitter is strongly influenced by the type of channel to be used, while the electronic modulating and control circuits for the light emitter in the transmitter are the same for both systems. Therefore, the design of the electro-optic portion of the atmospheric and fiber transmitters is treated separately, followed by a description of the electronics section. The chapter also includes a sample safety calculation for the atmospheric transmitter.

Atmospheric Transmitter Electro-Optics Discussion

Lenses. The lens system for the atmospheric transmitter has not been designed due to time constraints, but some comments about the lens system can be made.

Because of the highly elliptical spot pattern of CW laser diodes as shown in Fig. 22, the lens system employed must have different focusing actions in the x and y axes. This asymmetrical focusing may be accomplished by using cylindrical lenses as shown in Fig. 23. The lens system must change the very small, rectangular-shaped beam waist found inside the laser diode into a larger, symmetrically shaped waist at some point beyond the lens system (Fig. 24). Divergence from this symmetrical waist should then provide the desired spot size and circular shape at the receiver. Development of the actual lens package will involve the use of Gaussian beam propagation theory.

Since the exact lens system has not been developed, some assumptions must be made to provide a qualitative idea of the transmitter's
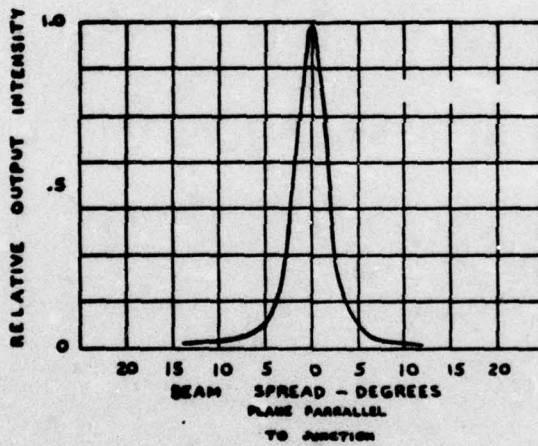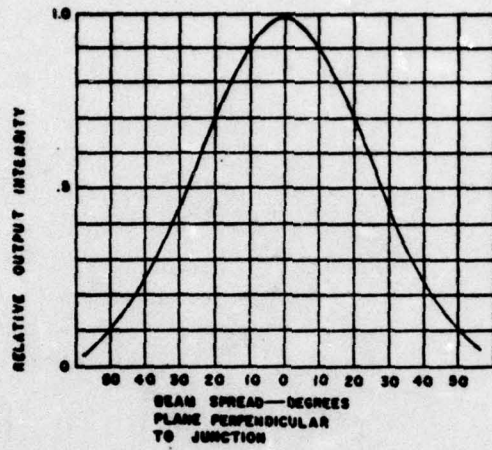
Fig. 22. Typical Beam Data For a CW Laser Diode
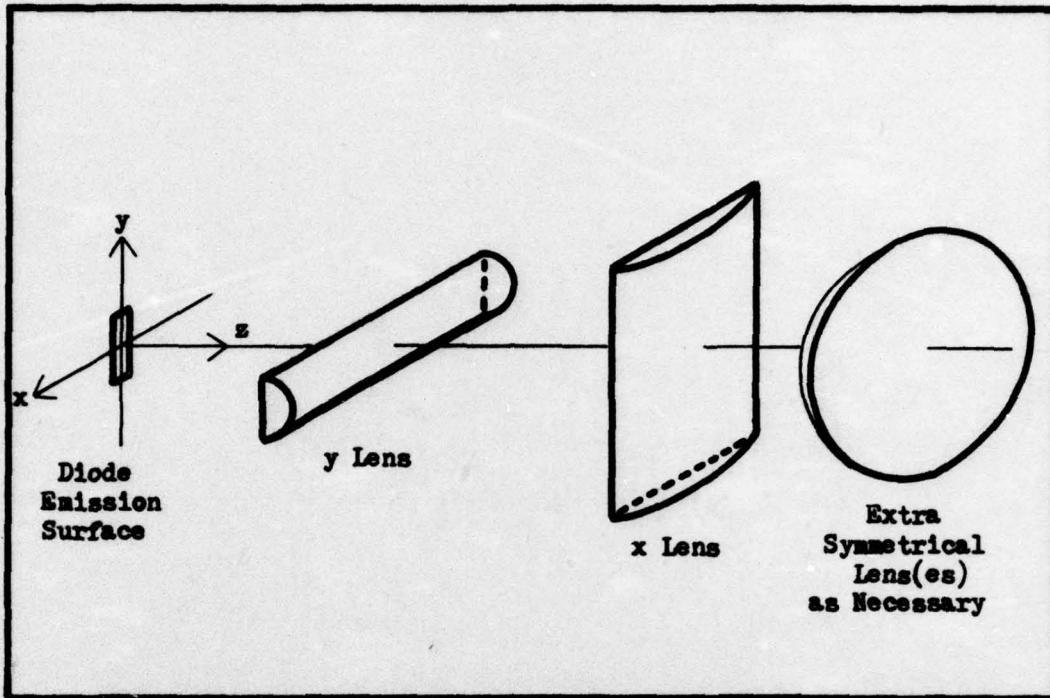(Laser Diode Laboratories LCW-10)

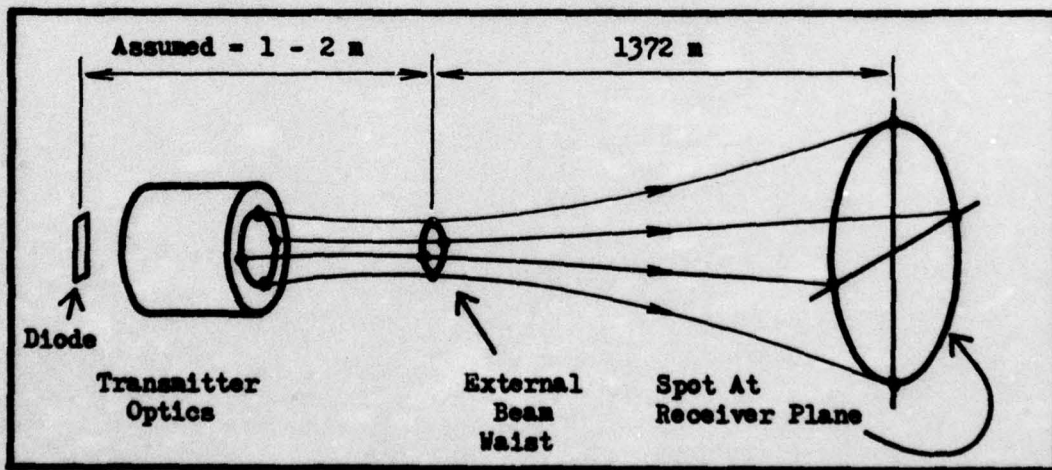Fig. 23. General Lens Configuration for Atmospheric Transmitter

Fig. 24. Beam Shape for Laser Diode Transmitter

84

operation. For purposes of this paper it will be assumed that the final lens system forms the external beam waist within a few meters of the lens system. As a result, the waist can be considered to be essentially at the transmitter when calculations involving beam divergence from the transmitter to the receiver are made. If this assumption later proves invalid, the only major effect should be on the calculation of the minimum safe direct viewing distance for the transmitter beam.

Required Transmitter Output Power. As mentioned in Chapter two, the signal power collected by the receiver input lens is affected by atmospheric attenuation and by the losses incurred from diverging the beam. The reader will recall a diverging beam is necessary to prevent spot dancing and beam bending from causing an outage. Now, the intensity pattern of the Gaussian beam at the receiver plane is shown in Fig. 25. Here, the intensity of the beam in watts/m^2 has fallen to half its maximum value at $X = a$. From work in Chapter two, the desired beam divergence angle α is one milliradian. As a result, a has a magnitude of 1.372 m as shown in Fig. 25. Now, $I_L = I_{Lmax}$ at $x = 0$ and $I_L = I_{Lmax}/2$ at $x = a$. Since the beam shape is circularly symmetrical at the receiver plane, the value of I_L at a radial distance r from the x-y axis is

$$I_L = I_{Lmax} \cdot e^{-\frac{r^2}{2.716}} \tag{68}$$

Next, the total amount of power at the receiver plane that falls on the circular area with radius q is given by
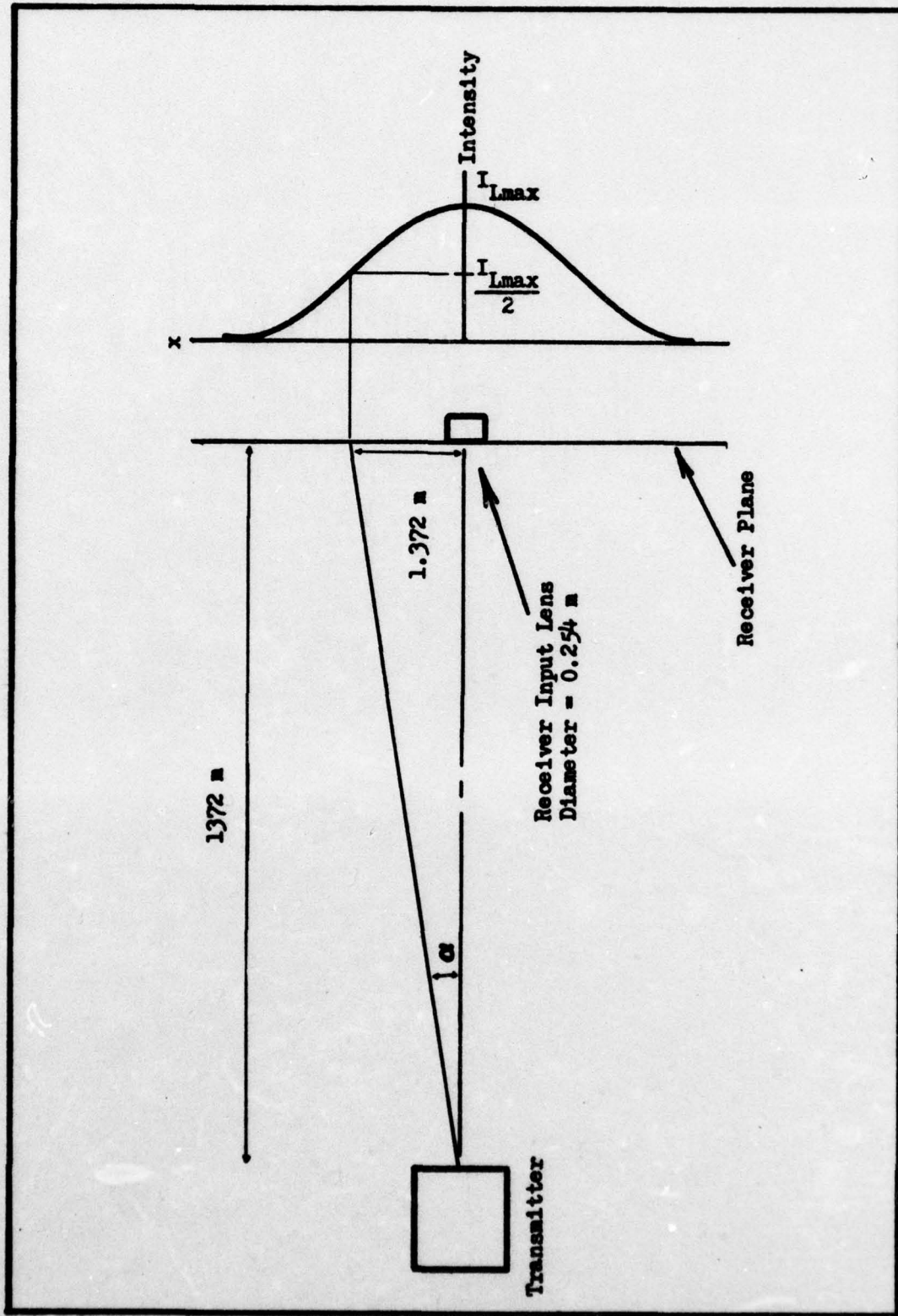
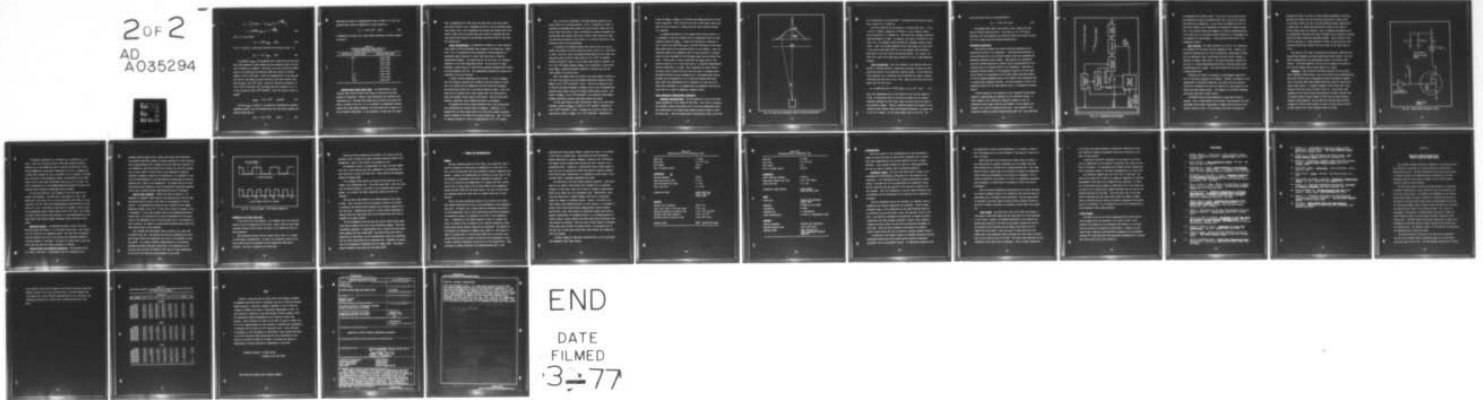85

Fig. 25. Beam Intensity Pattern at the Receiver

END

DATE
FILMED

3-77

1.0

4.5 2.8 2.5

3.2 2.2

3.6

4.0 2.0

1.1

1.8

1.25 1.4 1.6
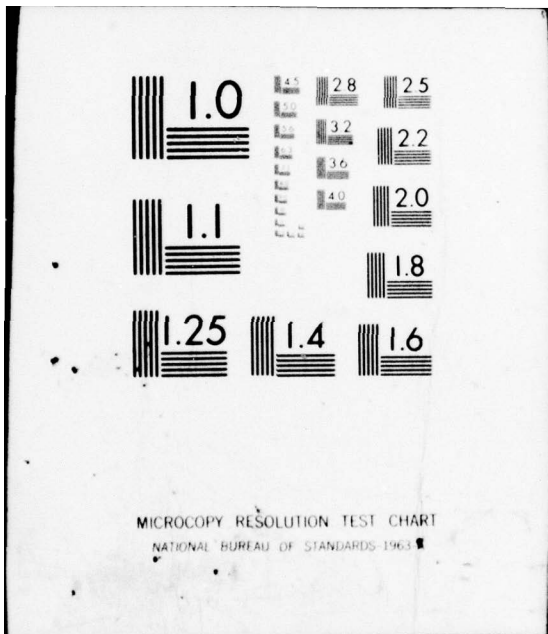
MICROCOPY RESOLUTION TEST CHART

NATIONAL BUREAU OF STANDARDS-1963

$$P_q = \int_o^q I_L \, 2\pi r \, dr = 2\pi I_{Lmax} \int_o^q r \, e^{-\frac{r^2}{2.716}} \, dr$$

$$= \pi \sqrt{2.716} \; I_{Lmax} \, (1 - e^{-\frac{q^2}{2.716}}) \tag{69}$$

For q = a, this yields

$$P_a = 2.589 \, I_{Lmax} \qquad \text{watts} \tag{70}$$

If q = ∞, then P_q = total power falling on the receiver plane. So

$$P_{rp} = 5.177 \, I_{Lmax} \qquad \text{watts} \tag{71}$$

To determine I_{Lmax}, the assumption will be made that the receiving lens input aperture is small enough that the intensity across the lens can be treated as a constant. From work in the last section of Chapter three, it is known that the detector diode must receive an optical signal of 3.90×10^{-8} watts. Given the transmissivity of the lens system (Eq 13), this means the power falling on the input receiver lens must be about 1.03×10^{-7} watts. Since the receiver lens aperture is 5.07×10^{-2} m^2 (see Fig. 12), this means that the intensity at x = a in Fig. 25 must be 2.03×10^{-6} watts/m^2. Since this value is equal to $I_{Lmax}/2$

$$I_{Lmax} = 4.07 \times 10^{-6} \qquad \text{watts/m}^2 \tag{72}$$

Now that I_{Lmax} is known, it is possible to determine the required transmitter power. Eq (71) indicates that the total power reaching the receiver plane must be

$$P_{rp} = 2.11 \times 10^{-5} \qquad \text{watts} \tag{73}$$

Recalling the clear air transmissivity given in Table II is 0.86, the required power from the transmitter in clear weather is

$$P_T = 2.45 \times 10^{-5} \quad \text{watts} \tag{74}$$

A tabulation of values of P_T versus other prevailing visibility appears in Table VI.

Table VI
Required Transmitter Output Power for
Various Prevailing Visibilities

Visibility in Statute Miles	Required Power Watts
14.3	2.45×10^{-5}
5	3.01×10^{-5}
4	3.30×10^{-5}
3	3.77×10^{-5}
2	4.06×10^{-5}
1	1.23×10^{-4}
0.75	5.86×10^{-4}
0.5	3.52×10^{-3}
0.25	4.69×10^{-1}

Required Laser Diode Output Power. The determination of the required power from the laser diode cannot be made until the lens package is determined. However, some preliminary work indicates that construction of a suitable lens system may be possible with three elements, as shown in Fig. 23. If it is possible to economically procure lenses with large enough diameters, the main power loss is going to be due to Fresnel reflections. If the assumption is made that the lenses

have a transmissivity of 90%, then the power loss in the lens system will only be about 1.4 dB. Assuming the use of a 10 mw continuous power laser diode, even if the transmitter lens system only couples 10% of the diode's output into the desired beam cone, Table VI indicates that the link should still function in prevailing visibilities down to less than one statute mile.

Safety Considerations. As mentioned in Chapter two, high intensity light beams at 860 nm wavelength pose a danger to the human eye. Therefore, a set of standards has been developed by several agencies for permissible power densities of laser light which may be viewed by unprotected personnel. For lasers used by the Air Force, the governing regulation is Air Force Regulation 161-32. As this thesis is being prepared, a major revision to AFR 161-32, presently designated AFR 161-xx, is being completed (Ref 22). The calculations included here comply with standards of this new revision.

To begin, several assumptions will be made. It will be assumed that the external, circular waist formed by the lens system is within one or two meters of the transmitter, and that far-field divergence conditions exist within one or two meters beyond the waist. Also, the laser will be assumed to be a point source under the definitions of point and extended sources given in AFR 161-xx. Once the final lens design is completed, these assumptions should be reexamined.

In applying AFR 161-xx, safety personnel take a very conservative view concerning the possible length of exposure. Presently, it is assumed that for open systems such as the data link, unaware personnel could be exposed to the beam for an entire working day. Thus, the time of exposure assumed is 8 hours, or approximately 2.88×10^4 seconds.

Now, the actual calculation of the MPE (maximum permissible exposure level) is a two-step process. First, a calculation is made to determine the maximum laser energy that can be safely viewed over the entire eight hour period. Next, a calculation is made to determine the maximum peak power density that may be safely viewed during one pulse. The controlling exposure is then taken to be the more restrictive value resulting from the two calculations.

To determine the maximum average power density that the eye can safely view during the entire eight hour period, Table 4-1 in AFR 161-xx is used. From this table, the maximum energy density for an eight hour long pulse train of 860 nm light pulses is 3.2×10^{-4} (t) exp(860 - 700/224) joules/cm^2, where t is the pulse train length in seconds. So, for 2.88×10^4 second exposure, $MPE_{ET} = 18.8$ joules/cm^2 - pulse train, where MPE_{ET} = maximum permissible exposure in energy units for the total energy of the pulse train.

Next, this MPE_{ET} value is divided by the total number of pulses in the eight hour period to get the maximum permissible energy per pulse, $MPE_{EP} = 4.35 \times 10^{-10}$ joules/cm^2 - pulse. This may be divided by the on time of the pulse developed in Chapter three to get the maximum permissible power density that can be safely viewed during a pulse. The result is $MPE_{PP} = 1.55 \times 10^{-3}$ watts/cm^2 = 15.5 watts/m^2, where MPE_{PP} = maximum permissible exposure beam power density per pulse.

For the peak power per pulse calculation, Table 4-1 in AFR 161-xx provides a value of MPE_{EP}' of (0.06)5.0×10^{-7} exp(860 - 700/224) or 6.13×10^{-8} joules/cm^2 - pulse. Dividing this by the on time of the pulse gives a value of $MPE_{PP}' = 2.2 \times 10^{-1}$ watts/cm^2. Comparing the

values for MPE_{pp} to MPE'_{pp}, it is obvious that MPE_{pp} describes the more severe limitation. Thus, during the on time of each pulse, human eyes must not view the beam in a region where the beam intensity exceeds 15.5 watts/m^2.

To complete calculation of the closest safe viewing distance, it is necessary to find the distance from the transmitter where the beam intensity equals the MPE_{pp}. To make this calculation, reference to Fig. 26 shows that AFR 161-xx uses a different definition of the divergence angle from the one presented earlier in this chapter. Also, the regulation permits the assumption that the beam intensity is constant across the spot subtended by the divergence angle and zero beyond that point. From Eq (68), it may be shown that the I_{max}/e point at the receiver plane is at X = 1.648 m and that α' is therefore approximately arctan (1.648/1370) = 1.2 mrad. Next, recalling the output power of the laser diode is about 10 mw and that this power is assumed evenly distributed across the spot subtended by α', the minimum safe viewing distance can be calculated as 11.9 m from the external beam waist. Thus, since both transmitters will be located at or near the top of multi-story buildings, it is unlikely that any personnel can enter the light beam in a region of dangerous intensity levels.

Fiber Transmitter Electro-Optics Discussion

Component Characteristics. The LED selected for use in the fiber system transmitter is the Plessy HR 954 diode. This diode is optimized for Corning's single fiber cables, and is the only commercially available diode known to the author which appears powerful enough to drive the fiber link. From the manufacturer's specification sheet, the HR 954
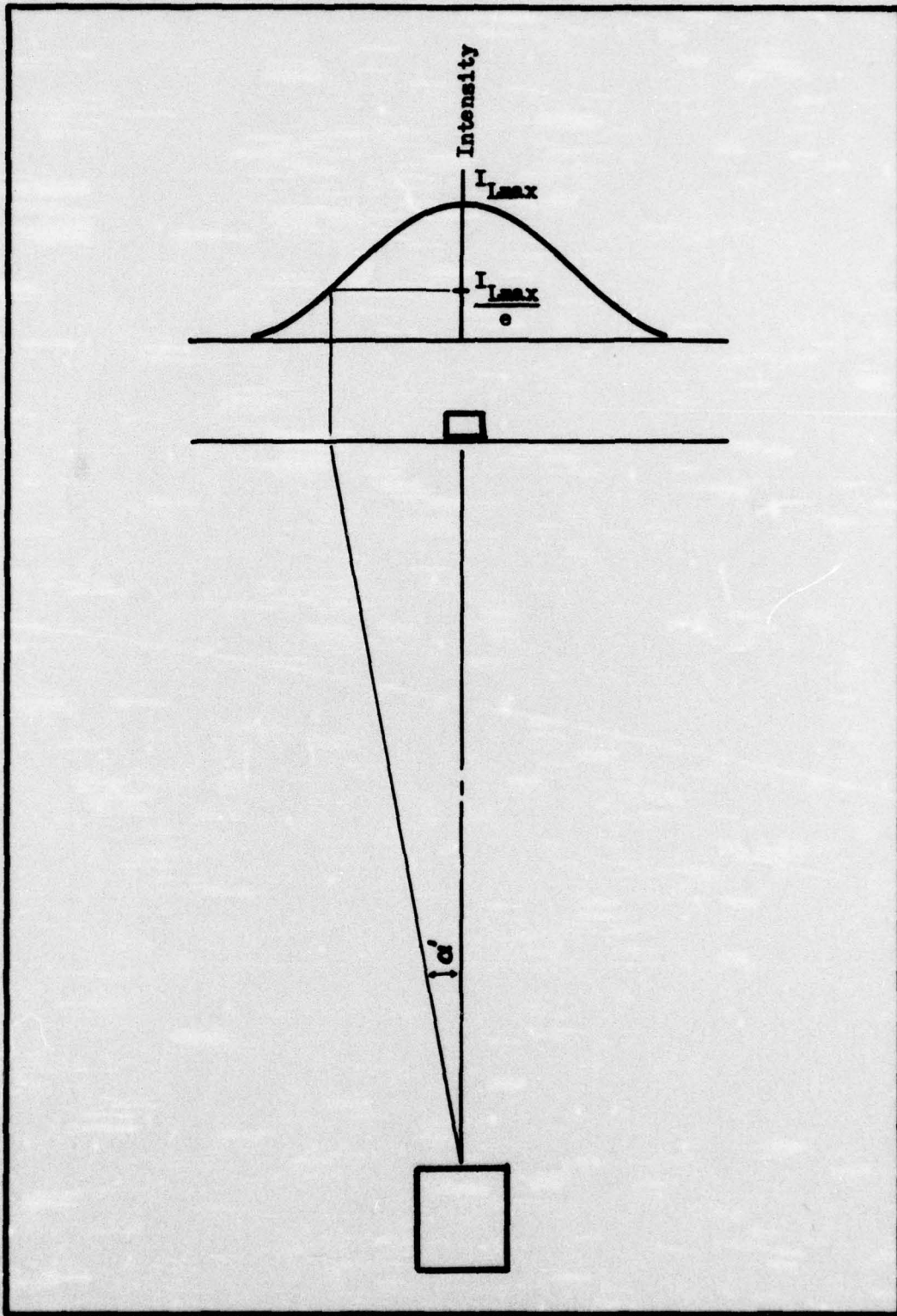
Fig. 26. Laser Beam Divergence Angle for Safety Calculations

has a brightness B of 35 watts/$(cm^2$ - steradian) and an emitting surface with a radius of b = 0.0025 cm.

The fiber selected for the system is a Corning 1158 fiber. It has a loss of 6 dB/Km, a bandwidth of 200 MHz in a one kilometer length, and core radius of a = 0.003125 cm. This fiber has a maximum refractive index difference Δ = 0.008. In addition, the fiber is available in two-fiber (i.e., two channel) cables suitable for telephone conduit installation. Also, the 200 MHz bandwidth of the fiber means the fibers have a rise time of only about 10^{-9} sec in 2 km lengths, which provides a good match to the rise time of the optical emitter. As a result, the fiber will cause little additional distortion in the 1.5 MHz Manchester signals.

Power Calculations. With the selection of the LED and fiber completed, it becomes possible to calculate the amount of power the fiber system can deliver to the receiver's detector diode. For the diode and fiber selected, Fig. 9 indicates that the HR-954 will insert a normalized power into the fiber of P_n = 0.86. Then, Eq (11) gives the actual power into the fiber P_f as

$$P_f = 0.86\pi^2(35)(3.125 \times 10^{-3})^2(0.008) = 2.32 \times 10^{-5} \text{ watts} \qquad (75)$$

Next, the transmission loss of the cable for the 2 km path length is 12 dB. An additional loss of 3 dB will be allowed for two Corning-supplied couplings for each fiber, since the fiber cables are made in one kilometer lengths. Finally, recalling comments from Chapter two on coupling losses between fibers and photodiode detectors, an output loss of 0.17 dB is added. So, the total channel loss is 15.17 dB. The

resulting optical power at the photodiode is

$$P_o = 7.05 \times 10^{-7} \text{ watts} \tag{76}$$

The minimum power level at the diode to give a BER of 10^{-5} was found in Chapter three (Eq (67)). This level is 3.9×10^{-8} watts. Therefore, the fiber channel with the HR 954 diode will provide an extra 12.5 dB of signal above the minimum required level.

Transmitter Electronics

This section discusses the various functions performed by the electronics section of the transmitter. These functions basically include providing drive to the optical emitter along with performing the Manchester encoding of data signals. Additionally, the transmitter circuitry includes functions to control initial synchronization of the receiver clock to the master clock in the transmitter. Time has not permitted detailed design of the transmitter circuitry, but the functional blocks to be described are all fairly simple, and there should be little problem implementing most of the circuit with inexpensive TTL or possibly MOS integrated circuits. The only exception to this is the modulator circuit for the light emitter, and it is described in greater detail.

A brief overview of the operation of the transmitter should prove helpful to understanding the operation of the functional blocks. A block diagram of the transmitter electronics appears in Fig. 27. Referring to this figure, when the data channel is to be opened, the computer will raise the request-to-send line. This results in the transmitter sending a special synchronizing signal for a time sufficient
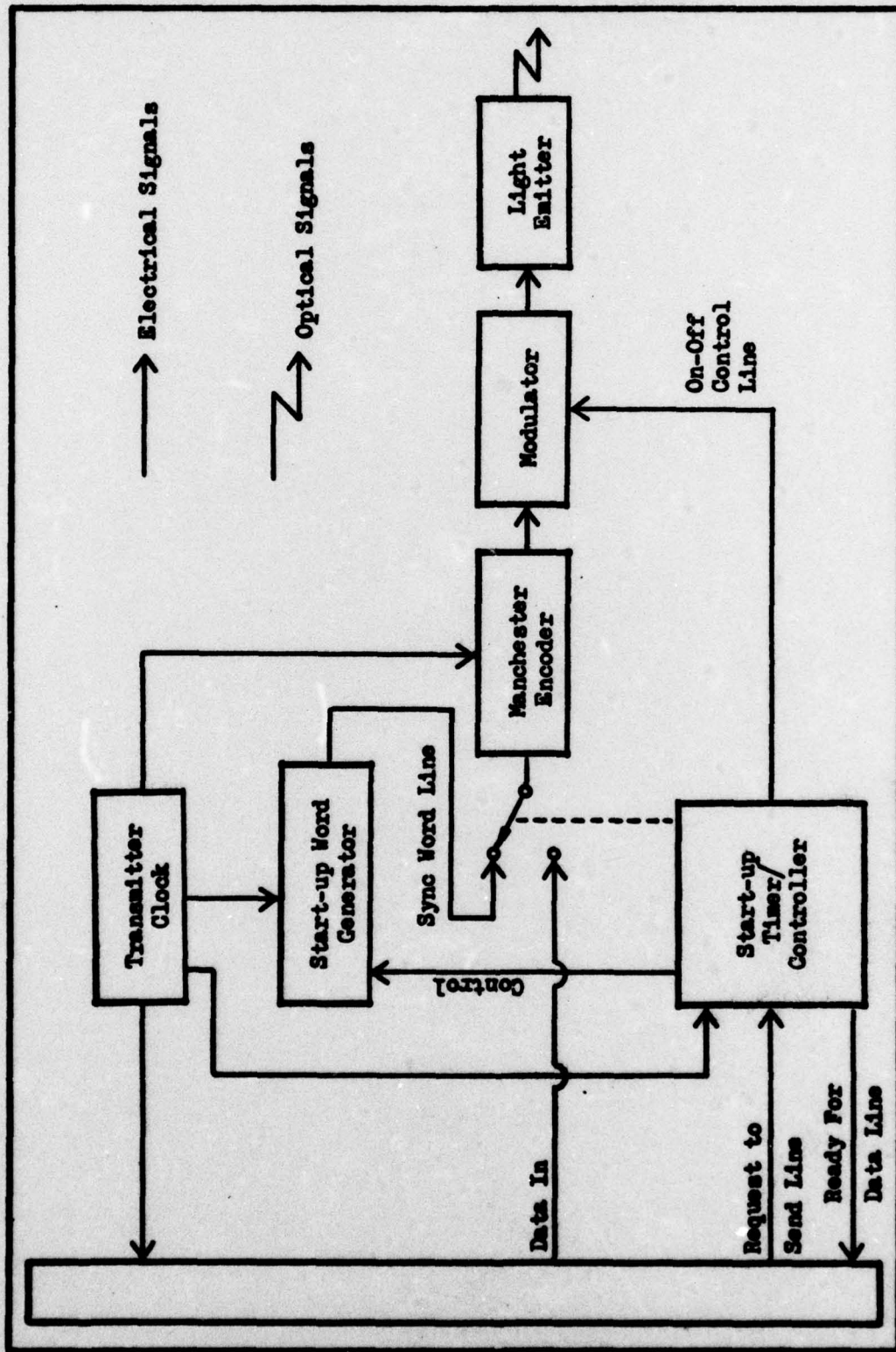
94

Fig. 27. Transmitter Block Diagram

95

to synchronise the receiver clock. At the end of the start-up period, the transmitter raises the ready-for-data line to notify the computer that data can be transmitted. At any time, the computer can shut off the optical output of the transmitter by lowering the request-to-send line. This feature permits the computer to initiate resynchronisation of the link, and it also permits safety functions to be programmed into the computer for link shutdown. A more detailed description of the transmitter follows.

Light Emitters. The light emitters to be used in the transmitter are different for the fiber link and atmospheric link. However, the electrical characteristics of the two devices are surprisingly similar. For the atmospheric link, a solid-state CW laser diode is needed to generate a coherent light source. The diode tentatively selected for the unit is a Laser-Diode-Laboratories LCW-10, although similar units from RCA may also be usable. The diode selected for the fiber link is a Plessy HR-954 LED.

Presently, the LCW-10 is available in developmental quantities, but its full scale testing is not complete. However, in addition to the manufacturer's published information, the author also has received a letter with information on tests per formed by Mr. Dick Swensen at the China Lake Naval Weapons Center. The comments on the LCW-10 presented below draw from both of these sources.

The LCW-10 diode has been modulated at rates above 20 MHz by Swensen. This is made possible by the diode's 100 picosecond rise time and modest drive current requirement of roughly 500 ma for full rated optical output of 10 mw. At full output, the diode's voltage drop

96

averages only about 1.8 volts, so power supply requirements are modest.
Swenson also reports that the diode has been pulsed at levels above
10 mw optical output, but that the diode emission pattern changes from
a single spot to a double spot pattern when levels on the order of
100 mw optical power are obtained. Also, a telephone conversation with
the manufacturer indicates that diode lifetimes will be severely shortened
when pulse levels exceed the published ratings. Since lifetime of the
diode is important, it seems advisable to limit the diode drive so that
the peak optical pulse outputs are on the order of the rated value of
10 mw.

The Plessy HR 954 diode is physically and optically compatible with
Corning Glass Company's low-loss single-fiber optical cables. The elec-
trical characteristics are surprisingly similar to the LCW-10 laser
diode's. The HR 954 requires a 300 ma drive to develop its rated out-
put, and the voltage drop at rated output is 1.6 volts.

Modulator. Both the HR 954 and LCW-10 emitters are best driven
from a constant current source. Due to the similar drive characteristics,
the author believes that an experimental circuit developed by Swenson
using a Siliconix VMP-1 power MOSFET transistor should be suitable for
either light emitter. A schematic diagram of the circuit with inter-
facing to TTL drive levels is shown in Fig. 28. This circuit takes
advantage of the current source characteristic the VMP-1 exhibits when
its drain-to-source voltage exceeds 10 volts and its gate-to-source
voltage is held constant. For the VMP-1 the required gate-to-source
voltage for a 300 ma drain current is about 3.3 volts, while a 500 ma
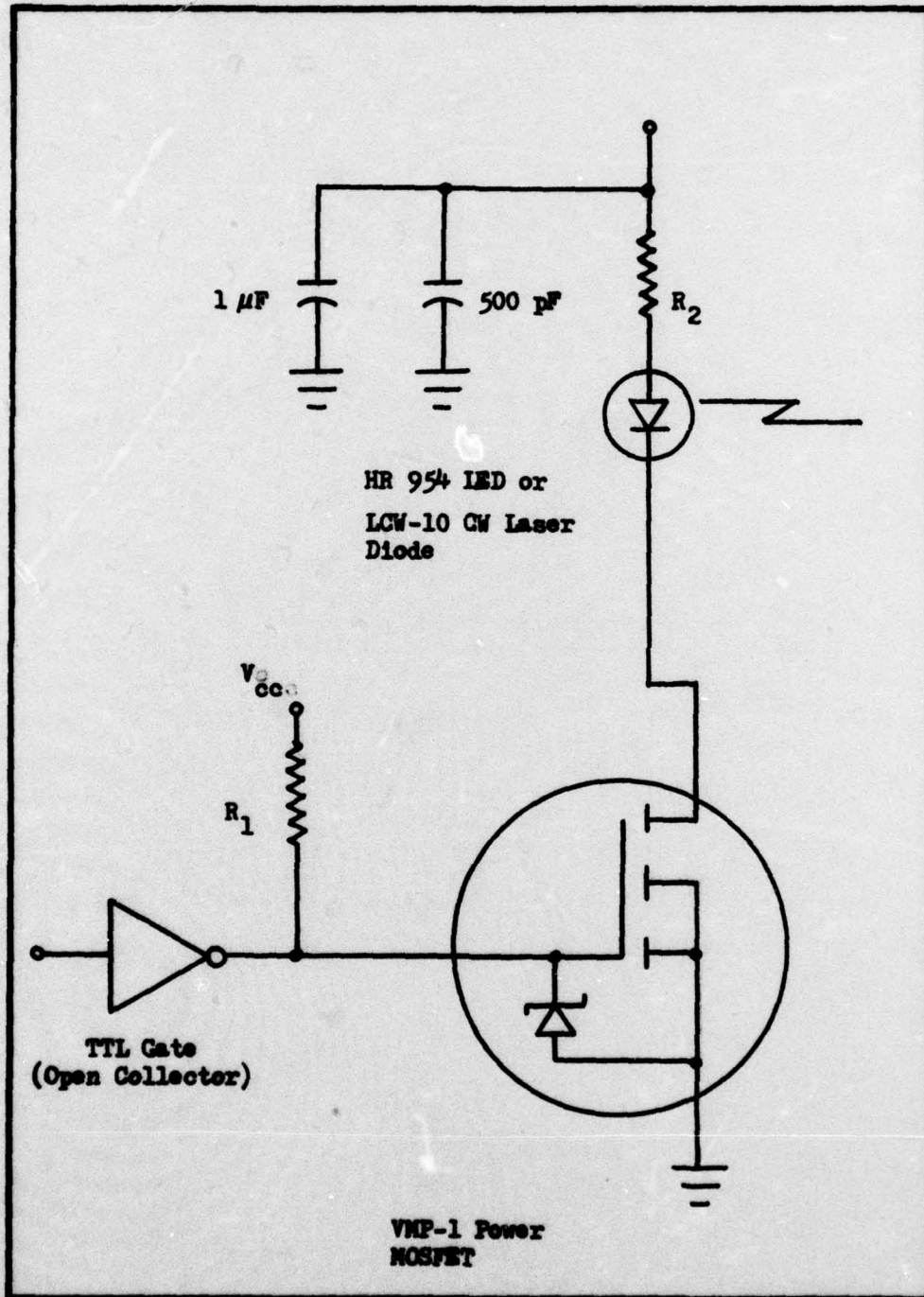current results with a gate voltage of about 4.3 volts.

Fig. 28. Light Emitter Modulator Circuit

In Swenson's prototype, $R_1 = 390$ ohms, $R_2 \approx 3$ ohms and $V_{cc} = 10$ volts. Also, the TTL gate was from a 7406 open collector inverter. Because V_{cc} in the transmitter does not need to be more than 5 volts, and the MOSFET has a gate-source capacitance of 40 pf, it appears that a faster gate voltage rise time is possible if R_1 is reduced to 130 ohms and a gate from a 7433 integrated circuit is substituted for the 7406. Using a 7433 IC does limit the maximum value of V_{cc} to 5.5 volts, but this is unimportant for the intended application because the high drive currents used in Swenson's experiments are not needed.

To close this section, a few comments on the rise time for the circuit are warranted. The VMP-1 has a rise time of 5 n sec. The LCW-10 has a rise time of 0.1 n sec and the HR-954 rise time is 5 n sec. Therefore, the rise time of the diode-modulator system should be on the order of 5 n sec. This value is only about 1.5 percent of the on time of the Manchester coded 1.5 MBit signal (3.33×10^{-7} sec). As a result, the output pulse from the light emitters is a good approximation of the ideal square wave shapes assumed throughout earlier portions of this paper.

Manchester Encoder. The Manchester encoder circuit will take a NRZ input pulse and convert it to the proper coded pulse. This circuit will be clocked by the transmitter clock. The input will be switched from the computer data line to the start-up word generator whenever a start-up sequence is initiated. The input will switch back to the computer data line when the start-up sequence is complete.

Start-up Timer and Transmitter Controller. Byrne mentions that, for certain conditions, a phase-locked loop will synchronize to a

suddenly applied signal within a known time period (Ref 21:588-589).
The required conditions include the proper selection of filter constants
for the phase-locked loop's low-pass filter and sufficient stability in
the transmitter clock and receiver VCO to ensure that the VCO frequency
with no input signal is fairly close to the transmitter frequency.
Therefore, assuming a stable set of oscillators, it is possible to con-
trol the synchronisation of the loop merely by controlling the start-up
sequence with a timer at the transmitter. The duplex form of the data
link allows either computer to test for successful closed-loop synchron-
isation and to request another synchronisation cycle if necessary.

Start-up Word Generator. During the start-up sequence, it is
important to transmit a data stream to the receiver which does not make
transitions from one state to the other at the beginning of the bit
periods. To understand the reason for this, consider the two sample
Manchester signals in Fig. 29. In Fig. 29b, a series of encoded 1 bits
is presented. If this data stream is fed to the unsynchronized phase-
locked loop, it is possible for the loop to synchronise on the transi-
tions at the beginning of the bit period rather than at the midpoint of
the bit period. The result is a quasi-stable synchronisation which will
cause gross errors in data decoding.

Now, consider the phase-locked loop's reaction to an input such
as shown in Fig. 29a. The only way the loop can synchronise with this
data stream is with the transitions that occur at the midpoint of each
bit period. As a result, improper synchronisation is not possible.
Assuming the design constraints mentioned in the subsection on the
start-up timer are met, the chance of the loop not being synchronized
at the end of the start-up timing interval is very small.

100
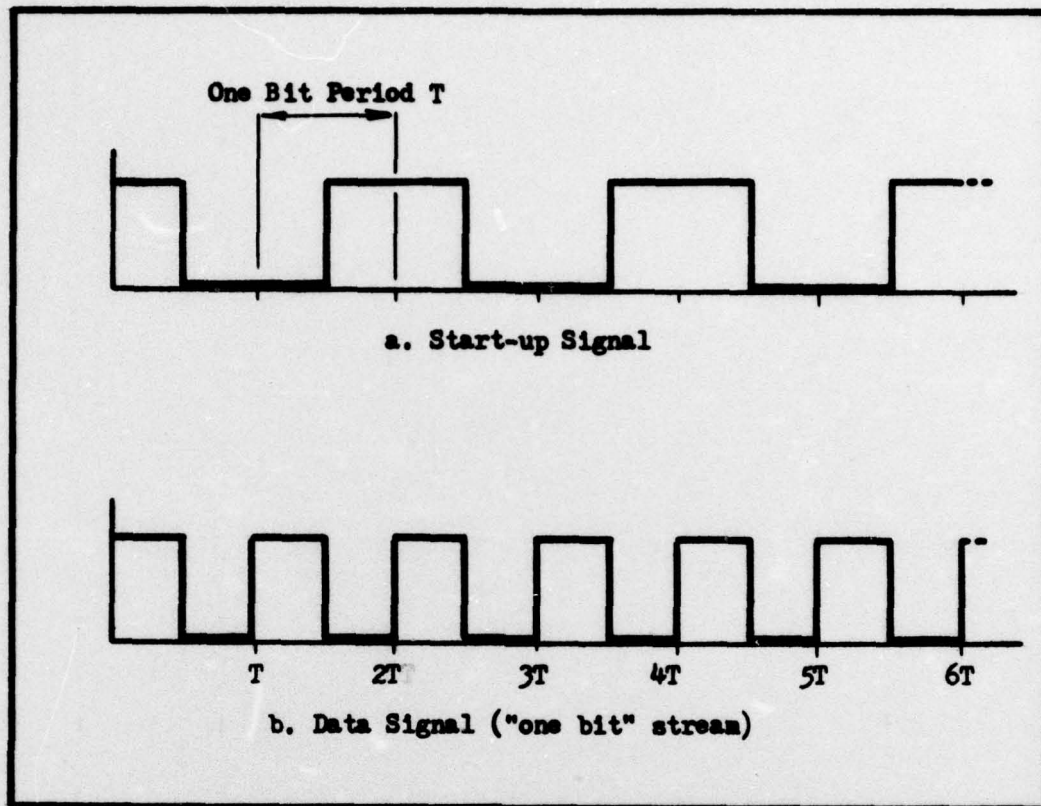
Fig. 29.   Start-up Signal - Data Signal Comparison

Transmitter and Fiber Cable Costs

As was done in the last chapter, a few comments about the projected costs of the two transmitters will be made. Again, these are only rough estimates because circuit details for much of the transmitter have not been completed.

The electronics section will be treated first, since it is common to both types of transmitters. To begin, the transmitter clock will be built around an LM 375 oscillator IC with appropriate 7400 series dividers. The cost is expected to be about $20.

Timing and control functions will include a 555 timer IC and the necessary logic to handle the simple switching functions needed in the transmitter. Cost of this circuit will probably be $20.

The modulator circuit is exceptionally low cost; the VMP-1 MOSFET unit cost is less than $8, and other components in the modulator will only raise this to about $15 total cost. Power supplies and packaging should add another $200.

For a complete fiber system, the Plessy HR 954 diode must be included in the transmitter cost. The HR 954 costs $300. Since the fiber will be epoxied directly to the LED, no extra hardware costs are expected. As a result, the fiber transmitter should cost $555 all together.

The two fiber cable needed by the system presently costs about $9.20/m. Thus, the cost for the 2 Km needed is going to be $19,200. In addition, the fiber-to-fiber couplers cost $78 each, adding $312 to the total cost. Recalling the costs of a fiber receiver mentioned in Chapter three, the total parts cost for the duplex fiber data link is expected to be about $21,830.

For the atmospheric link the lens cost and the LCW-10 laser diode costs must be added to the cost of the electronics package. From some preliminary designing, it seems possible that a suitable lens and focus mount package will cost around $400. The LCW-10 diode costs $230 in quantities of two-or-more, and the thermoelectric cooler and thermostat for the laser diode should add an additional $50. Therefore, the parts cost of an atmospheric transmitter will be roughly $935. This means a duplex atmospheric data link will cost about $4070.

V. Summary and Recommendations

Summary

The most important result of this study is the indication that it
should be possible to build either an atmospheric or fiber optic 1.5
Mb/s, 1-to-2 Km long data link using presently available commercial com-
ponents. Further, the transmitters and receivers for each type of link
can probably be constructed with fairly inexpensive components. The
cost of the receivers and transmitters for a duplex data link, exclud-
ing the cost of fiber cable, will be about $4100 for the atmospheric
system and about $2300 for the fiber system. The cost of fiber cable
and couplings brings the total cost of a duplex fiber link to about
$21,800.

One of the more interesting results of the study was the effect
that weather conditions will have on the performance of the atmospheric
data link. In chapter two, a simple model was developed using Beer's
law and Koschmeider's law to relate prevailing visibility measurements
to attenuation levels to be expected in the 1372 m long atmospheric
link. A tabulation of the results appears in Table II, chapter two.
Later, in chapter four, an analysis of the required transmitter output
power during various weather conditions was performed. The results of
the analysis are tabulated in chapter four, Table VI. The figures in
Table VI indicate that a 10 mw CW Laser Diode with an efficient lens
system should be able to provide the desired error performance in pre-
vailing visibility conditions as poor as 1/2 to 3/4 statute mile. Thus,
according to weather statistics for Wright-Patterson AFB, a link

installed here should suffer weather outages only about 1 to 2 percent of the time on a yearly basis. Even during the poor mid-morning weather conditions in January, Appendix A indicates that visibilities low enough to cause outages occur during less than 4 percent of the mid-morning hours. Therefore, in applications where a small amount of down time can be tolerated, and where the physical locations involved allow line-of-sight transmission, the atmospheric system offers a very low-cost means to implement high-speed data links.

The fiber-optic link also offers excellent potential. Fiber optic links do not require line-of-sight paths between the two computing systems, so fiber optic links can be used in a number of applications which do not permit use of an atmospheric link. Additionally, fiber links are impervious to weather changes, and the only significant reason for outages is equipment failure. Thanks to the small size, light weight, and strength qualities of fiber cables, it is possible to install fiber links using existing communications conduit systems. Additionally, since fiber cables are essentially immune from electro-magnetic interference of reasonable levels, it is probably possible to install fibers in power conduits and other areas where traditional wire links cannot be installed. While the cost of fiber cables is presently rather high (about $9.20/m for duplex cables), the projected cost in the next two to three years should make fiber systems very competitive with wire systems.

A tabular summary of some major characteristics of the fiber-optic and atmospheric data links follows.

Table VII
Characteristics of the Atmospheric Link

Data rate	1.5 Mb/s
Error rate	1 in 10^{+5} bits
Path length	1372 m
Cost for duplex system	$4070

Transmitter

Optical frequency	860 nm
Peak pulse output power	$\approx$ 10 mw
Beam divergence half angle	1 m rad
Pulse rise time	< 5 n sec
Transmitter laser	Laser Diode Labs LCW-10 GaAs CW laser diode

Receiver

Optical input frequency	860 ± 5 nm
Input lens field of view half angle	0.68 m rad
Required intensity at receiver lens	2.04×10^{-6} watts/m^2
Receiver lens input aperture	5.06×10^{-2} m^2
Required power at detector diode	3.90×10^{-8} watts
Receiver Diode	EG&G SHS-100 PIN Diode

Table VIII
Characteristics of Fiber-Optic Link

Data rate	1.5 Mb/s
Error rate	1 in 10^5 bits
Path length	2 Km
Cost for duplex system	$21,830

Transmitter

Center optical frequency	$\approx$ 900 nm
Peak power coupled into fiber	2.32×10^{-5} watts
Pulse rise time	< 5 n sec
Transmitter Light Emitter	Plessy HR-954 Light Emitting Diode

Cable

Fiber type	Corning 1158 multimode graded index
Bandwidth	200 MHs in 1 Km length
Attenuation	6 dB/Km
Coupling loss	1.5 dB/coupling
Cable configuration	2 fibers in strengthened cable

Receiver

Optical frequency	Suitable for transmitter
Required optical power	3.90×10^{-8} watts
Receiver Diode	EG&G SHS-100 with Texas Instruments TIXL-152 Amplifier

Recommendations

While the results of this investigation are very encouraging, a number of steps still must be taken before widespread use of optical high speed communications can be fully endorsed for use at Wright-Patterson. Since separate courses of action are deemed appropriate for the two types of systems, each is discussed separately.

Atmospheric System. The first step that should be taken is the development and experimental verification of a lens design for the transmitter. This investigation must include determining the actual amount of focusing that can be accomplished with inexpensive lenses and the resulting size and location of the beam waist formed by the lens package. With this information, a precise safety calculation can be performed, and the performance of the receiver can be redefined, if necessary.

Once the transmitter optics are selected, the important issue of transmitter and receiver aiming must be considered. Since the beam divergence angle of the transmitter and the beam acceptance angle of the receiver are both only about 1 mrad, this task may be quite difficult. The author has considered the possibility of making the photodiode/filter and laser packages removable to permit direct sighting through the optics trains, but time has not permitted development of this idea. Trial and error alignment by monitoring the detector diode's output signal may also be possible, although probably tedious.

In addition to the optical issues, the somewhat arbitrarily derived performance prediction of the timing circuit should be confirmed, preferably with an experimental circuit. If significant departure from

107

the predictions is noted, some redefinement of the values in Table VI will be necessary, and a revised estimate of the weather's effects will have to be made.

After solutions for the optical and timing issues are found, a test range should be created, preferably over the planned link path from Building 620 to Building 676 at Wright-Patterson AFB. This range should be used to gather data on the effects of weather on propagation before full-scale development of the receiver is attempted. The resulting information will indicate if a shift in transmitter wavelength, beam divergence, or output power is necessary to obtain the desired performance.

Once the desired transmitter characteristics are fully confirmed, the complete hardware design of the transmitter and receiver should be undertaken, and a prototype system constructed. The prototype should be exercised on the test range to ensure that the design criteria are met prior to making a decision to introduce the data links into general use.

Fiber System. The total parts cost of the fiber link design in this paper is about 40% higher than the rough goal set at the beginning of this study. However, an avalanche photodiode in the receiver may enable some reduction in the cost of the system, because the costs of the detector's bias circuitry may be offset by the lower cost of a higher loss fiber cable. Also, the use of a laser diode will also enable use of less expensive cables, although the laser diode's lifetime may not be as good as that of the LED. The timing issue mentioned for the atmospheric link should also be addressed. Thus, a further examination

of the fiber link seems warranted, although cost reductions of more than $2000 will probably be dependent upon future reductions in the costs of fiber cables.

In addition to possible refinements in the design of the fiber link, an examination of the problem of installing fiber cables in conduits is necessary. The engineering and economic factors involved may both be important issues in the actual implementation of a fiber link.

One additional comment about the fiber link is warranted. The author has learned that at least two commercial companies are offering developmental fiber optic data transmitters and receivers. At least one of these units may be capable of operating with a 2 Km system, and the costs of the finished units compare favorably with the cost of the designs described in this paper. Since the major cost of the fiber link is concerned with the fiber cable itself, the amount of money saved by constructing and testing yet another transmitter and receiver may not be justified. So, an evaluation of the actual capabilities of these commercial units seems warranted.

A Final Comment

The dawn of the era of optical communications has been continuously heralded since the discovery of the laser in 1960. Until recently, the promises of the laboratory have seemed to be far away from the realities of commercial practicability. However, as this report shows, commercial opto-electronic components are now becoming available at costs which make the operational implementation of optical data links practical and cost effective.

Bibliography

1. Woodman, Douglas P. "Limitations in Using Atmospheric Models for Laser Transmission Estimates." *Applied Optics*, 13:2193-2194 (October 1974).

2. Pratt, William K. *Laser Communication Systems*. New York: John Wiley and Sons, Inc., 1969.

3. McClatchey, R. A., et al. *Optical Properties of the Atmosphere* (Third Edition). AFCRL-72-0497. L. G. Hanscom Field, Massachusetts: Air Force Cambridge Research Laboratories, 1972. AD 753075.

4. McClatchey, R. A. and John E. A. Selby. *Atmospheric Attenuation of Laser Radiation from 0.76 to 31.25 um*. AFCRL-TR-74-0003. L. G. Hanscom Field, Massachusetts: Air Force Cambridge Research Laboratories, 1974. AD 779726.

5. Chu, T. S. and D. C. Hogg. "Effects of Precipitation on Propagation at 0.63, 3.5, and 10.6 Microns." *The Bell System Technical Journal*, 47:723-759 (May-June 1968).

6. Coolidge, Charles H. *Atmospheric Transmission of 1.06 Micron Laser Radiation: Application to Standoff Missile Performance*. Unpublished thesis. Wright-Patterson AFB, Ohio: Air Force Institute of Technology, March 1974. AD 779945.

7. Muench, Stuart H., et al. *Development and Calibration of the Forward Scatter Visibility Meter*. AFCRL-TR-74-0145. L. G. Hanscom Field, Massachusetts: Air Force Cambridge Research Laboratories, 1974. AD 783270.

8. Chiba, T. "Spot Dancing of the Laser Beam Propagated through the Turbulent Atmosphere." *Applied Optics*, 10:2456-2461 (November 1971).

9. Ochs, G. R. and R. S. Lawrence. *Measurements of Laser Beam Spread and Curvature over Near-Horizontal Atmospheric Paths*. ESSA TR ERL 106-WPL 6. Boulder, Colorado: Environmental Science Services Administration, February 1969.

10. Barnoski, Michael K., Editor. *Fundamentals of Optical Fiber Communications*. New York: Academic Press, Inc., 1976.

11. Gloge, D., et al. "Optical Fiber End Preparation for Low-loss Splices." *Bell System Technical Journal*, 52:1579-1588 (November 1973).

12. Rome Air Development Center. *Optical Cable Communications Study*. RADC-TR-75-187. Griffiss Air Force Base, New York: RADC, 1975. AD A016846.

13. Bisbee, D. L. "Measurements of Loss Due to Offsets and End Separations of Optical Fibers." _Bell System Technical Journal_, 50:3159-3167 (December 1971).

14. Miller, C. M. "Loose Tube Splices for Optical Fibers." _Bell System Technical Journal_, 54:1215-1225 (September 1975).

15. Marcuse, D. "Excitation of Parabolic Index Fibers with Incoherent Sources." _The Bell System Technical Journal_, 54:1507-1530 (November 1975).

16. Melles Griot Company. _Optics Guide_. Irvine, California: Melles Griot Co., 1975.

17. Klein, Miles V. _Optics_. New York: John Wiley and Sons, Inc., 1970.

18. Taub, Herbert and Donald L. Schilling. _Principles of Communications Systems_. New York: McGraw-Hill Book Company, 1971.

19. Riess, R. P. "High Speed Semiconductor Photodiodes." _The Review of Scientific Instruments_, 33:994-998 (September 1962).

20. Texas Instruments Inc. _The Optoelectronics Data Book_ (Third Edition). Dallas, Texas: Texas Instruments Inc., 1976.

21. Byrne, C. J. "Properties and Design of the Phase-Controlled Oscillator with a Sawtooth Comparator." _The Bell System Technical Journal_, 41:559-602 (March 1962).

22. AFR 161-xx. _Health Hazards Control for Laser Radiation_. Washington: Department of the Air Force (To be published, Draft dated 23 June 1975).

Appendix A

Additional Weather Statistics for
Winter, Spring and Summer Months

This appendix presents additional summaries of the average percent-
age frequency of occurrence of various prevailing visibilities at
Wright-Patterson AFB. The data presented has been derived from tables
of weather statistics for Wright-Patterson, maintained by the Data
Processing Division, USAF ETAC, Air Weather Service (MAC), Federal
Building, Ashville, North Carolina.

The ETAC data tables list the percentage frequency of occurrence
of weather conditions as a joint function of both the prevailing visi-
bility and cloud ceiling. To eliminate the dependence of the figures
upon ceiling height, the data in Table IX is derived from the row of
statistics in the ETAC charts which relate the percentage of time that
the ceiling was greater than or equal to zero feet while the visibility
was greater than or equal to the values in Table IX. Since the
percentage of occurrence of ceilings greater than zero is 100%, the
joint function listed in the ETAC charts becomes a function of the
ceiling only. The ETAC tables also provide tabulations in terms of the
percentage of time that observed weather conditions were better than
the stated levels. The figures in Table IX were derived by subtracting
the appropriate ETAC figure from 100%.

One additional note on the use of the ETAC data is warranted.
The data base includes weather observations made on an hourly basis
during the years 1936 to 1972. The time between observations is fairly

long compared to the rate of change of low-visibility weather conditions. However, because of the very large data base, the author assumes that the figures are a fairly accurate representation of the continuous time probability function for visibilities at Wright-Patterson Air Force Base.

Table IX
Percentage Frequency of Occurrence of Various Prevailing Visibilities for Three Selected Months

Hour (local)	Visibility							
	10	5	4	3	2	1	0.75	0.5
JANUARY								
0-0200	71.5	33.0	25.3	16.5	10.4	4.7	3.1	1.9
0300-0500	73.2	35.	26.3	16.7	10.1	5.1	3.8	2.5
0600-0800	79.6	41.1	31.6	22.1	13.2	5.2	3.6	2.0
0900-1100	84.8	46.5	36.2	25.3	15.5	6.3	3.7	1.7
1200-1400	79.7	34.7	26.5	16.9	9.9	3.9	2.3	0.6
1500-1700	75.0	32.4	22.7	15.1	9.1	3.7	2.1	0.9
1800-2000	74.3	32.3	23.2	15.0	8.9	3.6	2.2	1.0
2100-2300	70.7	31.3	23.3	15.1	9.6	4.4	2.7	1.6
APRIL								
0-0200	51.8	12.0	7.6	4.0	2.0	0.8	0.5	0.4
0300-0500	58.3	17.1	11.4	6.7	4.2	2.1	1.5	1.1
0600-0800	73.1	28.3	19.4	11.3	5.1	2.3	1.6	1.2
0900-1100	60.0	15.2	9.0	4.3	1.8	0.4	0.2	0.1
1200-1400	46.7	9.2	5.7	3.0	1.2	0.3	0.2	0.1
1500-1700	42.9	7.7	5.2	2.9	1.2	0.4	0.2	0.1
1800-2000	47.9	10.2	6.3	3.4	1.3	0.3	0.1	-
2100-2300	46.9	8.7	5.2	2.5	1.0	0.5	0.2	0.1
JULY								
0-0200	60.3	13.1	7.2	3.0	2.5	0.7	0.7	0.4
0300-0500	71.5	28.8	19.2	10.9	6.1	2.9	2.6	1.6
0600-0800	77.7	34.6	23.9	14.8	7.0	2.9	2.3	1.6
0900-1100	59.6	63.7	7.2	3.1	1.1	0.2	0.1	-
1200-1400	45.3	6.8	3.3	1.0	0.4	0.1	0.1	-
1500-1700	41.1	5.2	2.0	0.8	0.3	0.1	0.1	-
1800-2000	45.7	5.9	2.5	0.9	0.4	0.2	-	-
2100-2300	51.7	8.3	3.2	1.3	0.5	0.2	0.2	0.1

<u>Vita</u>

Richard G. Innes was born on 10 May 1945 in New Orleans, Louisiana. He graduated from high school in Scarsdale, New York in 1963 and attended Lehigh University, receiving a degree of Bachelor of Arts in 1967 and a degree of Bachelor of Science in Electrical Engineering in 1968. He also received a commission in the USAF through the ROTC program in 1968 and immediately entered undergraduate pilot training at Moody AFB, Georgia. After receiving his wings in July 1969, he served a combat tour in the A-37 fighter-bomber and then returned to Columbus AFB, Mississippi, in November 1970 for duty as a T-37 instructor pilot. While stationed at Columbus, he was instrumental in identifying a major design deficiency in the T-37 electrical power system and was later recognized for this effort by the Chief of Staff of the USAF. He entered the School of Engineering, Air Force Institute of Technology, in June 1975.

Permanent address: 24 Sage Terrace
                    Scarsdale, New York 10583

This thesis was typed by Mrs. Frances Jarnagin.

115

REPORT DOCUMENTATION PAGE		READ INSTRUCTIONS BEFORE COMPLETING FORM
1. REPORT NUMBER GE/EE/76D-25	2. GOVT ACCESSION NO.	3. RECIPIENT'S CATALOG NUMBER
4. TITLE (and Subtitle) LOW-COST OPTICAL DATA LINK DESIGN STUDY		5. TYPE OF REPORT & PERIOD COVERED MS Thesis
		6. PERFORMING ORG. REPORT NUMBER
7. AUTHOR(s) Richard G. Innes Captain, USAF		8. CONTRACT OR GRANT NUMBER(s)
9. PERFORMING ORGANIZATION NAME AND ADDRESS Air Force Institute of Technology (AFIT-EN) Wright-Patterson AFB, Ohio 45433		10. PROGRAM ELEMENT, PROJECT, TASK AREA & WORK UNIT NUMBERS
11. CONTROLLING OFFICE NAME AND ADDRESS Aeronautical Systems Division/XOG Wright-Patterson AFB, Ohio 45433		12. REPORT DATE December 1976
		13. NUMBER OF PAGES 125
14. MONITORING AGENCY NAME & ADDRESS(if different from Controlling Office)		15. SECURITY CLASS. (of this report) Unclassified
		15a. DECLASSIFICATION/DOWNGRADING SCHEDULE

16. DISTRIBUTION STATEMENT (of this Report)

Approved for public release; distribution unlimited

17. DISTRIBUTION STATEMENT (of the abstract entered in Block 20, if different from Report)

18. SUPPLEMENTARY NOTES

Approved for public release; IAW AFR 190-17

JERRAL F. GUESS, Capt, USAF
Director of Information

19. KEY WORDS (Continue on reverse side if necessary and identify by block number)

Atmospheric Propagation	Optoelectronic
Laser Transmittance	Electro-optic
Data Transmission	Fiber-Optics
Data Link	Optical Communication

20. ABSTRACT (Continue on reverse side if necessary and identify by block number)

This paper discusses some of the theoretical background and practical problems involved in designing a full duplex 1.5 Mb/sec optical data link. The actual design of a fiber-optic link and an atmospheric link is treated for an atmospheric path length of 1.372 Km and a fiber path length of 2 Km. Complete designs to the block diagram level are presented, and additional details are described for the modulator circuit for the CW laser diode and LED used in the atmospheric and fiber transmitters. Also presented is sufficient data to permit calculation of the various losses encountered in

DD FORM 1473 1 JAN 73 EDITION OF 1 NOV 65 IS OBSOLETE

Block 20. Abstract (continuation)

fiber and atmospheric links. It is shown that currently available LED's
and low-loss graded-index optical fibers should permit production of a 2 Km
long fiber optic data link to handle a data rate of 1.5 Mb/s with an error
rate of less than *10^{-5}. The atmospheric transmission theory presented permits
use of readily available weather statistics to roughly predict that an atmos-
pheric link operating in western Ohio can provide the comparable data
performance for more than 99% of the time. Parts costs for the transmitters,
receivers, and the cable in the fiber system are estimated at $21,800. Cost
of the receivers and transmitters in the atmospheric system cost about $4,030.

*10 to the minus 5th power.